Bergvesenet rapport nr	Intern Journal nr	Internt arkiv nr	Rapport fortrolig pga	Gradering
5264				

Kommer fra arkiv	Ekstern rapport nr	Oversendt fra	Fortrolig pga	Fortrolig fra dato:
Grong Gruber AS		Grong Gruber a.s.		

Tittel
THE GEOLOGY OF THE JOMA SULPHIDE DEPOSIT, NORD - TRØNDELAG, NORWAY
PART I - STRUCTURAL STUDIES OF THE ORE AND SURROUNDING AREA

Forfatter	Dato	År	Bedrift (oppdragsgiver og/eller oppdragstaker)
Noelle E. Odling		1986	Universitetet i Trondheim

Kommune	Fylke	Bergdistrikt	1: 50 000 kartblad	1: 250 000 kartblad
Røyrvik	Nord-Trøndelag		19241	Grong

Fagområde	Dokument type	Forekomster (forekomst, gruvefelt, undersøkelsesfelt)
Geologi		Grongfeltet Joma

Råstoffgruppe	Råstofftype
Malm/metall	Cu Zn Kis

Sammendrag, innholdsfortegnelse eller innholdsbeskrivelse

TABLE OF CONTENTS:

THE GEOLOGY OF THE

JOMA SULPHIDE DEPOSIT, NORD TRØNDELAG, NORWAY

PART I

STRUCTURAL STUDIES OF THE ORE AND SURROUNDING AREA

NOELLE E. ODLING

1986

UNIVERSITET I TRONDHEIM
NORGES TEKNISKE HØGSKOLE
GEOLOGISK INSTITUTT

TABLE OF CONTENTS

SECTION 3 : THE JOMA SULPHIDE DEPOSIT

SECTION 4 : SUMMARY AND CONCLUSIONS

SECTION 1 : INTRODUCTION

1.1 LOCATION AND GEOLOGICAL SETTING OF THE JOMA SULPHIDE DEPOSIT

The Joma massive sulphide deposit is situated in the north east of the Grong area of Nord-Trøndelag, some 4 km south of Huddinsgdalen and 15 km west of the Swedish border. The ore body outcrops in Røyrvik Group greenstones of the Leipikvattnet nappe, one of the Köli nappes in the Upper Allochthon of the Scandinavian Caledonides, see Fig.1.1. The Leipikvattnet nappe outcrops over a distance of 120 km, trending generally northeast and is separated from the overlying Gjersvik and underlying Gelvanåkko nappes by major thrusts. The Røyrvik group greenstones are correlated with the Remdalen Group found in the underlying Gelvanåkko and Stikke nappes (Zachrisson 1969, Sjöstrand 1978, Stephens 1982) and are inferred from fossil evidence in other parts of the Köli sequence to be Silurian to Ordovician in age.

The Leipikvattnet nappe is composed of intercalated layers of greenstone, quartzitic phyllite and graphitic phyllite. Minor amounts of serpentinite are associated with the greenstones while calcareous phyllites (the Brakkfjell schist) outcrop in the extreme east, see Fig.1.2. The lower thrust boundary with the Gelvanåkko nappe is marked by a highly deformed marble horizon. In the Joma area, the Leipikvattnet nappe is composed of three major greenstone units named from northeast to southwest, the outer, middle and inner greenstones, which are intercalated with quartzitic and graphitic phyllites, see Fig.1.2. The ore body outcrops within the middle greenstone unit. The metamorphic grade is upper Greenschist facies, the greenstones being composed of actinolite, albite, chlorite and epidote and the phyllites of quartz, muscovite and graphite.

The rocks have been deformed by several phases of deformation, which are locally strong, but original volcaniclastic layering and pillow structures are still

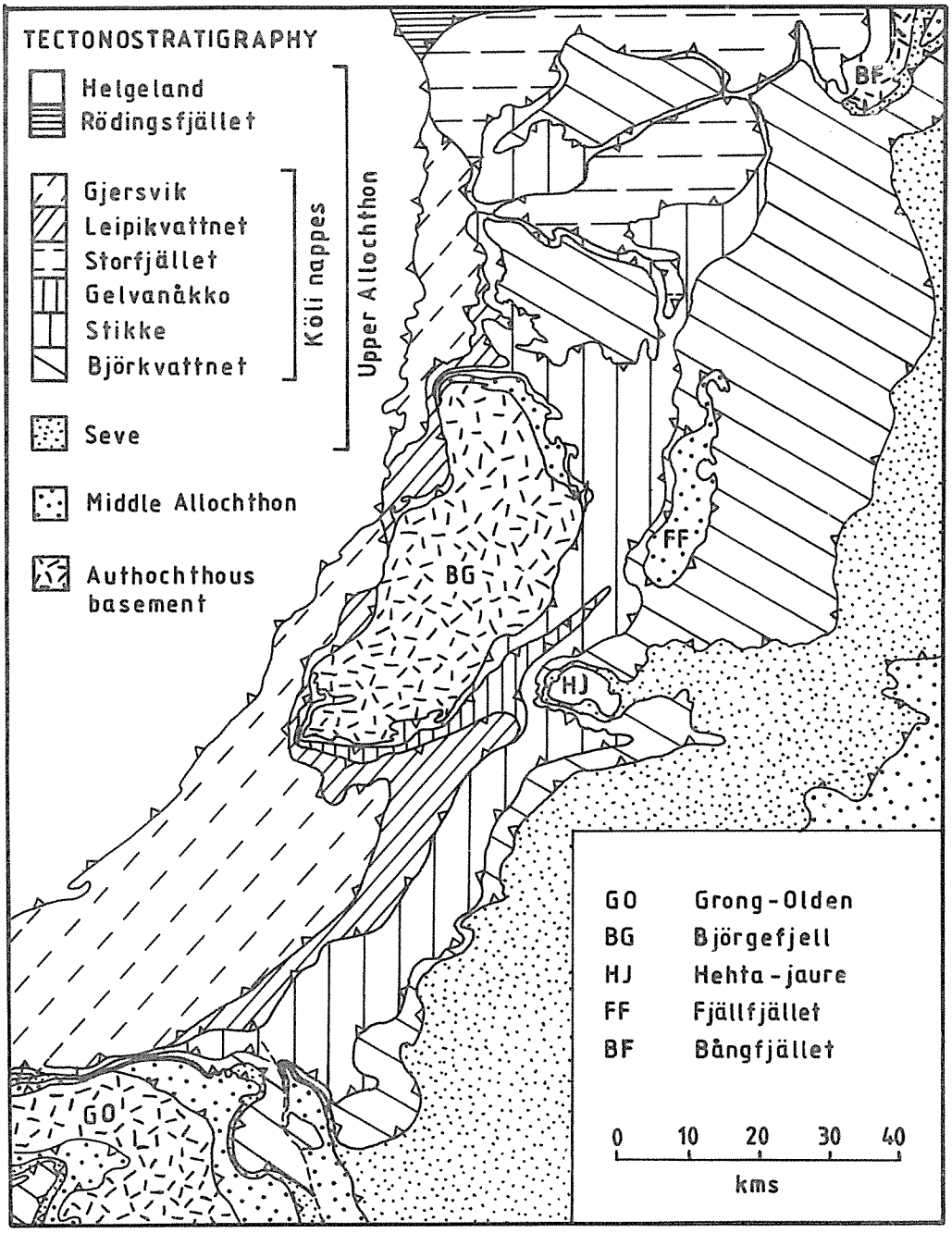

Fig.1.1 Map of the north, central Scandinavian Caledonides after Stephens and Reinsbakken (1981), Haggbom (1978), Ramberg (1981) and Reinbakken (unpublished data). The Leipikvattnet nappe outcrops over a distance of 120 kms from the north side of the Grong-Olden culmination to north of the Bjørgefjell massive.

Fig.1.2. STRUCTURAL GEOLOGY OF THE JOMA AREA, N. TRÖNDELAG

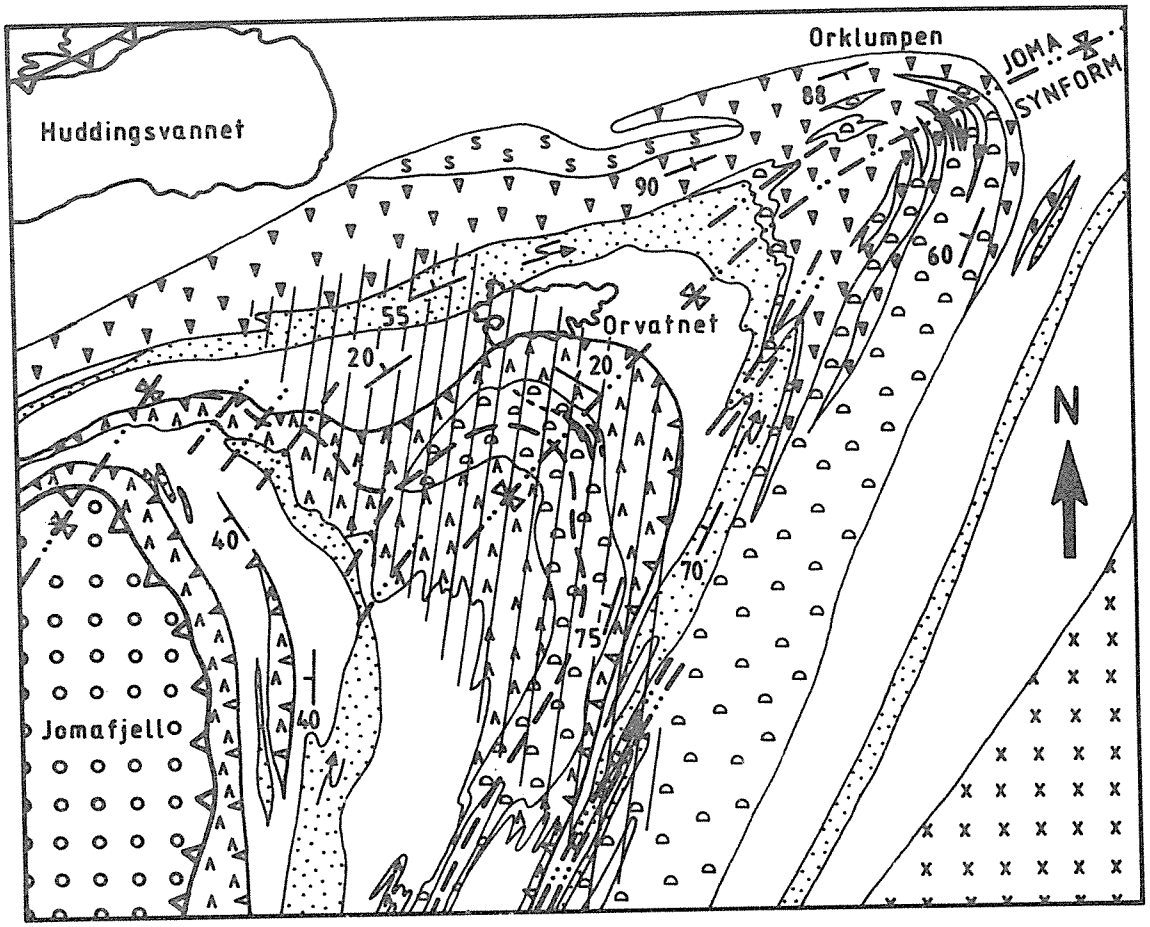

KEY

- Metasediments — Limingen Group — GJERSVIK NAPPE
- Graphitic phyllite
- Quartzitic phyllite
- Volcaniclastic greenstone
- Pillowed greenstone
- Massive greenstone
- Brakkfjell schist
- Röyrvik Group — LEIPIKVATNET NAPPE
- Serpentinite
- Outcrop of Joma sulphide deposit
- Major thrust contacts to Leipikvatnet nappe
- Minor thrusts within Leipikvatnet nappe
- F2 fold trace
- F2 fold vergence, arrow indicates plunge
- F3 fold trace
- Average dip of S2 deavage
- Zone of subhorizontal F3 fold axes

0 1 2 3 4 5 kms

discernible in the greenstones and original layering preserved in the quartzitic phyllites. The rocks have suffered four phases of deformation of which the second is responsible for the overall flat-lying penetrative schistosity, isoclinal folding and northwest trending mineral lineation common to all rocks. An early phase of deformation is seen in locally preserved S1 schistosity and F1 folds. These features have been refolded by the major, northeast trending Joma synform, with which minor folds and a variably developed crenulation cleavage are associated. The Joma ore body lies in the hinge zone of this structure. Minor structures belonging to the latest phase of deformation are only developed adjacent to the thrust with the overlying Gjersvik nappe.

1.2 PREVIOUS REASEARCH AND THE MINING HISTORY OF THE JOMA SULPHIDE DEPOSIT

The Joma massive sulphide deposit was first described by Munster (1915) in a report on the exposure of sulphides in the the Orvasselv river at Joma and the area first mapped by Foslie in 1922 to 1925. Early exploration of the deposit started with some preliminary drilling in 1912 (Munster 1915) and later drilling by the Germans during the second World War. The deposit was, however, not mined at this time and activity ceased until attention was again drawn to Joma by reviews of sulphide deposits in the Grong area (Foslie 1949, Oftedahl 1958 and Bjørlykke 1959).

Renewed efforts in exploration began in the 1960's when the ore deposit was extensively drilled by N.G.U. under the supervision of H. Bjørlykke. Detailed mapping on the scales of 1:200 and 1:500 of the immediate area of the sulphide exposures was done by Juve in 1964. The ore deposit was taken over by Grong Gruber A/S in 1969 and when production started in 1972, total massive sulphides were estimated at 20 million metric tons, with ore reserves calculated as 6.8 million metric tons averaging 1.70% copper and 1.11% zinc.

Exploration after the mining started has included the use of the 'Turam' geophysical technique, which has outlined the

location of subsurface sulphide horizons (Løgn and Bølviken 1974). Recent geophysical exploration using the 'differential electromagnetic potential' technique by Elvebakk in 1984 and 1985 has added to these results. A detailed 1:50,000 map of the Leipikvattnet nappe in the Joma area was completed by Kollung in 1978 and has served as a basis for further detailed mapping. The middle greenstone unit was mapped on the scale of 1:5,000 as an undergraduate project by Romaya in 1982 and the continuation of the three greenstone units to the west mapped on a similar scale by Horbach during 1983 to 1985. A preliminary report on the greenstone mineralogy and geochemistry is given in Horbach and Leissmann (1985).

The mineralogy and composition of the sulphide lithologies were first described by Anger et.al. (1963) and are presently under investigation by Liessmann who gives a preliminary report in Horbach and Leissmann (1985). The occurence of silver and silver bearing minerals in the sulphides has been described by Eidsmo et.al. (1984). Underground mapping of the ore body was undertaken by Olsen from 1975 to 1977 who constructed sections in the upper part of the ore body (Olsen 1984). These are revised and extended to the lower parts of the ore body by Reinsbakken in the present study. Olsen (1980) described the geochemistry of the the ore types and adjacent greenstones, interpreting the ore deposit to have been deposited in an ocean floor environment. The tectonic setting and genesis of the deposit are further dicussed by Stephens and Reinsbakken (1981).

1.3 OUTLINE OF THE PRESENT PROJECT

The present project has as its aims, an analysis of the structural setting, stratigraphy and chemistry of the Joma sulphide deposit and its country rocks. The project has been tackled in two sections, Part I, a study of the structures by N. Odling and Part II, a study of the stratigraphy and chemistry by A. Reinsbakken. The project was funded jointly by N.T.N.F. and Grong Gruber A/S. Odling was in possession of a two year post-doctoral fellowship from N.T.N.F. from 1st June 1984 to 1st June 1986 and Reinsbakken was funded jointly by Grong Gruber A/S and N.T.N.F., administered by SINTEF, from 1st May 1984 to 1st June

1986.

The structural analysis by Odling involved structural mapping on the scale of 1:5,000 of the area outlined in Fig.1.2 and incorporated the measurement of minor structures and mapping of lithological types in the greenstones. Finite strain was analysed for ten specimens of pillowed greenstone containing variolites from the outer greenstone. The structure of the ore deposit was studied by underground mapping and minor structure measurement, concentrated in the newer deeper parts of the mine. A total of 12 weeks were spent on surface mapping and 12 weeks on underground mapping from June to September in 1984 and 1985.

The stratigraphical study of the ore horizon by Reinsbakken involved the construction of 28 vertical and 5 planar sections of the ore body, extending those of Olsen (1984) to greater depth, and reclassifying the sulphide and country rock lithologies. To this end a number of the levels in the mine were mapped in detail during a total of six months spent at Joma. Fifteen deep drill holes from the surface to the ore horizon and 6 underground drill holes were were logged and sampled for a total of 460 chemical analyses to study the hydrothermal alteration associated with the sulphide deposit. In addition, 72 samples of sulphide ore were analysed for base and trace metal content.

SECTION 2 : REGIONAL GEOLOGY OF THE JOMA AREA

2.1 OUTLINE OF GEOLOGY AND STRUCTURE OF THE JOMA AREA.

An area of some 12 square kilometers, centered on the outcrop of the ore body has been mapped on the scale of 1:5,000, using the 1:50,000 map by Kollung (1979) as a basis to conduct more detailed structural mapping. Special attention was paid to the mapping of the minor structures: cleavage, lineation and fold orientations, with qualitative estimations of deformation intensity. Contacts were mapped in structurally complex areas and different lithologies within the greenstone units were identified and mapped.

The area consists of two main lithologies, phyllites and greenstones. The phyllites have varying contents of quartz as thin, subparallel layers. Phyllite with over approximately 50% quartz has been called quartzitic phyllite and mapped as a separate lithology by Kollung (1979). The greenstones are composed of three major types, pillow lavas, massive lavas and volcaniclastic deposits. The pillow lavas locally show well preserved pillow structures and are associated with pillow breccias. The massive lavas are homogeneous, coarse to fine grained and contain thin zones of graphitic phyllite and agglomerate. The volcaniclastic deposits vary from massive to well laminated and are generally fine grained.

The area has been affected by four phases of deformation. The second phase is the main event, giving rise to a penetrative schistosity and mineral lineations throughout the area which has almost completely overprinted a pre-existing schistosity. The main schistosity is folded by the third phase into a large scale, partially overturned, synformal structure known as the Joma synform. The fourth phase of deformation is restricted to sporadically developed minor structures, mainly in the southern part of the area.

2.2 LITHOLOGIES AND THEIR RESPONSE TO DEFORMATION

2.2.1 The Phyllites.

The phyllites grade from quartzitic to graphitic varieties with quartzitic phyllites concentrated in the structurally lower part of each of the three phyllite units, see Fig.2.1. The quartzitic phyllites are composed of intercalated quartz and graphite-rich layers which have recorded all phases of deformation as folds and cleavage. The quartzitic horizons vary from laterally continuous layers 5 to 10 cms thick to discontinuous, anastamosing layers down to a few mms thick. Mineralogically, they are composed of quartz, muscovite and graphite with minor chlorite. The quartz-rich layers, containing only small amounts of other minerals, show good polygonal textures while a strong cleavage is developed in the phyllitic layers. The large contrast in competency between quartzitic and phyllitic layers makes the rock highly susceptible to folding. The rock type is thus a very sensitive indicator of the deformation history and is structurally the most useful lithology in the area.

The dominant folding phase is D2. F2 folds are tight to isoclinal with sharp hinges and show a penetrative cleavage in the phyllitic layers. A strong rodding lineation is developed on the quartzitic layer surfaces parallel to F2 hinges (Fig.2.2), and where the quartzitic layers are thick with respect to phyllitic layers, a strong refraction occurs between a penetrative cleavage in phyllitic layers and the fracture cleavage in quartzitic layers, see Fig.2.3. Where the layering is thin (less than 0.5 cms), the concentration of muscovite and graphite in the limbs and quartz in the hinge zones of small scale F2 folds has caused local layer transposition, Fig.2.4.

Occasionally in the field and more frequently in thin section, S2 is seen to be a strong crenulation cleavage, folding a pre-existing S1 cleavage. F1 folds were detected at one out-

Fig. 2.1 STRUCTURAL GEOLOGY OF THE JOMA AREA, N. TRÖNDELAG

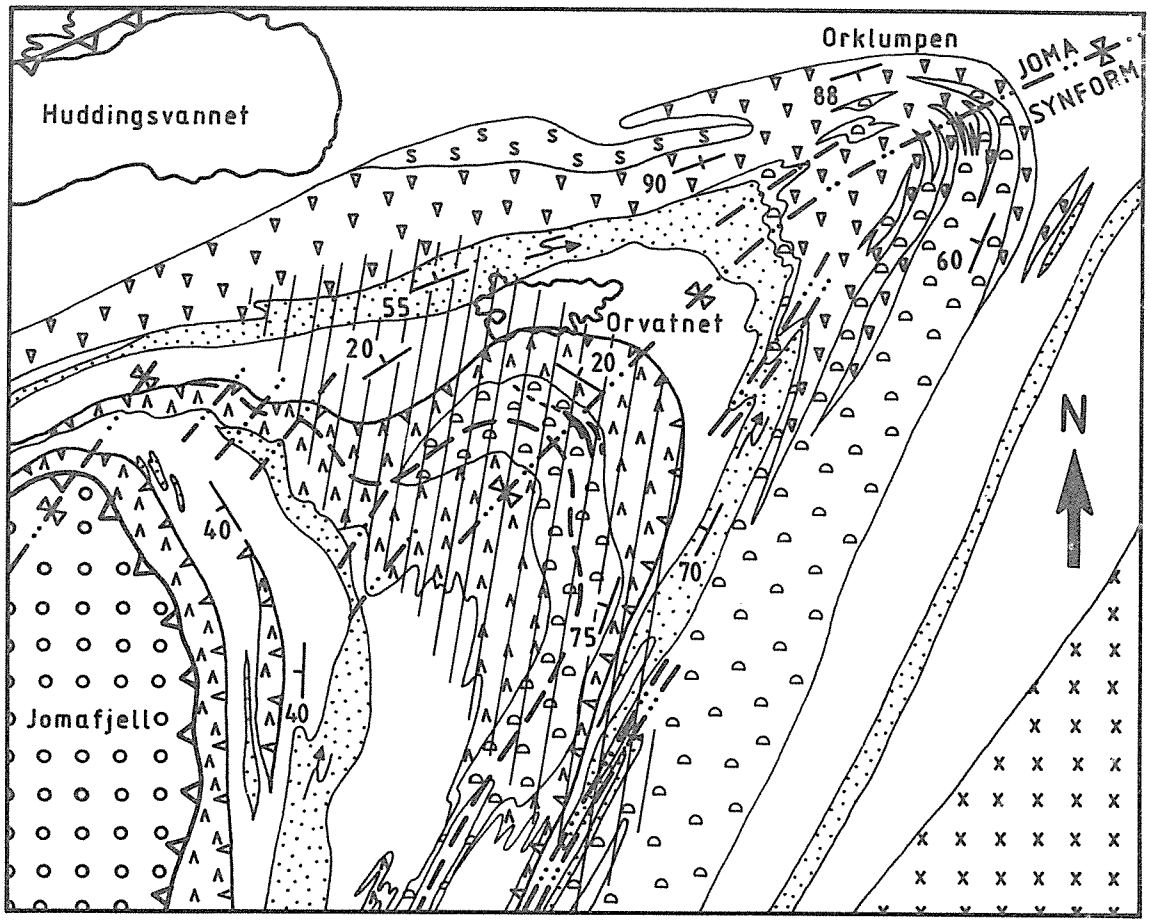

KEY

- Metasediments — Limingen Group — GJERSVIK NAPPE
- Graphitic phyllite
- Quartzitic phyllite
- Volcaniclastic greenstone
- Pillowed greenstone
- Massive greenstone
- Brakkfjell schist

  — Röyrvik Group — LEIPIKVATNET NAPPE
- Serpentinite
- Outcrop of Joma sulphide deposit
- Major thrust contacts to Leipikvatnet nappe
- Minor thrusts within Leipikvatnet nappe
- F2 fold trace
- F2 fold vergence, arrow indicates plunge
- F3 fold trace
- Average dip of S2 deavage
- Zone of subhorizontal F3 fold axes

0 1 2 3 4 5 kms

Fig.2.2

Fig.2.2 Photograph of a quartz layer surface from the quartzitic phyllite showing L2 rodding lineation (parallel to the pencil) and F3 minor fold hinges perpendicular to L2 lineation.

Fig. 2.3

Fig.2.3 F2 fold in quartzitic phyllite showing refraction of S2 schistosity from phyllitic to quartzitic layers.

Fig. 2.4

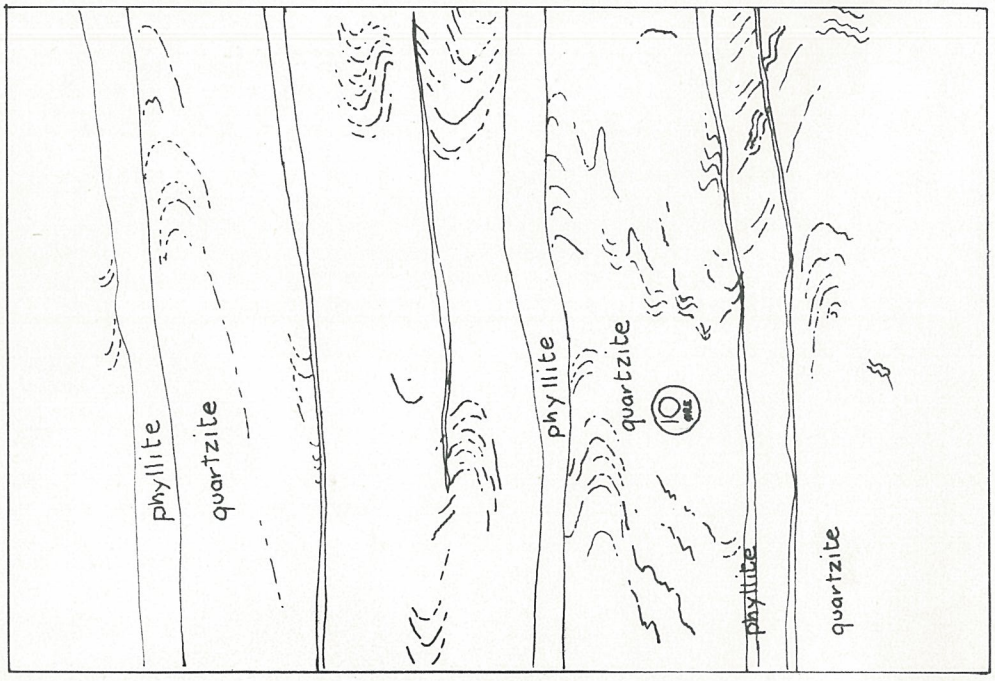

Fig.2.4 Layer transposition in quartzitic phyllites due to D2 deformation. F2 fold hinges form quartzitic layers and F2 fold limbs, the phyllitic layers.

crop on the northwestern side of Orklumpen (map reference X765000 Y31550) refolded by both F2 and F3, and small scale refolding of F1 by F2 was seen in thin sections from a number of locations. F1 folds and S1 cleavage are only locally preserved being overprinted by D2 throughout most of the area.

F3 folds refold both F1 and F2 folds. F2 and F3 hinges are strongly oblique and thus the refolding produces striking fold interference patterns, see Fig.2.5(a) and (b). F3 folds range from open to tight and are generally more open then F2 folds. Box-shaped folds, in which the limbs are zones of strong, and hinges zones of weak, deformation are commonly developed, see Fig.2.6. The L2 rodding lineation on quartz layer surfaces is well preserved in the hinges of these folds. Axial plane orientations of F3 folds are variable and the folds themselves tend to be disharmonic. On both outcrop and thin section scales, conjugate sets of F3 folds with highly variable axial plane orientations occur.

2.2.2 The Greenstones.

The Leipikvattnet nappe contains three greenstone units in the Joma area which have been called from northeast to southwest, the outer, middle and inner greenstone units, see Fig.2.1. The outer and middle greenstone units comprise most of the greenstone outcrop while the inner greenstone is represented by a thin strip adjacent to the thrust contact with the overlying Gjersvik nappe. The middle greenstone has been studied in some detail as it contains the Joma massive sulphide deposit and will be described first.

a) The middle greenstone.

The middle greenstone is composed of two major lithological types, volcaniclastic deposits and pillowed lavas. Pillow lavas form an elongate wedge-shaped outcrop, parallel to the main trend of the greenstone, which is flanked by volcaniclastic deposits.

The volcaniclastic deposits vary from fine-grained, well-laminated to coarse-grained, massive units. The laminated lithology (Fig.2.7), comprises alternating light and dark laminae,

Fig. 2.5 (a)

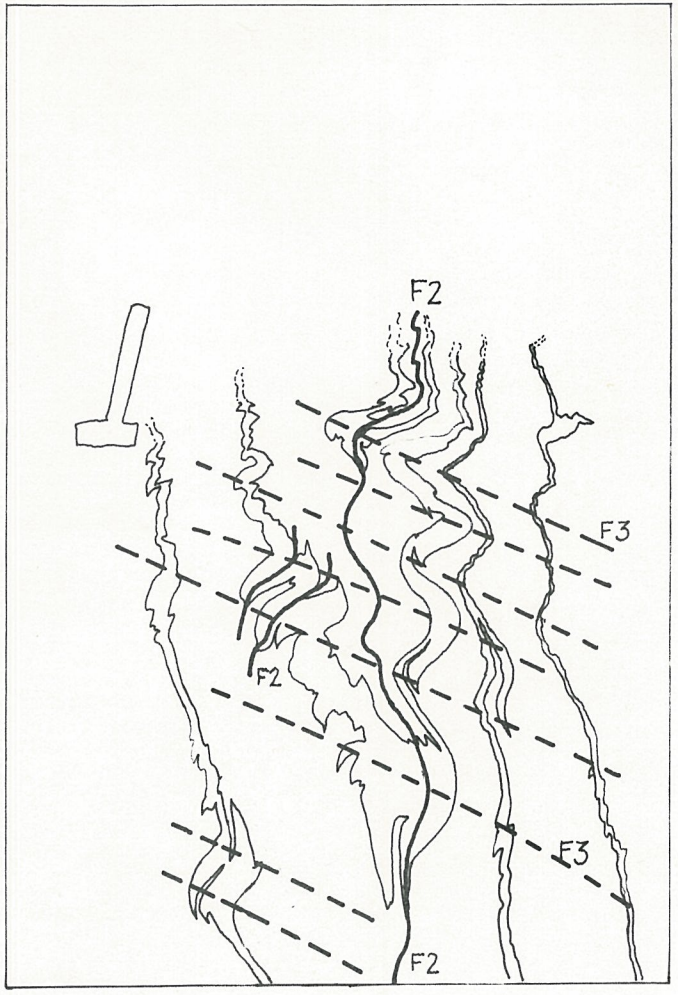

Fig.2.5(a) Interference patterns produced by F2 and F3 folds in quartzitic phyllites from the northwest limb of the Joma synform.

Fig. 2.5(b)

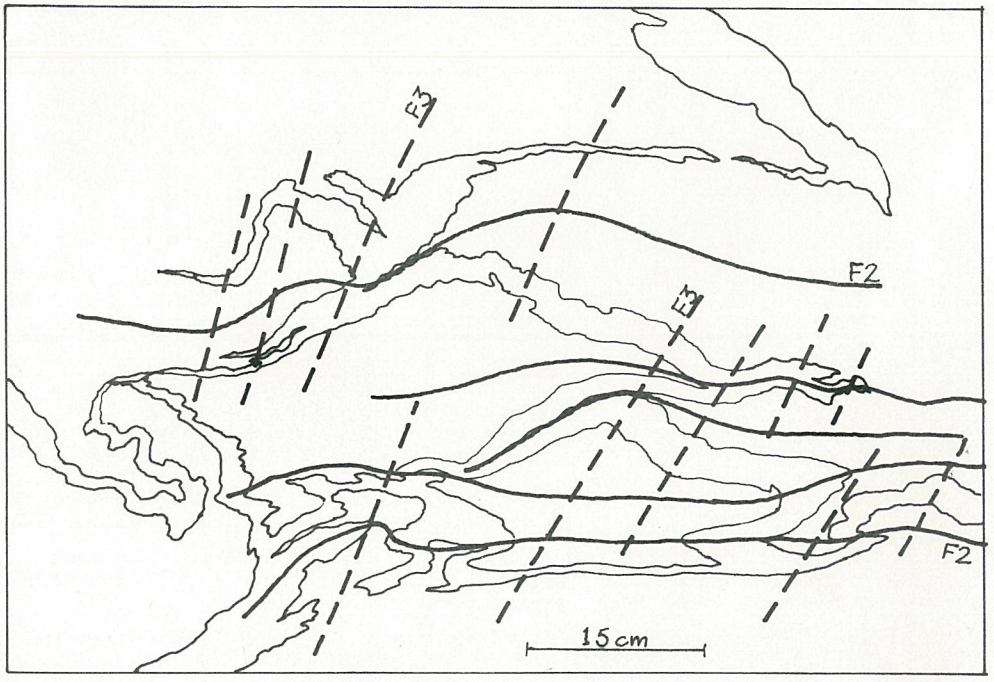

Fig.2.5(b) Interference patterns produced by F2 and F3 folds in quartzitic phyllites from the hinge zone of the Joma synform.

Fig.2.6 Box-shaped F3 folds in quartzitic phyllite. The hinges are zones of weak and the limbs zones of strong D3 deformation.

Fig.2.7 Laminated volcaniclastic deposits crenulated by small scale F3 folds from the middle greenstone.

mineralogically composed of actinolite-plagioclase-muscovite-clinozoisite-sphene and clinozoisite-opaques-plagioclase-sphene-actinolite-chlorite, respectively. The relative increase of clinozoisite, sphene and opaques gives rise to the darker colour. Thin quartz-calcite layers, locally abundant, cut obliquely across the layering and therefore probably represent early veining. F3 crenulation is common and the dark clinozoisite-sphene rich layers show evidence of higher competency than the pale actinolite-muscovite rich layers during D3. F2 folds are only rarely developed in the volcaniclastic deposits. The more massive units within the volcaniclastic deposits are coarser-grained and contain clinozoisite-muscovite pseudomorphs after plagioclase. Mineralogically, they are similar to the paler layers in the laminated deposits, and in thin section faint layering is commonly seen. The presence of layering, their concordance to layering in the laminated deposits and the lack of any igneous features, such as pillow structures or relict ophitic textures, suggests that they are also volcaniclastic in origin.

The pillow lavas of the middle greenstone locally show well preserved pillows with pale centers, dark rims and finely laminated deposits between pillows, see Fig.2.8. Mineralogically, the pillowed lavas are similar to the volcaniclastic deposits but with generally less clinozoisite, sphene, chlorite and muscovite. Pillow centers are fine to medium grained and actinolite, composing the bulk of the rock, has a commonly clouded appearance caused by many small inclusions. Lath-shaped aggregates of fine-grained plagioclase with actinolite, clinozoisite and chlorite probabely represent original phenocrysts. The dark colouration of pillow rims is due to an increase in clinozoisite and sphene towards the pillow margin. The finely laminated material between pillows resembles closely the laminated volcaniclastic deposits, though with less regular layering and probably represents a fine-grained clastic deposit that filled the gaps between pillows.

The pillows themselves are extensively fractured on micro and macro scales, the fractures now being filled with quartz-calcite or clinozoisite-chlorite. Within individual pillows, the fracturing is concentrated into elongate lens-like features, 30x15cm or less, oriented subparallel to the pillow length.

Fig. 2.8

Fig.2.8 Pillow lavas from the middle greenstone showing dark pillow rims and pale centres.

These are contained within pillows and are not found crossing pillow margins. The occurance of these lenses is confined to pillow lavas and they are thought to represent original features related to contraction during cooling. The lenses weather to give a characteristic appearance and serve as a diagnostic feature of pillows where exposure is bad or deformation so high that the pillow margins are indiscernible, see Fig.2.9.

b) The outer greenstone.

The outer greenstone is composed of two main rock types; pillow lavas and massive greenstones. The pillow lavas comprise most of the outcrop on the eastern limb of the Joma synform, but finger out into massive greenstones which are the dominant rock type on the western limb, see Fig.2.1. The pillow lavas resemble those of the middle greenstone in both mineralogy and texture, showing pale centres with fractured lenses, dark margins, and little interstitial material. Generally, the pillows are better preserved due to the lower deformation, (Fig.2.10) and they are also better exposed. The degree of deformation makes the determination of way-up difficult. However, the curvature on the upper and lower surfaces and the orientation of probable pedicles on pillows, tentatively suggests that they are the correct way up.

In the zone of pillow lavas adjacent to the upper contact of the outer greenstone with quartzitic phyllites, the pillows contain variolites ranging from 2mm to 4cm long, see Fig.2.11. The variolites, which are not found in the pillow lavas of the middle greenstone, contain higher proportions of clinozoisite than their matrix and are concentrically layered with plagioclase cores surrounded by zones consisting dominantly of clinozoisite and actinolite. Their shape is now subspherical to ellipsoidal.

The massive greenstones are fine to coarse grained and mineralogically composed dominantly of actinolite and plagioclase with minor amounts of clinozoisite, sphene, muscovite, chlorite and hornblende. The coarsest grained examples (up to 3mm grain size) show relict ophitic texture, see Fig.2.12, with actinolite and relict hornblende pseudomorphing pyroxene and large (2mm) interlocking laths of plagioclase. Finer grained examples show a

Fig. 2.9

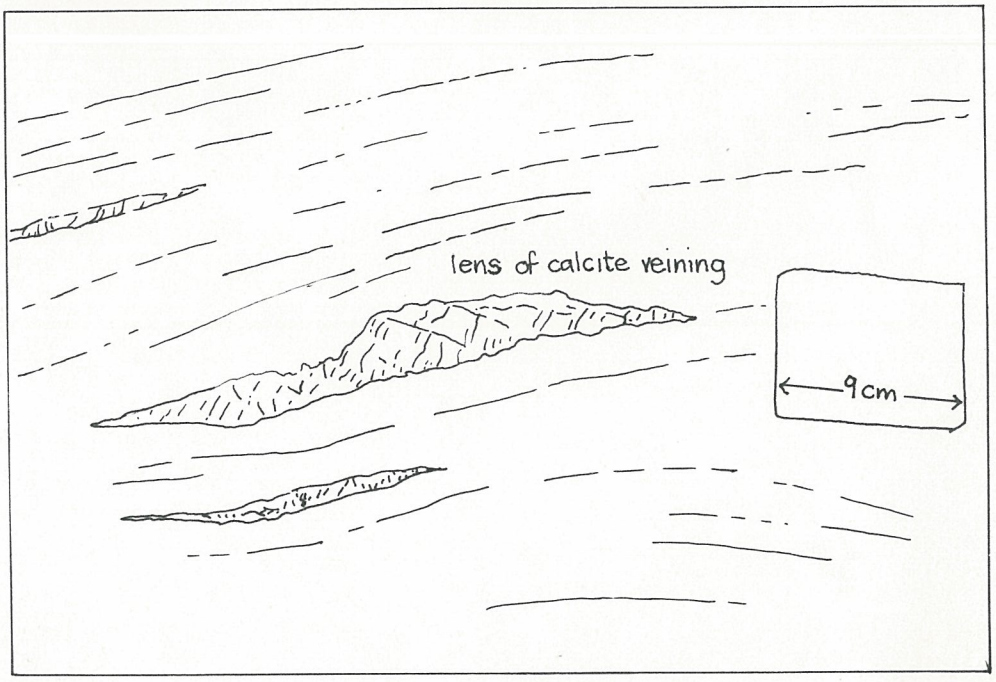

Fig.2.9 Weathered-out calcite veins forming characteristic lens-shaped features in highly deformed pillow lavas of the middle gresnstone.

Fig. 2.10

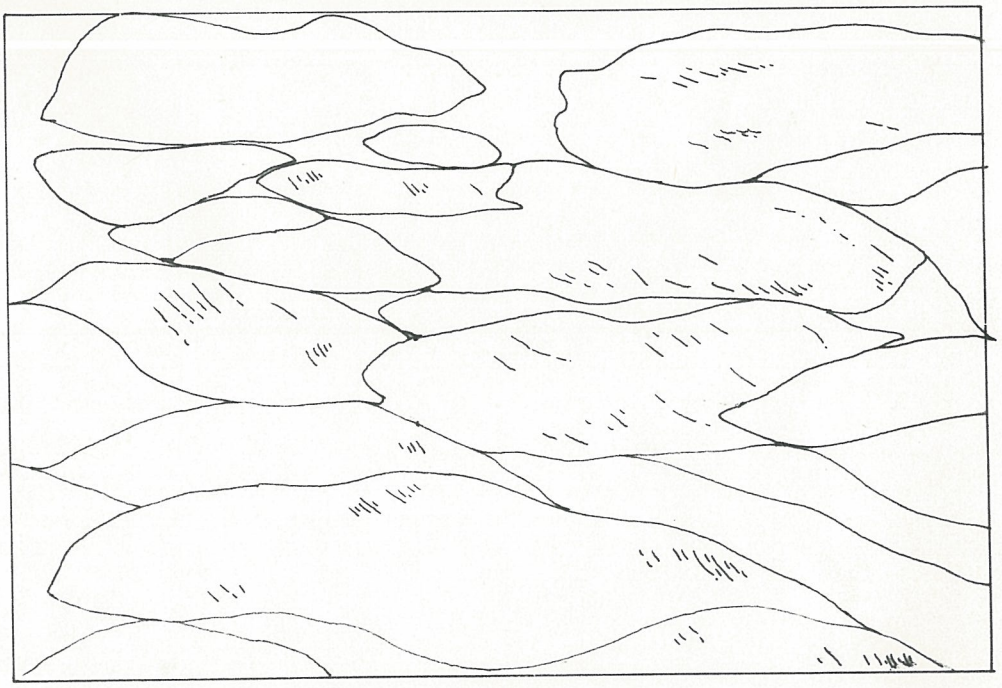

Fig.2.10 Pillow lavas from the outer greenstong showing dark pillow rims, which weather out, and pale pillow centers.

Fig. 2.11

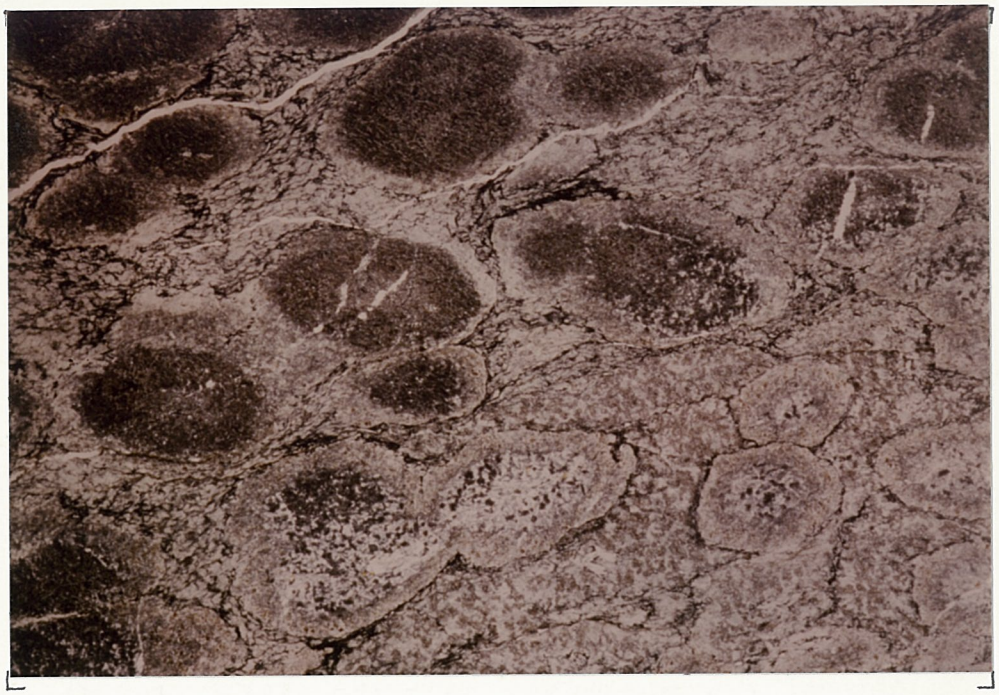

Fig.2.11 Thin section of variolites from the margin of a pillow from the outer greenstone. The photograph is 1.6 cm across.

Fig. 2.12

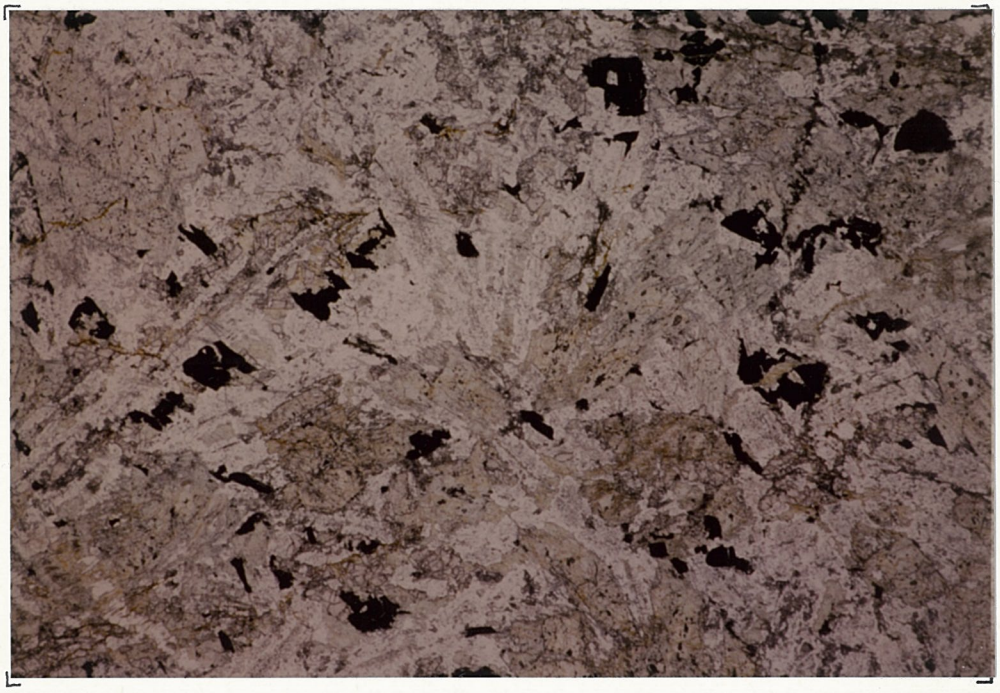

Fig.2.12 Thin section of relict ophitic texture in coarse grained massive greenstone from the outer greenstone. The photograph is 1.6 cm across.

similar mineralogy but textures are less obviously ophitic with a few large actinolite pseudomorphs after pyroxene and recrystallized plagioclase laths. Grain size is independent of foliation development and is therefore an original feature of the massive greenstones, although the coarser grained rocks tend to be preserved as lenses of weak deformation. The massive greenstones show sharp to gradational contacts with the pillow lavas, locally grading into a rock with abundant fracture lenses but without discernible pillow margins which is thougnt to represent a pillow breccia, see Fig.2.13. The presence of relict ophitic textures and the gradational contacts with the pillow lavas indicate that the massive greenstones are igneous in origin, representing massive flows that were probably extruded subaerially and did not form pillows.

The massive greenstones are associated with thin horizons of black graphitic and quartzitic phyllite* which occur in elongate, commonly en echelon, lenses arranged subparallel to the pillowed-massive greenstone contacts. In places, these phyllites show regular quartzitic layering up to 4 cm wide, subparallel to the contacts, and closely resemble the phyllites found between the main greenstone units. They contain variable amounts of pyrite, pyrrhotite and chalcopyrite as disseminated grains or a network of veins. Associated with the phyllites in the greenstones are breccias containing greenstone and calcite fragments in a phyllitic matrix and impure marbles. The breccias, which are also locally found in the greenstones away from the phyllitic horizons, are composed of angular greenstone fragments up to 10cm across, see Fig.2.14. A very fine-grained dark greenstone found at the contact of a phyllitic horizon is composed of actinolite, biotite and chlorite with euhedral garnet, opaques and sphene. The mineralogy indicates an increase of Fe and Al over the normal massive greenstone and the rock probably represents a fine-grained tuffaceous sediment. ~ Calcard ?

The association of phyllitic horizons with breccias, marbles and fine-grained tuffaceous sediments indicates that they are sedimentary in origin. The absence of greenstone fragments in the phyllitic horizons, suggests that they are formed largely by biological activity and chemical precipitation with little

* subaerial ?

Fig. 2.13

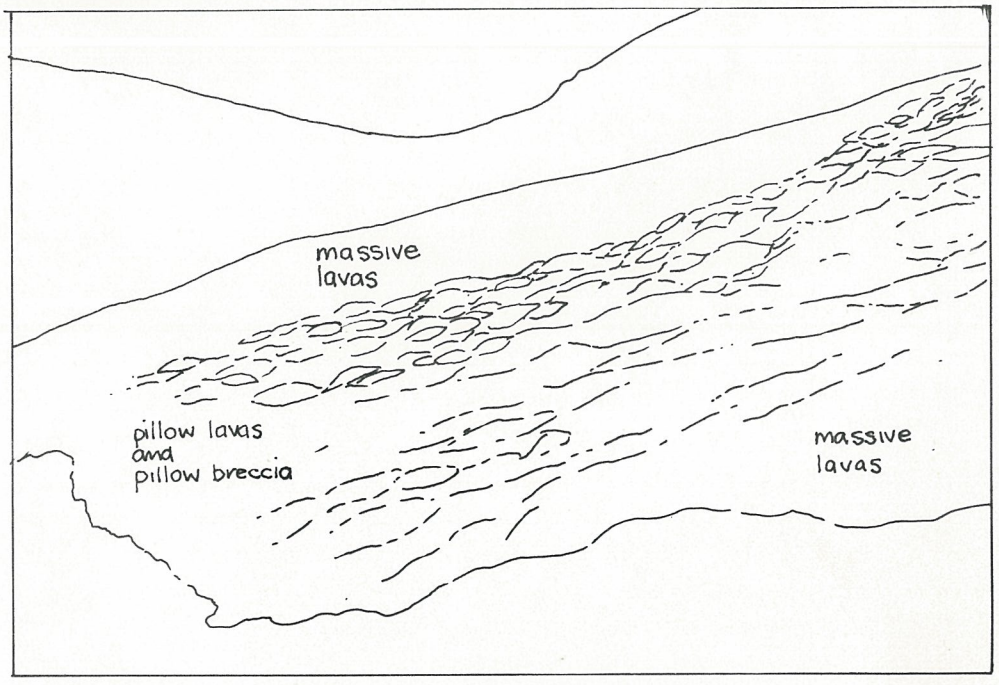

Fig.2.13 Massive greenstone grading into pillow lavas and pillow breccias from the outer greenstone.

Fig. 2.14

Fig.2.14 Breccia from the margin of a phyllitic layer in the massive greenstones of the outer greenstone, showing angular greenstone fragments in a phyllitic matrix.

Fig 2.15

Fig.2.15 F3 folds in laminated volcaniclasic deposits of the middle greenstone showing characteristic straight limbs and sharp hinges.

terrigenous input. Their association with massive, subaerial flows suggests that they formed in quiet pools of water on the lava surface where anaerobic conditions resulted in sulphide precipitation. No such phyllitic horizons have been found within the pillow lavas. The formation of pillowa indicates the presence of a larger body of water which was probably too turbulent to allow the deposition of phyllite.

c) The inner greenstone.

The inner greenstone has limited outcrop, being cut by the main thrust beneath the Gjersvik nappe. Lithologically, it is composed of medium to fine grained, massive, homogeneous greenstones, which show occasional layering. Mineralogically, the greenstones consist of actinolite, plagioclase, muscovite, chlorite, opaques, sphene, clinozoisite and calcite. Coarser grained specimens show large actinolite grains up to 3mm and plagioclase up to 1mm. The subhedral to euhedral plagioclase grains which are partially recrystallised, contain abundant inclusions of chlorite, clinozoisite and actinolite. Finer grained specimens show good layering resembling that of the volcaniclastic deposits of the middle greenstone. Calcite occurs with quartz in veins and as large irregular, equidimensional grains (2mm) which have grown across the foliation.

The coarse grained massive greenstones of the inner greenstone unit, show no relict ophitic textures and their mineralogy, which includes chlorite and muscovite with abundant clinozoisite and sphene, resembles the middle greenstone volcaniclastic deposits. These factors, together with the presence of laminated greenstones and the absence of any features relating to pillow lavas, indicates that they are most likely to be volcaniclastic deposits similar to the massive units of the middle greenstone. The large, partially recrystallized actinolite and plagioclase grains therefore most probably represent large crystals in a tuffaceous matrix.

2.2.3 Structural styles in the greenstones.

Throughout all three greenstone units the dominant penetrative schistosity is S2 which is formed mainly by the parallel

alignment of actinolite and muscovite. It is subparallel to the layering in the volcaniclastic deposits and axial planar to minor F2 folds in the layering and in thin quartz veins. F2 folding is rare and the main effect of increasing D2 deformatin is to cause the layering to become markedly thinned and less distinct. In the more massive units clinozoisite-chlorite pseudomorphs after plagioclase become elongate, large actinolite grains recrystallise and there is a marked decrease in grain size. D2 deformation in the pillow lavas is expressed as a penetrative cleavage formed largely by the parallel alignment of actinolite. As D2 deformation increases the pillows become elongate and the pillow margins indiscernible. The lenses of intense fracturing, however, survive strong deformation, becoming extremely elongate and in the most strongly deformed rocks are the only surviving original features of the pillow lavas. The massive lavas of the outer greenstone respond to increasing D2 deformation by recrystallisation of the large actinolite and plagioclase grains and the development of a penetrative cleavage by the parallel alignment of actinolite.

F3 folds in S2 cleavage, showing wave-lengths of 2m or less, are common throughout all the greenstone units. They tend towards a chevron style with sharp hinges and straight limbs (Fig.2.15) and intense crenulation cleavage is developed in the short limbs. Small scale folding and crenulation cleavage are most strongly developed in the layered volcaniclastic deposits where the clinozoisite-sphene rich layers act as relatively competent units and show signs of brittle failure during D3. In the pillow lavas where D2 is weak and pillows well preserved, D3 is expressed as a spaced cleavage in the pillows and as small scale folding and crenulation cleavage in the laminated interstitial deposits.

2.3 STRUCTURAL ANALYSIS

2.3.1 Late Phase Structures - D4.

Late phase, D4 deformation is expressed as minor kink-like folds often occuring in conjugate sets. Though they occur spor-

adically throughout the area, they are largely restricted to the area adjacent to the main thrust with the Gjersvik nappe, becoming more abundant towards the thrust boundary. Their axial plane orientations, shown in Fig.2.16(a), are highly variable. However, using observations on individual conjugate F4 fold sets (Fig.2.16(b)), the distribution consists of a gently southeast dipping set (open triangles in Fig.2.16(a)), and a steeply east to moderately west dipping set (open squares in Fig.2.16(a)). The intersection of the conjugate pairs parallels the F4 hinges which plunge subhorizontally southwest or northeast, (Fig.2.16(a)). The relationship between conjugate folds indicates a maximum stress dipping moderately to steeply northwest.

D4 and D3 structures tend towards an antithetic relationship. That is, as the main thrust boundary with the overlying Gjersvik nappe is approached, F3 folds become less, and F4 folds more, abundant. In the Gjersvik nappe itself, F3 folds are rarely found and F4 folds are dominant. Of the F4 conjugate sets observed in the Leipikvatnet nappe, the shallow southeast dipping set becomes dominant within the Gjersvik nappe. In the transition zone between dominant F3 and F4 folding, F4 folds were always observed to overprint D3 structures and therefore postdate them, but their spatial relationship suggests that these deformation phases are not widely separated in time and may well overlap.

3.2. D3 - The Joma Synform and Related Structures.

The major Joma Synform belongs to the third phase of deformation. This structure trends northeast-southwest and has a steeply west to northwest dipping eastern limb and shallow southeast to moderately northwest dipping, partially overturned, northwest limb. The synform plunges gently southwest to northeast. Minor D3 structures comprise folds and crenulation cleavage which are plotted in Fig.2.17(a) and (b) for the southeastern and northwestern limbs of the Joma synform. The plots show that some fanning of the S3 surfaces occurs across the synform, being steeper in the southeastern limb. D3 deformation is most intense on the northwestern limb of the Joma synform. This is

FIG. 2.16

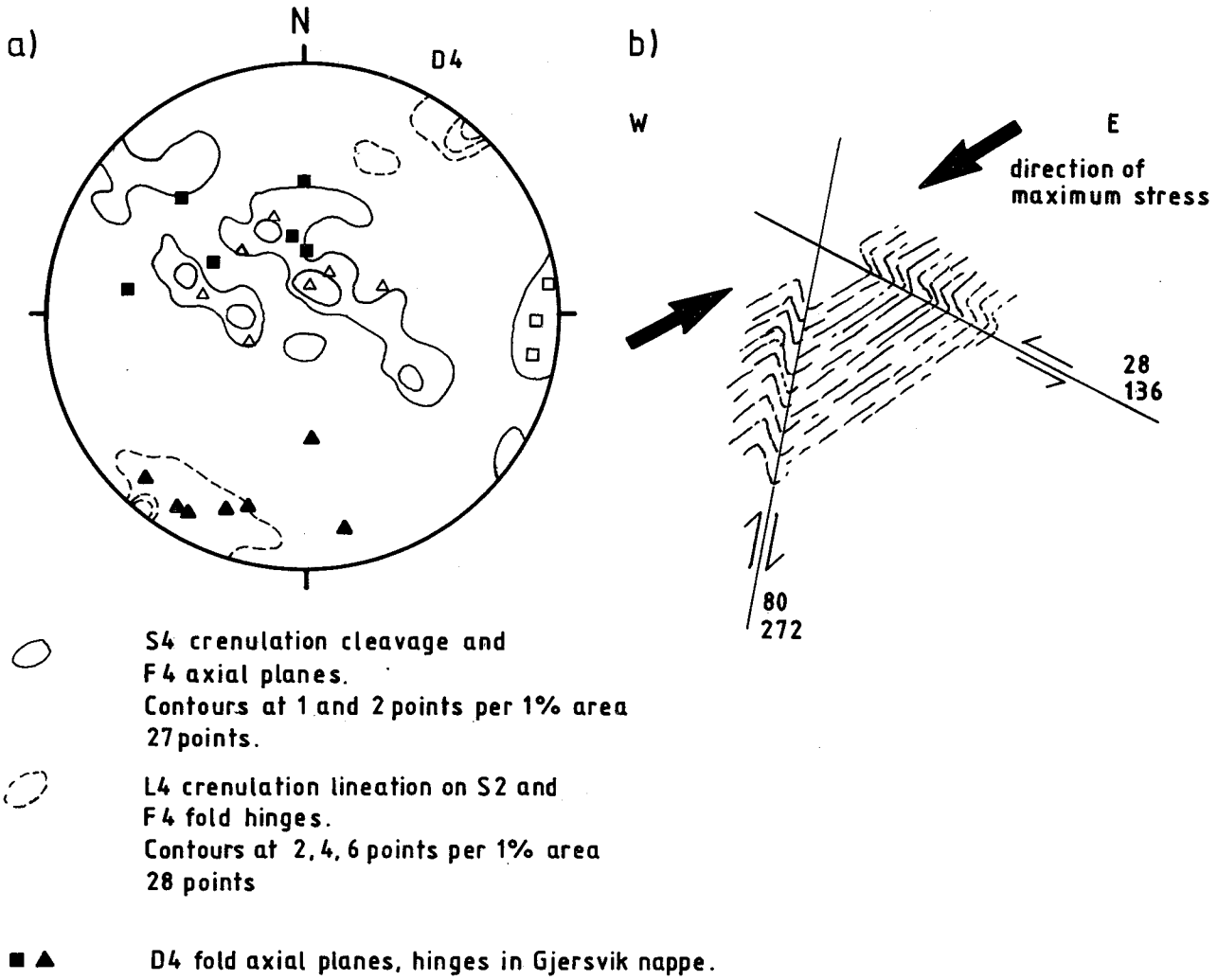

Fig.2.16 (a) Stereonet showing orientations of D4 minor structures in the Leipikvattnet nappe (contoured) and the Gjersvik nappe (solid symbols). (b) Sketch showing conjugate sets of F4 folds.

FIG. 2.17

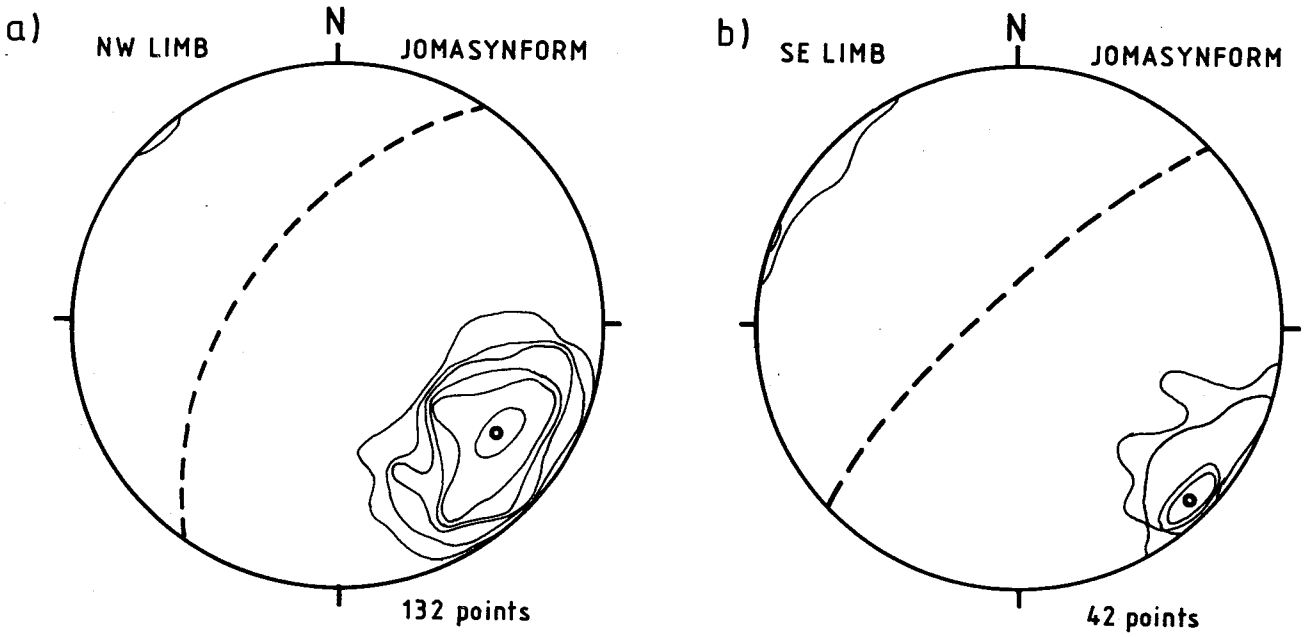

Poles to S3 crenulation cleavage
and F3 fold axial planes.
Contours at 2, 4, 6, 8, 10 and 20 points per 1% area

Fig.2.17 Stereonets of D3 planar structures on (a) the northwest limb and (b) the southeast limb of the Joma synform.

illustrated for the middle greenstone in Fig.2.18 which shows zones of qualitatively determined, weak to stong D3 deformation. Zones of intense D3 deformation, determined by the strength of the crenulation cleavage and frequency of F3 folding, form lenses concentrated on the northwest limb and around the inner arc of the middle greenstone unit. F3 folding is similarly intense on the inner arc and western limbs of the outer greenstone and adjacent quartzitic phyllites. The discontinuous style of F3 folding shown by the distribution of D3 deformation in Fig.2.18 is also shown by the Joma synform. In the northeast, the synform is tight and overturned and becomes more open to the southwest as the western limb flattens out. In the extreme southwest, this major synform dies out and is transferred some kilometers to the west, via a series of intermediate scale folds, some where it continues southwestwards through the Gjersvik nappe.

F3 minor fold hinges and intersection lineations associated with S3 crenulation cleavage plunge variably throughout the area, as shown on the map of L3 in Fig.2.19(a). L3 lineations plunge generally southwest except for a zone around the middle greenstone in which they plunge gently northeast. In Fig.2.19(a), the area has been divided into three zones of similar L3 plunge, A, B and C. Zone B of gently northeast plunging L3 lineations trends obliquely across the middle greenstone and includes some of the quartzitic phyllites on the northwestern limb of the Joma synform. The trend of zone B in the extreme southeast of Fig.2.19(a) is uncertain due to lack of data but the overall trend is approximately north-northwest. In Fig.2.19(b), L3 lineation plunges are projected onto a perpendicular to the overall trend of zone B (027°) and plotted against distance along the section X-Y. The graph shows areas of relatively constant southwest plunges in the southwest and northeast (zones A and C), with transition zones showing highly variable plunges, to a zone with relatively constant northeast plunges (zone B). Fig.2.20 shows stereoplots of L3 lineations for zones A, B and C. The maxima indicated by the contoured plots shows a change in L3 plunge from 30° southwest to 8° northeast to 20° southwest through zones A, B and C.

The possible causes of this variation in L3 plunge include

FIG. 2.18

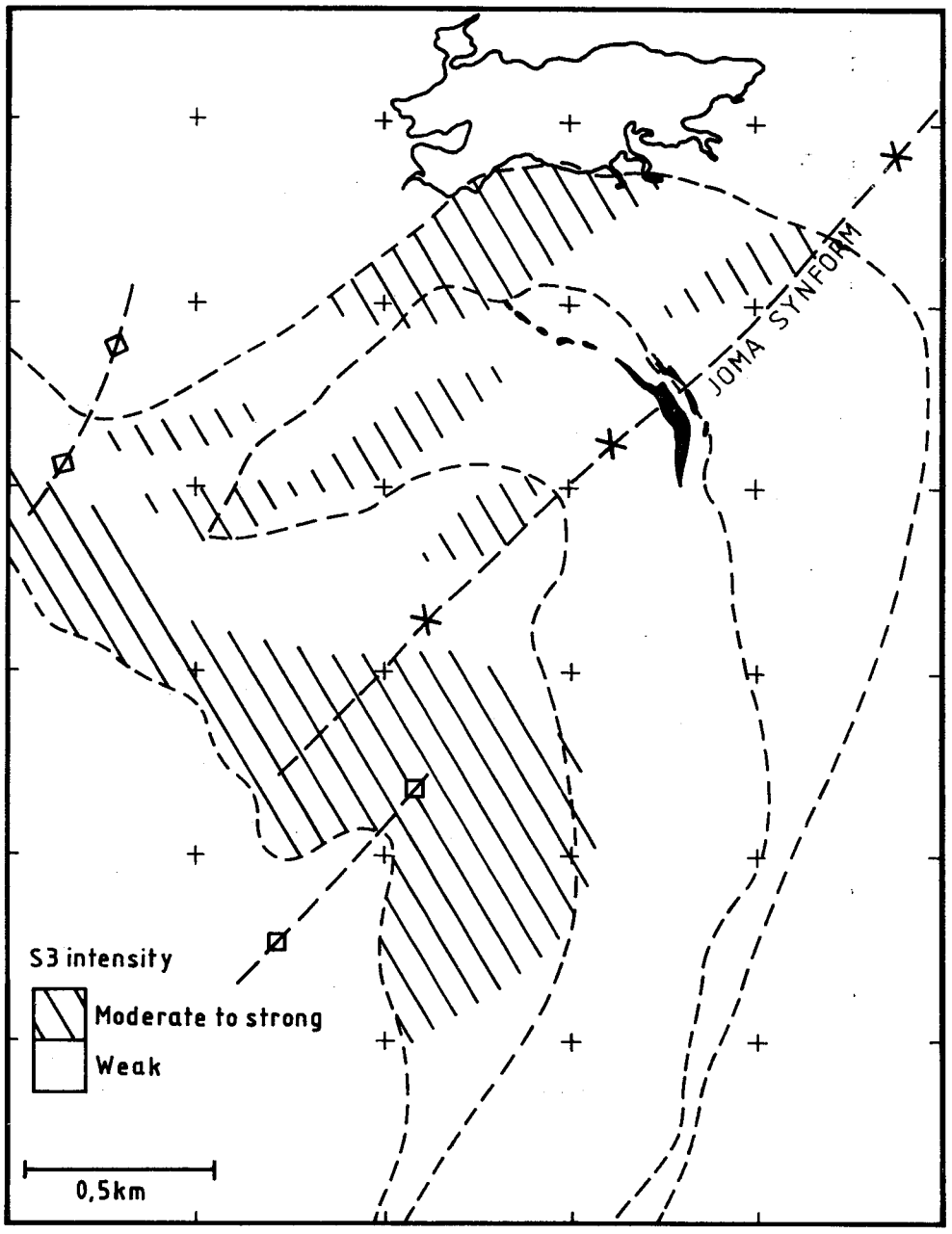

Fig.2.18 Map of D3 deformation intensity estimated from development of S3 crenulation cleavage and F3 minor folds for the middle greenstone. D3 deformation is concentrated in the northwest limb of the Joma synform.

FIG. 2.19

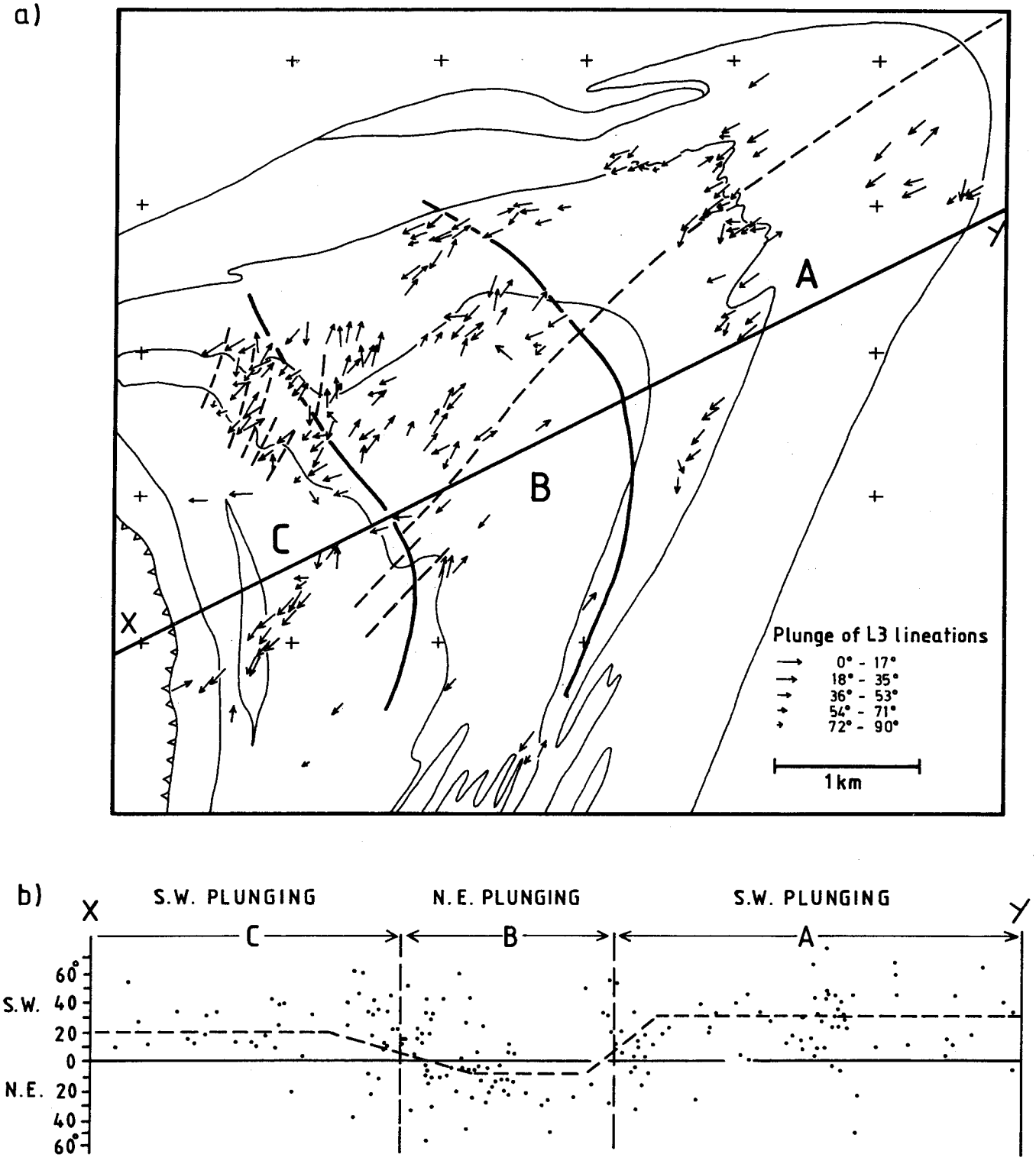

Fig.2.19 (a) Map of L3 plunges in the Joma area. Zones A, B and C show L3 plunging southwest, northeast and southwest, respectively. (b) Graph of L3 plunges projected onto section X-Y, showing zones A, B and C of varying L3 plunge.

FIG. 2.20

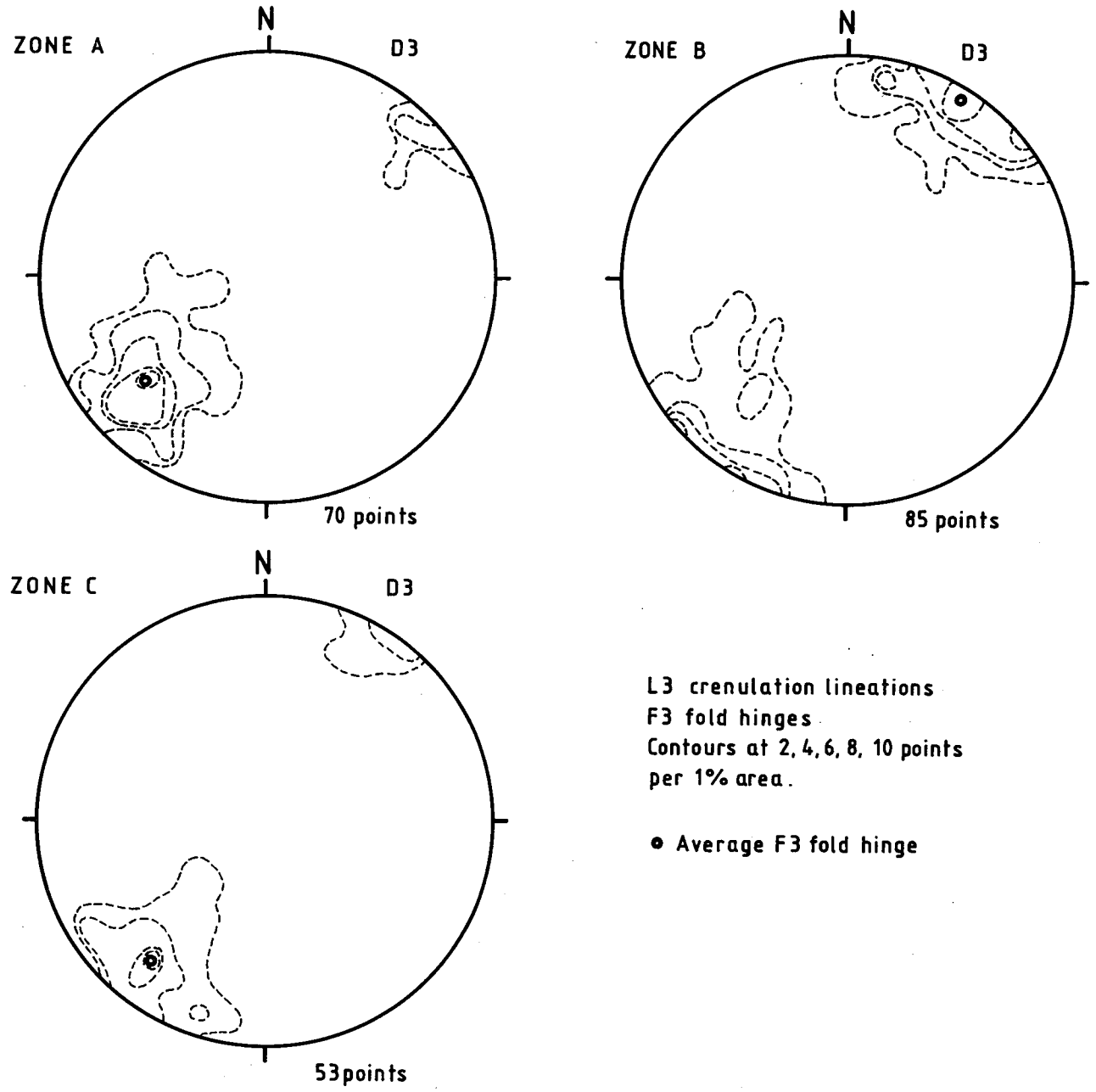

Fig.2.20 Stereonets of L3 plunges for zones A, B and C (Fig.2.19). Average L3 plunges are, zone A - 30° southwest, zone B - 8° northeast and zone C - 20° southwest.

post D3 folding, variation in intensity of D3 deformation and variation in the pre-D3 attitude of the S2 surface. The only structures found to postdate D3 are D4 minor folds. These are, however, very poorly developed throughout the greater part of the area and have no large scale structures associated with them. There is also no indication of a corresponding variation in the S3 orientations and thus D4 folding is an unlikely cause. D3 deformation is most intense on the western limb of the Joma synform, which trends at a high angle to zone B and therefore cannot be the cause of the variation in L3 plunges. Thus, the third cause, a variation in the S2 surface orientation prior to D3, is the most likely.

2.3.3 D2 - Main Phase Deformation.

a) The analysis of D2 minor structures.

The main penetrative cleavage and mineral lineations throughout the area belong to the second phase of deformation. Minor structures associated with this phase are cleavage, mineral lineations, rodding lineations and, within the quartzitic phyllites, minor folds.

The variation in L3 plunges has been shown to indicate a variation in the pre-D3 orientation of the S2 surface. Stereoplots of S2 (schistosity and minor fold axial planes) for zones A, B and C (Fig.2.21(a)), show partial girdles, the poles to which correspond to the maxima for L3 plunges. The girdles are partial because minor F3 folding of S2 causes flat lying dips to be uncommon. Zone B shows the widest scatter of data corresponding to the largest scatter in L3 plunges. Fig.2.21(b) shows the plots of L2 (mineral and rodding lineations) for each of the zones A, B and C. There is no significant difference in the L2 lineation patterns of these zones. L2 mineral and rodding lineations form an arcuate trend on the stereoplots of Fig.2.21(b), due to folding by D3 about the Joma synform axis. The simplest models of a folded lineation are a) by concentric folding, where the lineation maintains a constant angle to the fold axis, and b) by shear folding, where the lineations lie within the plane containing the initial lineation orientation and the shear direction. To construct either model, the initial

FIG. 2.21(a)

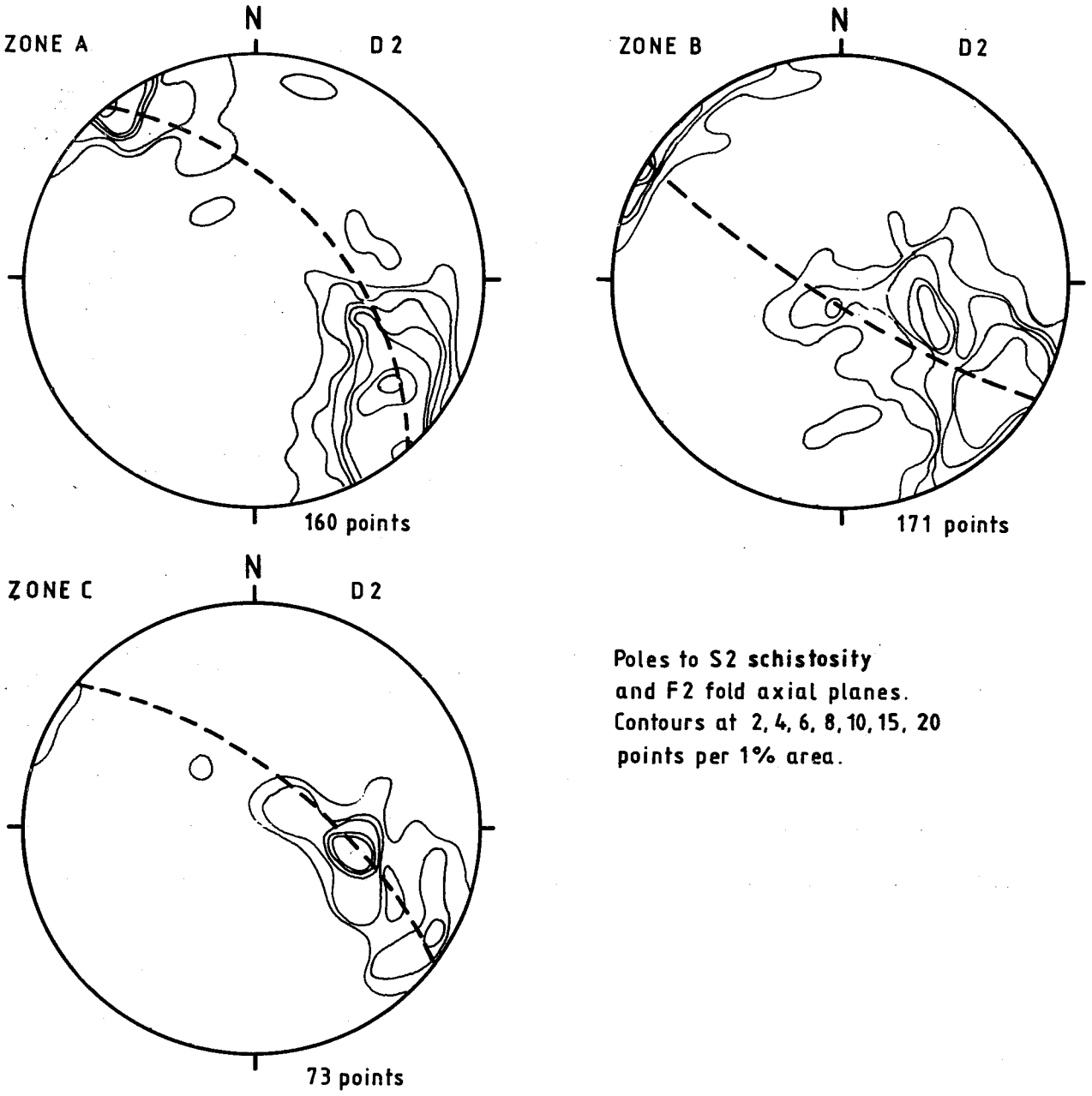

Fig.2.21(a) Stereonets showing D2 planar structures for zones A, B and C. The distributions approximate partial great circles whose poles are the maxima of L3 plunges.

FIG. 2.21(b)

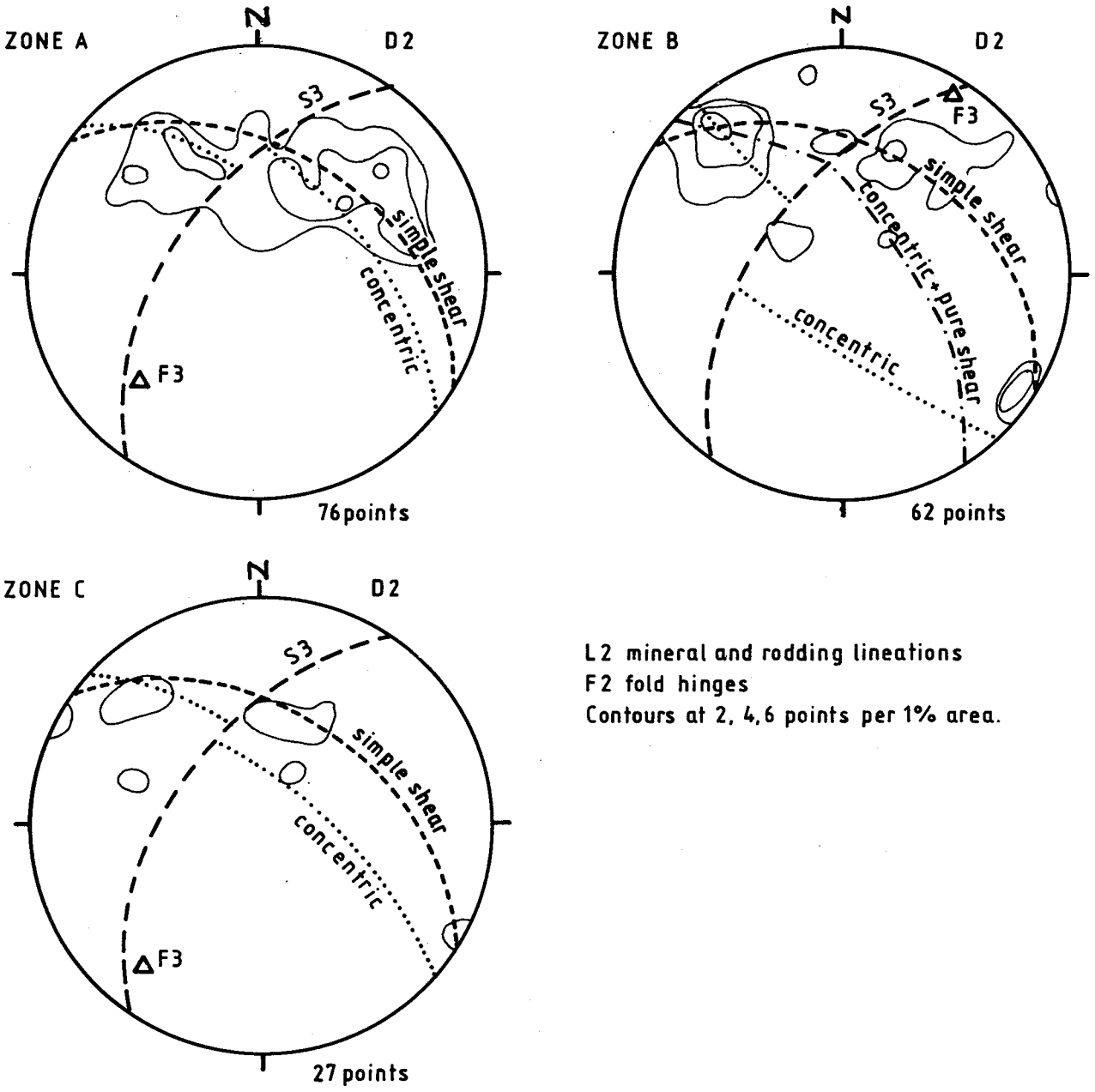

Fig.2.21(b) Stereonets of L2 distributions for zones A, B and C showing the expected distri-butions for a shear fold, a concentric fold and concentric fold modified by pure shear. The shear fold model provides the best fit to the L2 distribution.

orientation of L2 prior to D3 must be known.

L2 lineations are most likely to be preserved in their original orientation where the layering has been least rotated into the F3 axial plane direction. S2 surfaces at a high angle to the S3 orientation are not common due to minor F3 folding but do occur in the hinges of box-shaped folds within the quartzitic phyllites of zone B. In these folds the deformation has been concentrated in the limbs of the folds leaving the flat hinges as areas of relatively weak deformation. The L2 rodding lineation here plunges gently northwest and this provides the best available estimate for the pre-D3, L2 orientation.

Using this orientation as an initial direction, simple folding models were constructed for each of the zones A, B and C and these are shown in Fig.2.21(b). In the concentric folding model, L2 forms small circle distributions about the F3 fold axes and in the shear fold model, the best fit great circle to the L2 distribution containing the intial L2 direction was estimated. The concentric and shear fold models produce similar patterns for zones A and C, but markedly differing patterns for zone B, where the shear fold model gives the best fit. The concentric folding model can be further modified by superimposed pure shear. If the D3 pure shear maximum strain direction plunged moderately north, the L2 lineations would rotate into this direction with deformation. This would modify the concentric pattern of zone B towards better agreement with the L2 distribution. However, intense D3 deformation would also rotate F3 fold hinges towards the pure shear maximum direction and, since these have remained at high angles to the required strain direction, it is unlikely that L2 lineations have undergone large amounts of rotation due to pure shear. Since the variation in F3 fold plunges has no marked effect on the L2 distribution, a shearing model with a constant shear direction for all parts of the Joma synform gives a better fit to the data.

F2 minor folds are common in the quartzitic phyllites where they are usually refolded by F3. However, in areas of less intense F3 folding, enough of the F2 folds can be seen to work out the F2 fold vergence, and this has been recorded in a number

of localities for both horizons of quartzitic phyllite. Although there is some variation in vergence, the folds show an overall consistent pattern, such that F2 and F3 minor folds show opposite vergences, see Fig.2.1. On 'undoing' or flattening out the Joma synform, the F2 fold vergence indicates a synformal structure to the south.

b) The distribution of D2 deformation.

As discussed in section 2.2, the intensity of D2, recorded by S2 strength and development of F2 folding, is variable throughout the area. Variation in D2 deformation intensity within the quartzitic phyllite is difficult to quantify due to overprinting by F3. However, in the greenstones, inhomogeneous D2 deformation has led to varying S2 schistosity strengths and this has been mapped in a qualitative way for the middle greenstone, using the categories, strong, moderate and weak S2 development, see Fig.2.22. The most noticable features of the pattern are the zones of strongly developed S2 along the lower contact and weakly developed S2 in the centre of the middle greenstone. The zone of strong D2 deformation suggests the presence of a thrust at the middle greenstone lower contact. Supportive evidence of this was found at the southeastern contact between greenstone and quartzitic phyllite (map reference X761500, Y31500), see Fig.2.23. The zone of strong S2 schistosity here is narrow, confined to 5 or 10m adjacent to the contact. S2 cleavage is slightly oblique but swings to become parallel some 30 cm from the contact where isoclinal folds are developed in laminated volcaniclastic greenstone. The truncation of quartz layering in the phyllites with the swing in S2 cleavage, indicates that movement has occured along the contact and supports the existence of a thrust.

The area of low D2 deformation on Fig.2.22, coincides approximately with the outcrop of the pillow lavas except in the west where a zone of strong S2 cleavage passes through the wedge tip. This pattern suggests that the wedge shaped outcrop of the pillow lavas may represent the core of an F2 fold. There are no F2 folds in the pillow lavas to indicate the presence of a major fold, but F2 folds occur in part of the outcrop of massive sulphides, known as the 'elvegangen', in the river on the

FIG. 2.22

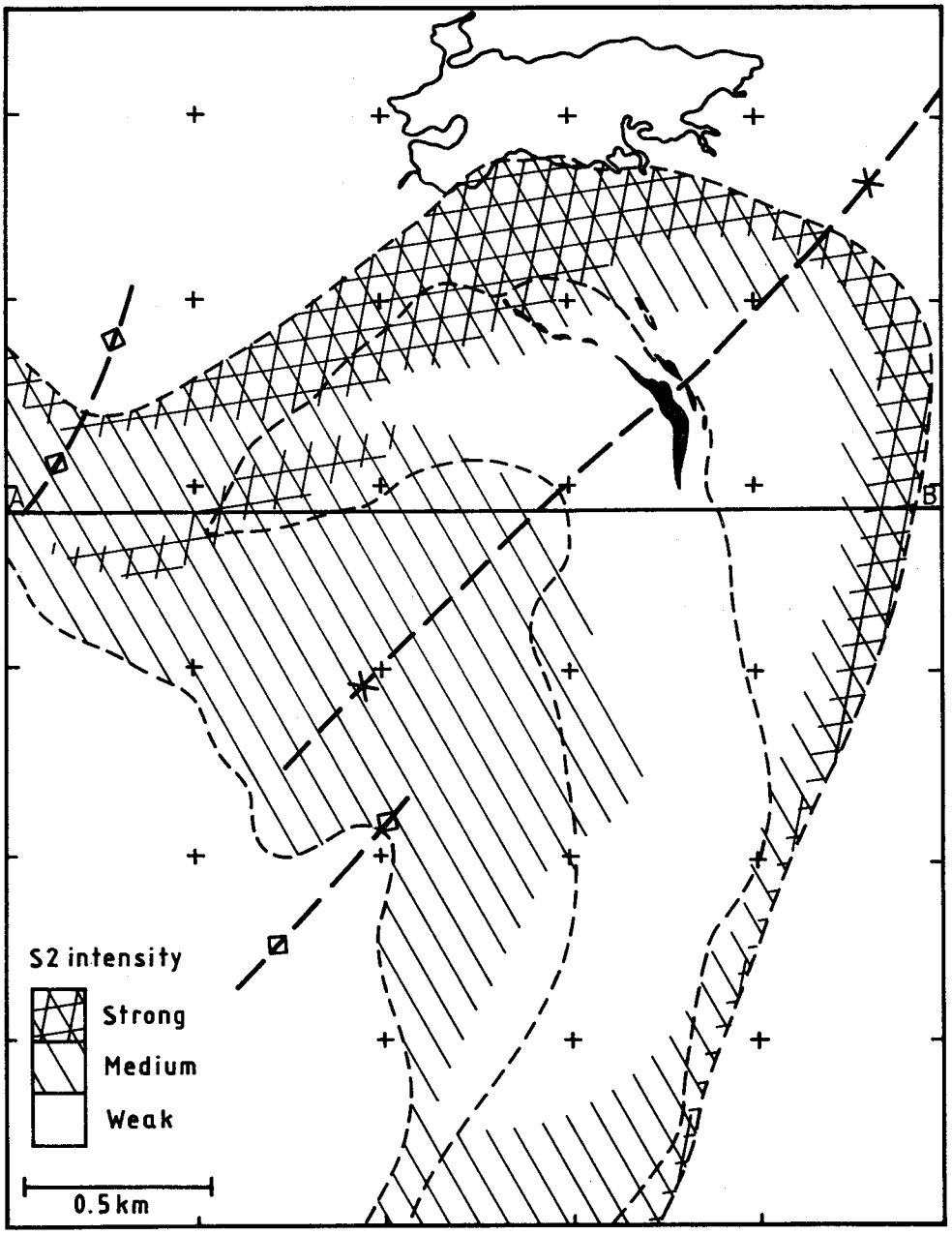

Fig.2.22 Map of D2 deformation intensity as estimated from the strength of the S2 cleavage in the middle greenstone. D2 is most intense adjacent to the lower contact and least intense in the vicinity of the pillow lava outcrop.

Fig. 2.23

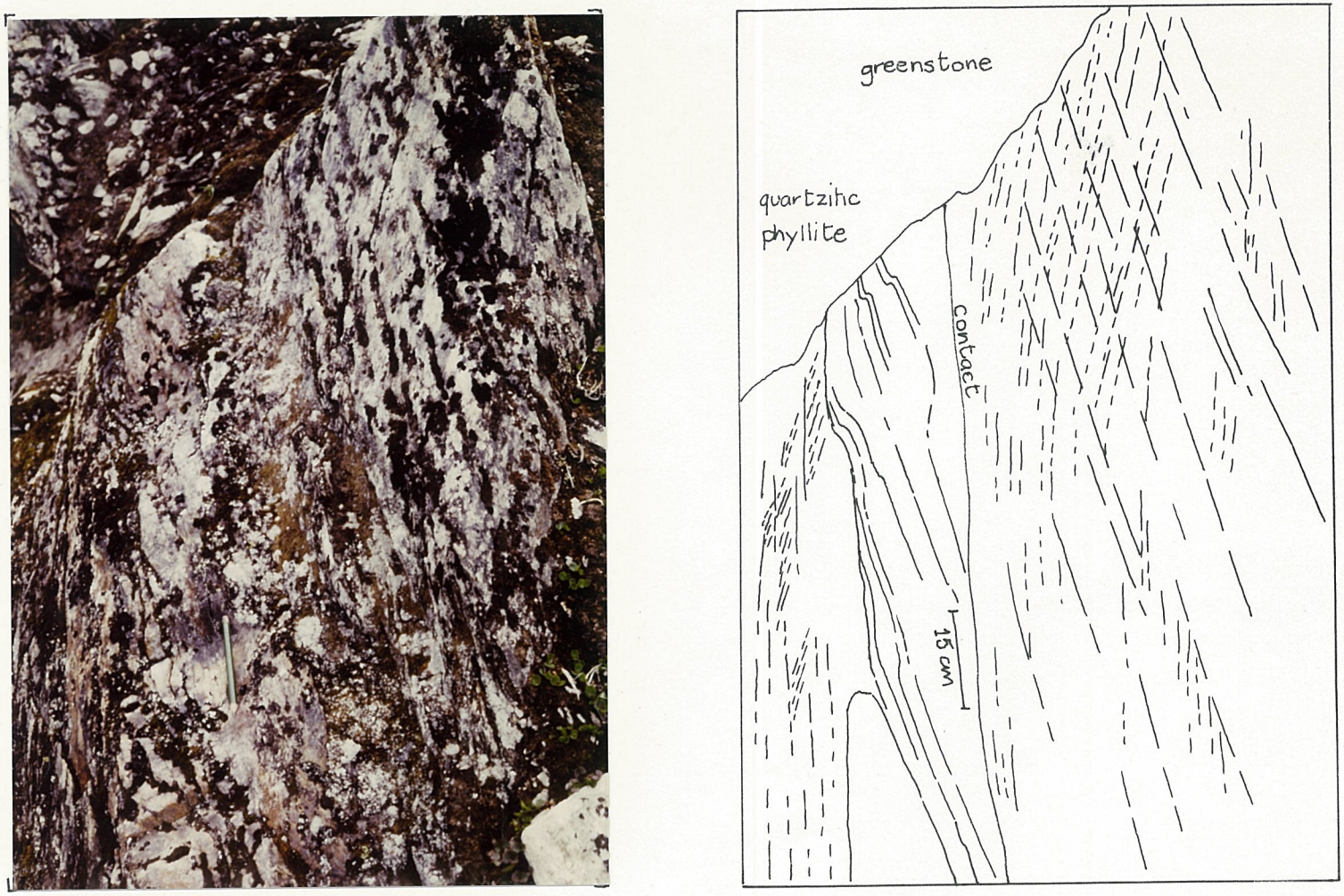

Fig.2.23 Photograph of the lower greenstone-quartzitic phyllite contact on the east limb of the Joma synform. S2 schistosity in the greenstone swings in to become parallel to the contact and layering in the quarztitic phyllites is obliquely cut by the contact.

northern margin of the pillow sequence (map reference X763560, Y31550), see Fig.2.24. Intermediate scale F2 folds refolded by small scale F3 folds were mapped in the contact between sulphides and greenstone and from schistosity-bedding relationships in the volcaniclastic deposits. The fold traces and the outcrop pattern of the sulphides, imply a vergence that indicates an antiformal F2 fold to the south. This is the opposite vergence to that indicated by the graphitic phyllites (synformal F2 fold to the south) and indicates the presence of a major F2 antiform situated within the middle greenstone.

Further evidence for an F2 fold in the middle greenstone is shown in long drill holes of an east-west section (section A-B in Fig.2.22) logged by Reinsbakken (Part II). Three major greenstone types have been identified; volcaniclastic deposits, younger, unaltered pillow lavas and older, altered pillow lavas (Reinsbakken, Part II). The three greenstone types show a symmetrical pattern with the older pillow lavas in the centre flanked by younger pillow lavas and volcaniclastic deposits, which indicates the presence of an F2 fold whose axial plane lies in the older greenstones, see Fig.2.25. The lower limb of this fold is cut obliquely by the thrust at the base of the greenstone. Due to folding by the Joma synform, the section shows the thrust cutting upwards through the lower F2 limb towards the hinge zone of the major F3 fold, see Fig.2.25.

The F2 fold in the middle greenstone occurs within zone B of gently northeast plunging L3 lineations which indicates a differentorientation of the pre-D3, S2 surface from that to the northeast and southwest. It has been shown that the L2 orientation from the flat hinges of box-shaped folds in the quartzitic phyllites, plunging gently northwest, estimates the original L2 orientation. Assuming that there has been little rotation of the F3 hinges, the L2 orientation and the F3 fold hinge for each of the zones A, B and C, can be used to estimate the orientation of the pre-D3, S2 surface. This gives pre-D3 S2 surface orientations that vary from gently west dipping in zones A and C, to gently north dipping in zone B. This variation is a D2 feature and may be caused by movement along non-planar D2 thrust planes.

FIG. 2.24

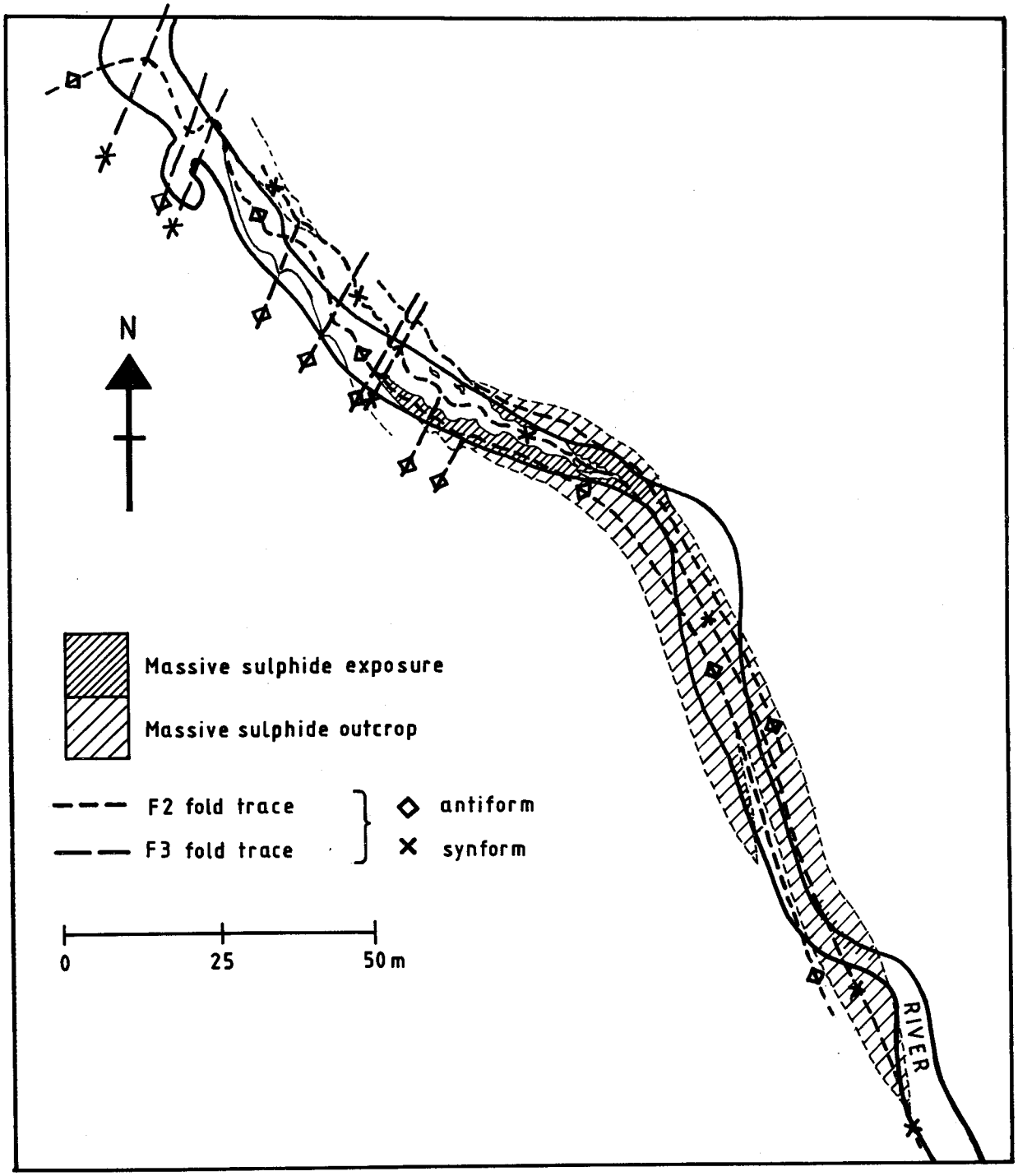

Fig.2.24 Map of massive sulphide exposure in the river at X763560, Y31550, known as the 'elvegangen', showing F2 and F3 fold traces. F2 folds here show the opposite vergence to those in the quartzitic phyllites.

Fig.2.25

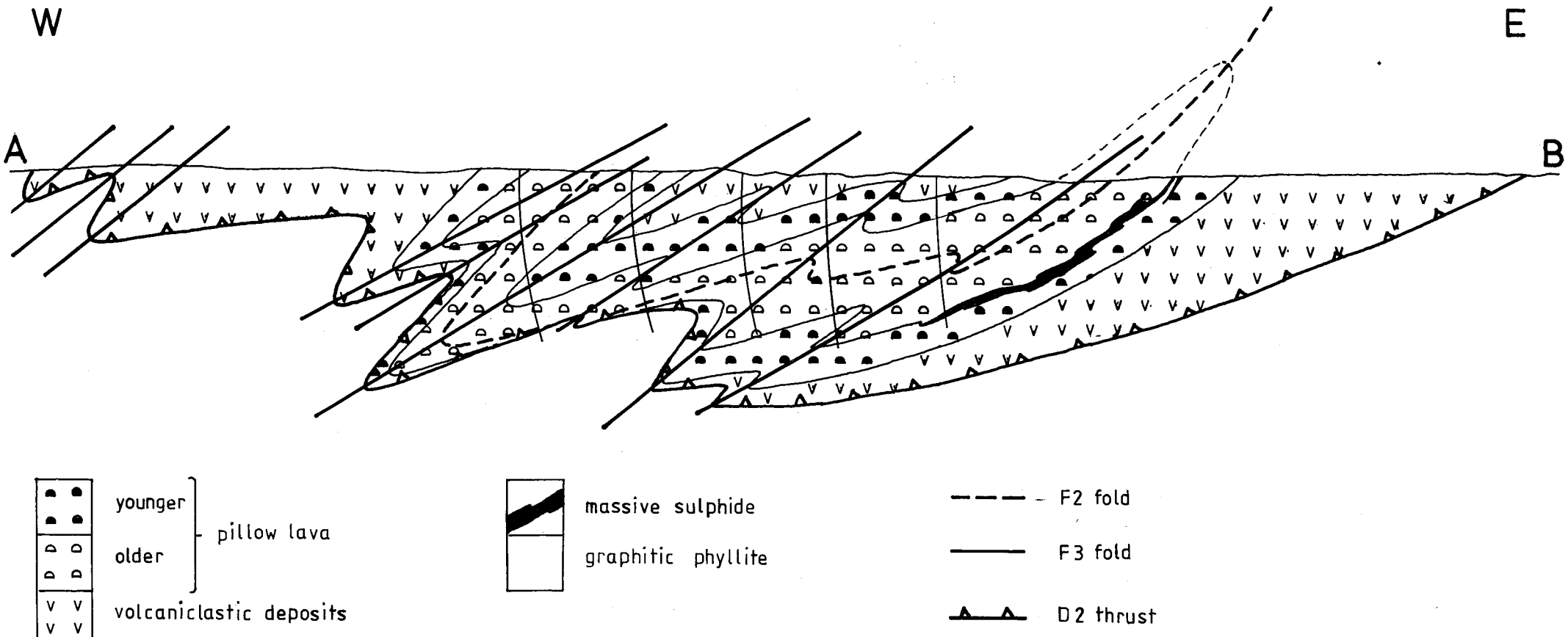

Fig.2.25 Structural section A-B (Fig.2.22) through the middle greenstone constructed from long drill holes logged by Reinsbakken (unpublished data, 1985). The greenstone rock types are folded by a major F2 fold with the ore body on its lower limb. The fold's lower limb is cut by the thrust at the base of the middle greenstone. Both the F2 fold and the thrust plane are folded by the F3 Joma synform.

The inner greenstone outcrops as a thin strip adjacent to the major thrust with the Gjersvik nappe and as an isolated lens between this and the middle greenstone, Fig.2.1. The lower contacts of these outcrops are marked by zones of strong S2 schistosity and complex interlayering of greenstone and phyllite on the scale of 10 cm to 2 m. Upwards from these contacts, S2 schistosity becomes weaker. From analogy with the middle greenstone, the lower contacts of the inner greenstone components are tectonic in nature and mark the probable location of thrusts.

The outer greenstone shows a rather different distribution of S2 intensity than the middle and inner greenstones. S2 schistosity is strongly developed in the thinner western section and weakly developed in the eastern thicker section. In the east, S2 development is inhomogeneous and consists of narrow zones of intense S2 schistosity, 1 to 2m wide, often associated with the phyllitic horizons. Zones of intense S2 schistosity do not correspond to the interlayering of pillowed and massive flows, which is thus likely to represent an original feature rather than one caused by intense F2 folding. The nature of the lower contact of the outer greenstone is uncertain as it has nowhere been found exposed. However, similarities in the outcrop pattern with the middle and inner greenstones suggest that it may also mark the location of a thrust.

The repeated sequence of greenstone, quartz phyllite and graphitic phyllite, and the thrust nature of the lower contacts of at least the middle and inner greenstone units, suggests that the sequence has been tectonically repeated. The three greenstone units therefore may have originated from the same horizon and the variation in lithologies represents a facies change through volcaniclastic deposits, pillow lavas and subaerial flows, from the inner to the outer greenstone units.

2.3.4 D1 - Eariest Phase of Deformation.

F1 folds and associated S1 cleavage were observed on outcrop scale at only one locality, which lies within quartzitic phyllites, on the northwestern side of Orklumpen (map reference

X760450, Y31530). Here the effects of D3 are low and tight to isoclinal F2 folds with limbs lengths of up to 2m are well developed. In some of these F2 folds, a penetrative S1 cleavage is observed suparallel to the quartz layering and folded with it. A few F1 folds were identified and the interference patterns developed with F2 suggest that F1 and F2 are close to coaxial, see Fig.2.26(a). This is also supported by the orientations of rodding lineations which correspond throughout the outcrop to the L2 orientation. Other examples of S1 and small scale F1 folds were found in thin sections of quartzitic phyllite from other localities, see Fig.2.26(b). S1 occurs as an intensly crenulated cleavage which is, in places, completely overprinted by S2. Minor F1 folds in thin quartzitic layers are refolded by F2 and the interference patterns produced are similar to those on the outcrop scale, suggesting that F1 and F2 are coaxial. Both S1 and S2 are refolded by conjugate sets of F3 kink folds in the phyllitic horizons, Fig.2.26(b).

F1 folds or S1 cleavage have not been identified in any of the greenstone units. Where the rocks show weak deformation, as indicated by the preservation of original features such as pillow structures and relict ophitic textures, S2 is poorly developed and there is no indication of a pre-existing cleavage. This, with the evidence that F1 and F2 folds are essentially coaxial, suggests that they represent the same deformation phase. The high competency contrast between quartzitic and phyllitic layers encourages the early development of folds (D1) which, on becoming isoclinal, are easily refolded at a later stage during the same phase (D2). In the greenstones, there is no such pronounced competency contrast to produce early folding so that such refolding of the cleavage is unlikely, and D1 structures are thus not represented.

2.4 STRAIN ANALYSIS

Variolites were found in some horizons of pillow lava in the outer greenstone and are most abundant in the layer adjacent to the upper contact (section 2.2.2). Individual variolites, now ellipsoidal in shape, range from 1 to 10 cm long and are either

Fig.2.26(a)

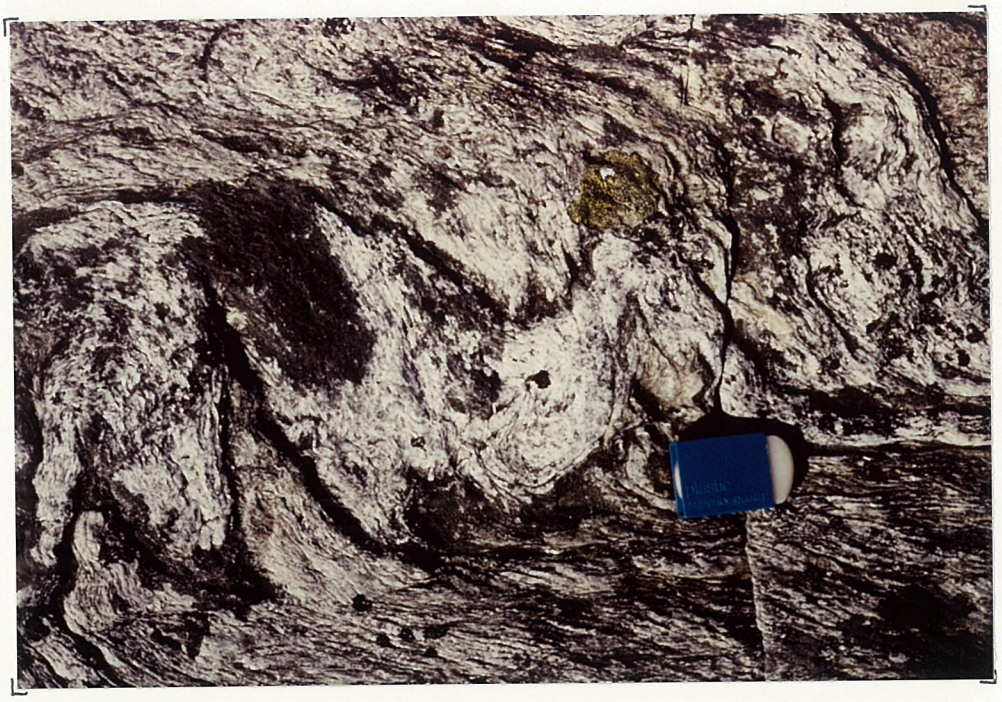

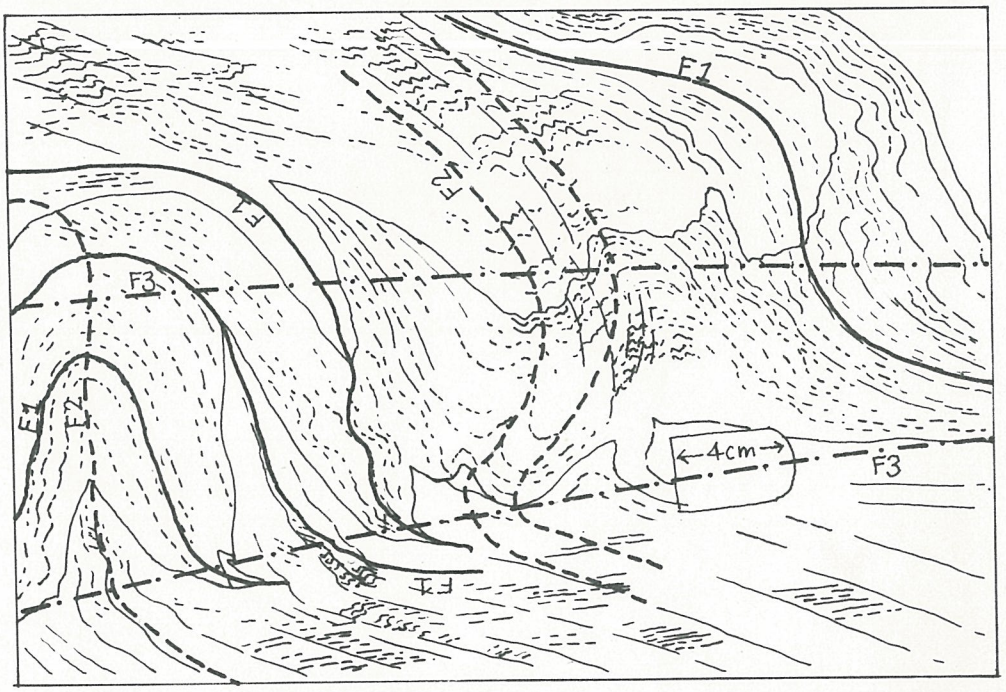

Fig.2.26(a) Photograph showing F1, F2 and F3 folds in quartzitic phyllite from the northwestern limb of the Joma synform, at X765000, Y31500.

Fig. 2.26 (b)

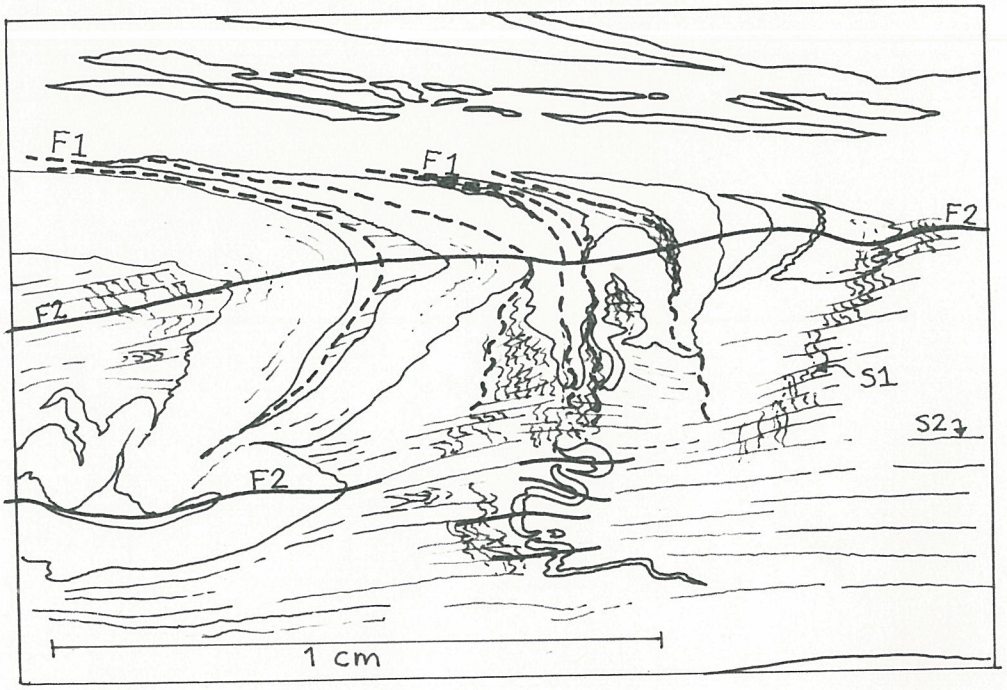

Fig.2.26(b) Thin section of quartzitic phyllite from the eastern limb of the Joma synform showing F1, F2 and F3 folds and S1, S2 and S3 cleavages.

darker or paler than their matrix due to different concentrations of clinozoisite and sphene . The origin of variolites in pillow lavas is unknown but evidence from recent pillows shows that their formation takes place soon after pillow extrusion and appears to be related to sea-floor alteration and cooling (Augustithis, 1982). In undeformed recent pillows, the variolites are subspherical and the constancy of axial ratio in the deformed examples from the outer greenstone is consistent with an initial subspherical shape.

Ten oriented specimens containing deformed variolites from locations within the outer greenstone (Fig.2.27), have been analysed for finite strain. The variolites are generally elongate parallel to the S2 cleavage and L2 lineation. D3, shown by the development of S3 crenulation cleavage, has affected the specimens to varying degrees.

2.4.1 The Method.

Each specimen was cut along three mutually perpendicular planes such that two of the planes coincide as closely as possible to the S2 schistosity and a plane perpendicular to S2 containing L2. These planes approximate the principal planes of the strain ellipsoid and measurement on them improves accuracy. The cut faces were smoothed and spray varnished to enhance the contrast between variolites and their matrix. Since many of the variolites were too small to be measured at their natural size, photographic colour transparencies were made of each face and projected on to a transparent screen, from which the enlarged variolites were traced. The long axis orientation of each variolite, estimated by eye, was measured relative to a reference line to the nearest degree. The long and short axes were measured to the nearest 0.01mm using a micrometer and the axial ratio (long axis length/short axis length) calculated for each variolite.

For a group of initially spherical particles, their shape and orientation after deformation defines the strain ellipsoid. Thus, if the initial shape of the particles is subspherical, the strain ellipsoid may be estimated by calculating the arithmetic

FIG. 2.27

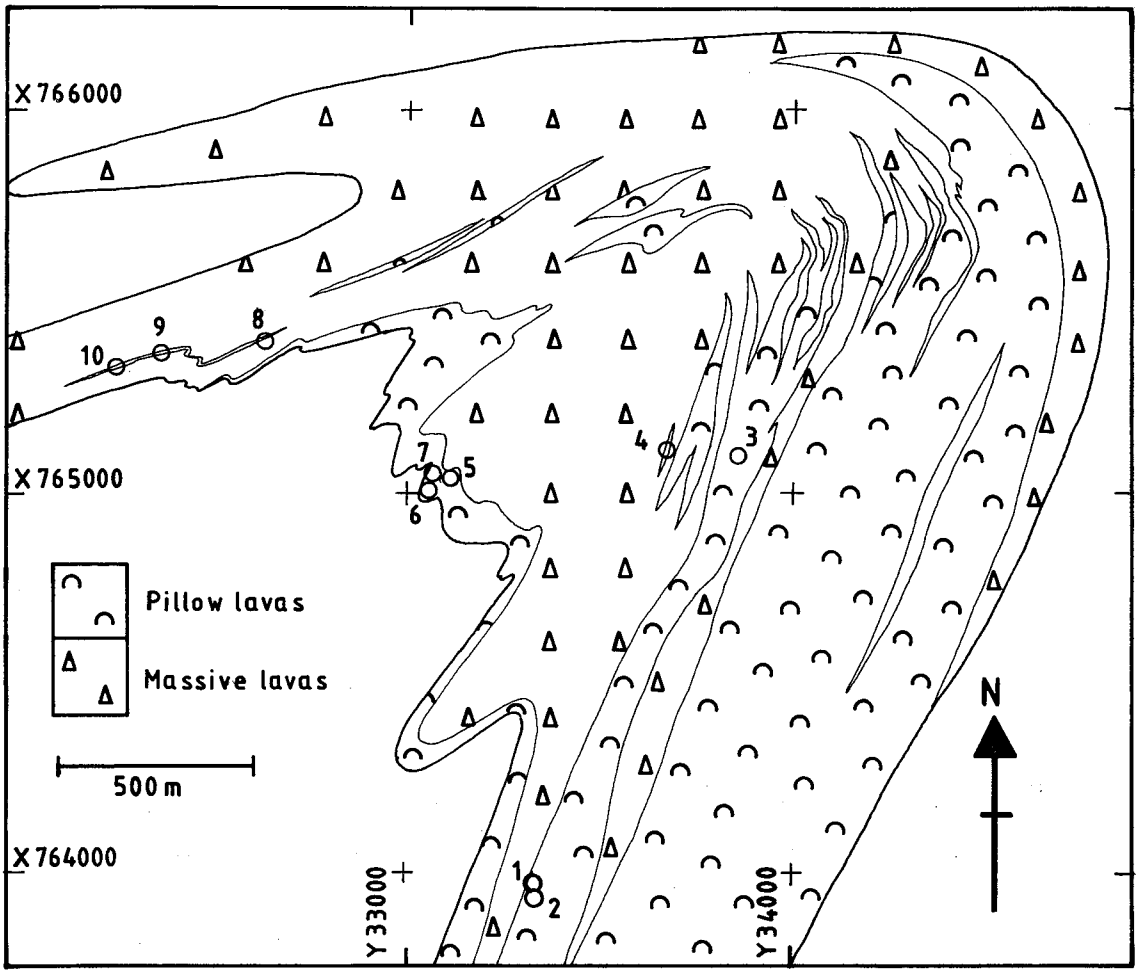

Fig.2.27 Map of the outer greenstone at Orklumpen showing the localities of specimens containing variolites used for strain analysis.

TABLE 1 Results of average ellpse (Shimamoto and Ikeda (1976) and arithmetic average methods applied to specimen 7, faces 1 to 3, for 20, 30, 40 and 50 particles per face.

	θ		R	
n	Ave. Ellip.	Arith. Ave	Ave. Ellip.	Arith. Ave.
Specimen 7, face 1				
20	9.5	10.0 - 3.3	2.14	2.26 - 0.17
30	10.3	10.7 - 2.7	2.13	2.24 - 0.12
40	10.9	11.3 - 2.2	2.10	2.20 - 0.10
50	9.9	10.4 - 2.0	2.14	2.25 - 0.09
Specimen 7, face 2				
20	-3.5	-3.5 - 2.4	1.74	1.77 - 0.06
30	-0.0	0.0 - 3.3	1.63	1.70 - 0.06
40	0.1	0.6 - 2.9	1.62	1.69 - 0.06
50	1.6	1.8 - 2.7	1.63	1.71 - 0.06
Specimen 7, face 3				
20	1.3	1.1 - 2.0	3.22	3.39 - 0.24
30	1.2	1.1 - 1.8	3.06	3.25 - 0.20
40	0.5	0.3 - 1.5	3.15	3.35 - 0.20
50	0.5	0.4 - 1.4	3.13	3.33 - 0.17

average of their axial ratios and orientations. However, for a group of intially ellipsoidal particles of varying orientation, the shapes and orientations after deformation are variable and using the arithmetic averages of axial ratios and orientations to calculate the finite strain ellipsoid leads to serious error. Shimamoto and Ikeda (1976) have developed a two dimensional mathematical method of calculating the strain ellipse of a group of initially elliptical particles with random orientations in which the corresponding components of 2X2 matrices, each representing a particle, are averaged. This 'average' particle is equivalent to the strain ellipse.

The variolites appear to have a relatively consistent shape and orientation for any one section and thus calculating the arithmetic average of these quantities would seem to be a valid method of estimating the strain ellipsoid. To test the validity of this assumption, each face of a test specimen was analysed by the average-ellipse (Shimamoto and Ikeda, 1976) and arithmetic-average methods. For the arithmetic method the 95% confidence intervals on the axial ratios and orientations were calculated. The orientations were assumed to approximate a Von Mises distribution and the 95% confidence intervals were calculated by a method outlined by Cheeney (1983). Each method was applied for 20, 30, 40 and 50 particles per face to determine the number of particles needed for a reproducible result and the results for both methods are listed in Table 1. The results show that for the strain ellipse orientation (θ), the two methods differ by less than 1^{o}, which lies well within the 95% confidence interval of the arithmetic average and is therefore not significant. The arithmetic-average method gives results which are consistently greater than the average-ellipse method but the discrepancies between the two methods are not great, just bordering on significance at the 95% confidence level. There is therefore, little error in assuming an initial spherical to subspherical shape for the variolites and using the arithmetic-average method to estimate the strain ellipse for each face.

The resulting strain ellipses obtained for the three faces were then combined using a program by Gendzwill and Stauffer (1981). The program adjusts the ellipse ratios and orientations

until a compatible set of data is obtained and then calculates the axis lengths and orientations of the strain ellipsoid. The adjustments made by the program lay within or close to the 95% confidence confidence interval on the two-dimensional data.

In specimen 10, the variolites have become highly elongate due to extreme D1-D2 deformation and have later been folded by D3, see Fig.2.28(a). Unfolding the variolites gives an estimation of the D1-D2 strain and measuring the variolites in their folded state gives an estimation of the total finite strain (D1-D2-D3). Thus, two stages in the strain history of specimen JA10 are obtained. The D1-D2 shape of the variolites was estimated by using the total length of the now folded, long axis and the breadth to calculate the axial ratio. The long axis orientations were measured on the longer, less crenulated limbs, see Fig.2.28(b). The D3 state of strain was estimated using the present length of variolites with their 'average' orientations, see Fig.2.28(b). The short axes were then recalculated from the D1-D2 values assuming no loss in area for each variolite.

2.4.2 The Results.

The three dimensional finite strain ellipsoids of specimens 1 to 10 are plotted on a logarithmic deformation plot where the logarithm of the ratio 'a' (maximum/intermediate) is plotted against the logarithm of the ratio 'b' (intermediate/minimum), in Fig.2.29(a). Maximum and minimum axis orientations are plotted on an equal-area projection, lower hemisphere stereonet in Fig.2.29(b). From the logarithmic deformation plot in Fig.2.29(a), all specimens show nearly plane strain (a=b), lying consistently on the flattening strain side of the k=1 line (where $k=(a-1)/(b-1)$). Strain values show a wide range with 'a' strain ratio values from 1.15 to 5.15. The intensity of strain shows a correlation with geographical position, with the lowest strains (specimens 3 and 4) in the centre of the eastern limb of the Joma synform and the highest strains (specimens 9 and 10) on the western limb. Intermediate strain values come from the Joma synform hinge area close to the contact with the quartzitic phyllites. This distribution is in general agreement with the field observation that D2 deformation is more intense in the west

Fig. 2.28(a)

Fig.2.28 (a) Photograph of specimen 10, face 2 showing strained and folded variolites.

FIG. 2.28

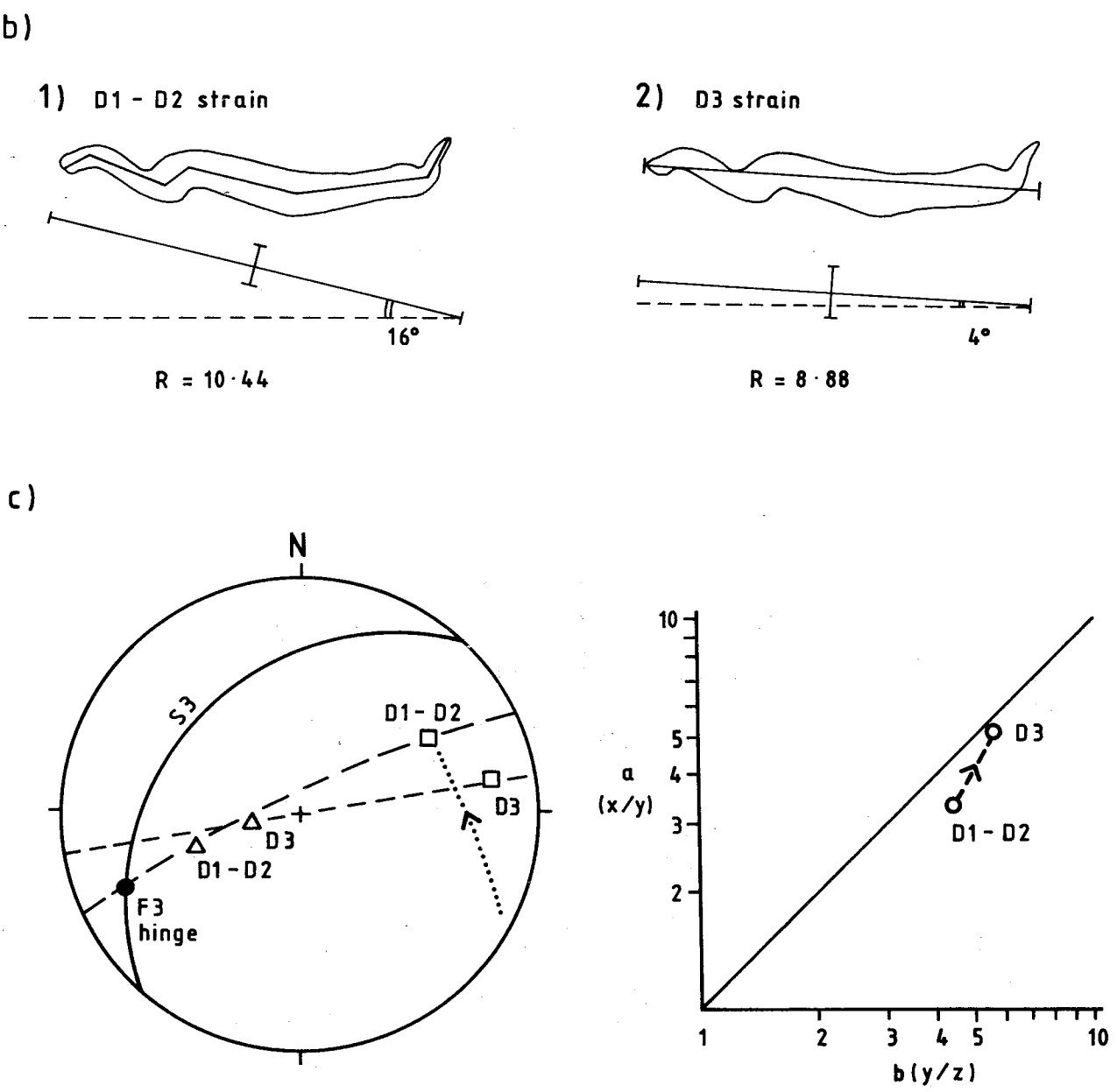

Fig.2.28(b) Measurement of variolites for (1) D1-D2 strain by measuring total variolite length, and (2) for D3 by measuring variolite folded length and recalculating breadth from (1) assuming no area loss. (c) strain results for D1-D2 and D3 strains on logarithmic deformation plot and stereonet. Dotted path on stereonet shows D3 rotation path of D1-D2 strains.

FIG. 2.29

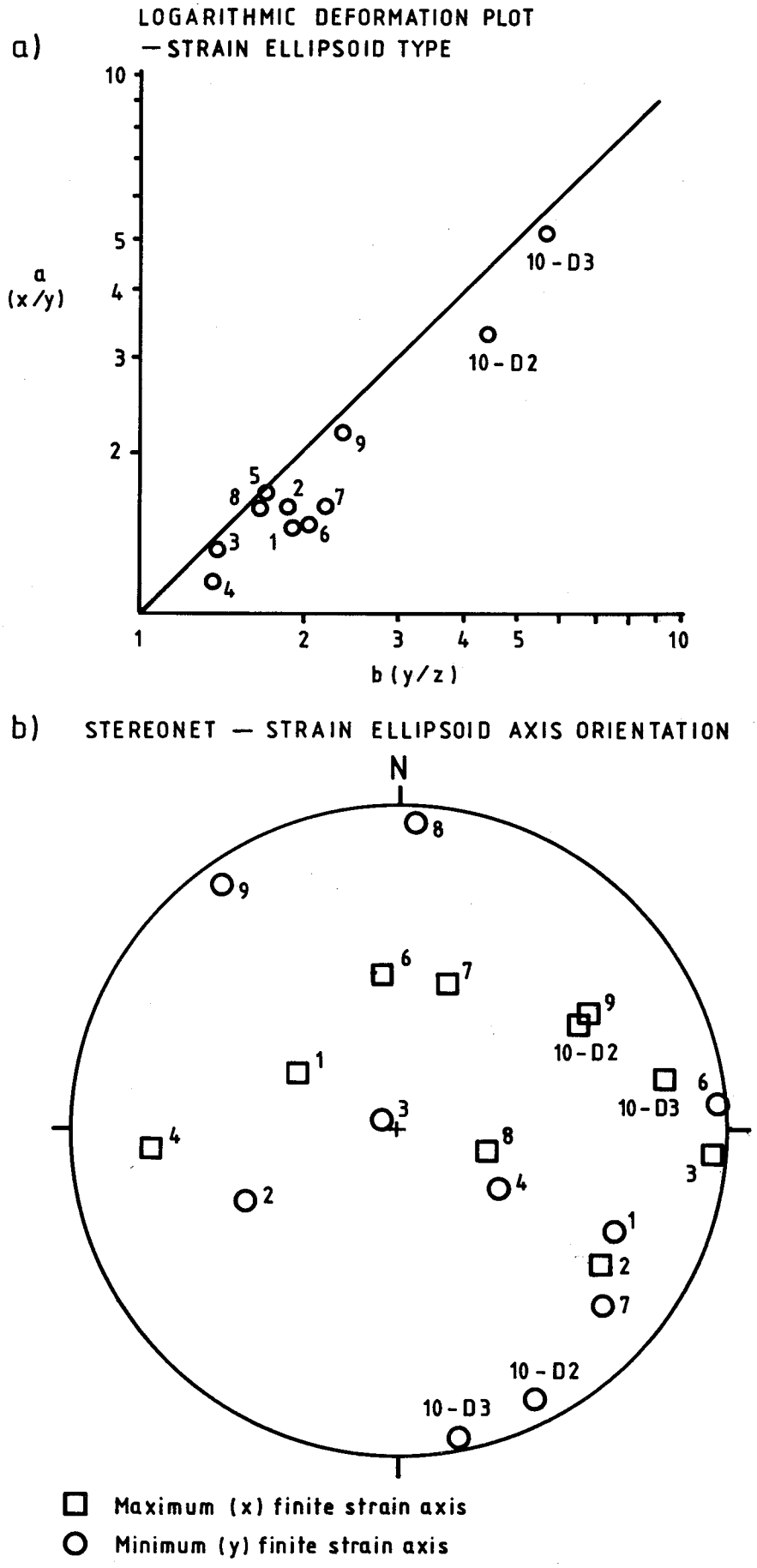

Fig.2.29 (a) Finite strain axial ratios of specimens 1 to 10 plotted on logarithmic deformation plot. (b) Finite strain axis orientations for specimens 1 to 10 plotted on a lower hemisphere equal area projection stereonet.

TABLE 2 Results of strain analysis for specimens 1 to 10.

Specimen	a	b	X	Z
1	1.45	1.92	62 300	28 116
2	1.57	1.79	25 124	46 244
3	1.31	1.40	04 095	86 294
4	1.15	1.39	24 266	60 123
5	1.65	1.71	unknown orientation	
6	1.47	2.03	50 355	02 086
7	1.52	2.09	34 054	17 312
8	1.57	1.68	66 104	05 004
9	2.18	2.39	33 059	07 325
10-D2	3.33	4.38	36 059	06 154
10-D3	5.15	5.63	18 079	01 169

and less intense on the eastern limb of the Joma synform (section 2.3.3). S3 cleavage in the specimens also shows a correlation with intensity of strain. Specimens showing lowest strain also show the least development of S3 (specimens 1, 2, 3, 4, 6, and 7) while those showing highest strain show an S3 spaced cleavage, crenulation and small scale F3 folding (specimens 5, 8, 9 and 10). This agrees with the field observation that S3 crenulation and folds commonly occur in areas of strong S2, S2 providing an anisotropy to be folded by D3.

The distribution of principal axis orientations (Fig.2.29(b)), shows a considerable range in orientations, with the maxima (X) following an arcuate trend similar to L2 lineations, (Fig.2.21(a)). The minima (Z) show largely shallow plunges indicating steeply dipping X-Y planes for all specimens close to the upper contact with the quartzitic phyllites. This is due to the intense F3 folding which has rotated S2 to become subparallel to S3. Specimens 3 and 4, located in the more central portions of the outer greenstone, show more shallowly dipping orientations, indicating positions close to the hinge of the Joma synform.

The two finite strain results for specimen 10 illustrate the effect of D3 superposition on D2-D1 strain. Fig.2.28(c) shows that both strain values lie close to the k=1 line and that D3 strain has increased the finite strain by a factor of 'a'=1.82 and 'b'=1.25. In the measurement of D1-D2 strain, variolite orientations were taken from F3 fold long limbs. It is probable that these limbs have suffered some rotation during D3 and thus the orientation of D1-D2 strain contains a component of D3 rotation. The D1-D2 strain value has been rotated about the F3 fold axis which lies within S3. Rotating the D1-D2 strain about the F3 fold axis away from the S3 plane gives the approximate path of the D1-D2 strain during D3. The S3 cleavage and F3 hinge for specimen 10 are plotted with the finite strain results in Fig.2.28(c). The D1-D2 Y strain axis plots close to the F3 hinge, it has thus suffered relatively little rotation during D3. In plane strain (k=1) and under conditions of no volume loss (assumed here), the Y strain axis is a direction of no strain and thus any changes in the strain of specimen 10 during D3 therefore

occured largely in the X-Y plane. Thus, a k=1, plane strain deformation path is maintained. This is supported by the other strain results which plot close to the k=1 line regardless of the intensity of D3 deformation, as recorded by development of S3 cleavage and F3 folding.

2.5 THE DEFORMATION HISTORY OF THE LEIPIKVATTNET NAPPE.

The strain results show that both the D1-D2 and D3 strains result in a k=1 deformation path. Both deformations are therefore by plane strain and must be subcoaxial in at least the Y strain direction. In plane strain deformation there are two possible 'end-member' mechanisms, pure shear (irrotational strain) and simple shear (rotational strain), between which infinitely many combinations of these two 'end members' are possible.

It has been shown (section 2.3.4) that D1 and D2 deformations are coaxial and probably represent different stages of the same deformation phase. D1-D2 deformation is associated with the main thrusting event that produced the nappe pile of which the Leipikvattnet nappe is a part. The deformation phases therefore have a large simple shear component. The orientation of the S2 surface has been reconstructed using the F3 fold hinge and the least disturbed L2 lineation orientation (section 2.3.3). Since S2 schistosity, the lithological layering and the D2 thrust planes are subparallel, this also provides an approximation to the D2 shear plane. As shown by the variation in L3 plunges, the S2 surface (D2 thrust plane) had a different orientation in zone B (gently north dipping) from zones A and C (shallowly east dipping), see section 2.3.3. A possible reason for the change in attitude is refraction of the D2 thrust plane in the relatively competent greenstone unit, causing a steepening of the dip. This refraction of the D2 thrust plane formed a 'ramp and flat' structure (Boyer and Elliot 1982), (Fig.2.31(a)). The formation by shearing of the F2 fold in the middle greenstone produced a highly deformed short limb (Fig.2.31(a)), which then acted as a zone of weakness and thus provided a suitable location for the development of a thrust. Movement along the curved shear plane then causes variation in the orientation of the S2 surface, see

Fig.2.31(b). This shallowing of S2 dips in zone B has resulted in the greatly increased outcrop width of the middle greenstone in the hinge of the Joma synform, (Fig.2.31(c)).

D3 deformation has been superimposed on D1-D2 strains in such a way as to maintain plane strain (k=1). This is possible if the D3 deformation is the result of either 1) simple shear with shear plane, direction and sense similar to that for D1-D2 deformation or 2) pure shear, in which the Y strain direction remains approximately constant throughout the deformation, so that all changes in strain occured within the X-Z plane. During the formation of the Joma synform, the D1-D2 strains are rotated first into an orientation where D3 'undoes' strain in the X-Z plane and thereafter into a position where D3 increases strain, see Fig.2.30. Since the Y strain direction is constant, this results in a strain path confined to near plane strain, first moving towards the origin of the plot (decreasing strain) and afterwards moving away from the origin (increasing strain). Both pure and simple shear models produce strain paths which are compatible with the finite strain results.

Though pure and simple shear produce similar strain results, several factors suggest a dominantly simple shear mechanism for D3 deformation. The average S3 plane for the western overturned limb of the Joma synform lies at 45° to the D1-D2 shear plane (Fig.2.30). This is the angle at which cleavage is first developed in a simple shear regime and thus the development of S3 is compatible with continuing shear on the D1-D2 shear plane. The form of the Joma synform is also compatible with the D1-D2 shear sense in which the overlying rocks move eastwards, which is the general sense of nappe translation within the Scandinavian Caledonides. D3 deformation is concentrated in the overturned Joma synform limb, section 2.3.2. This is compatible with a simple shear model in which which shearing is concentrated on the short limb of the shear fold. In the pure shear model, D3 deformation would be expected to be more evenly developed on both limbs. A simple shear model is also indicated by the distribution of L2 lineations around the Joma synform, described in section 2.3.3, and Fig.2.21(b). If the D3 deformation were dominantly pure shear, the lineation pattern of zone B could only

FIG. 2.30

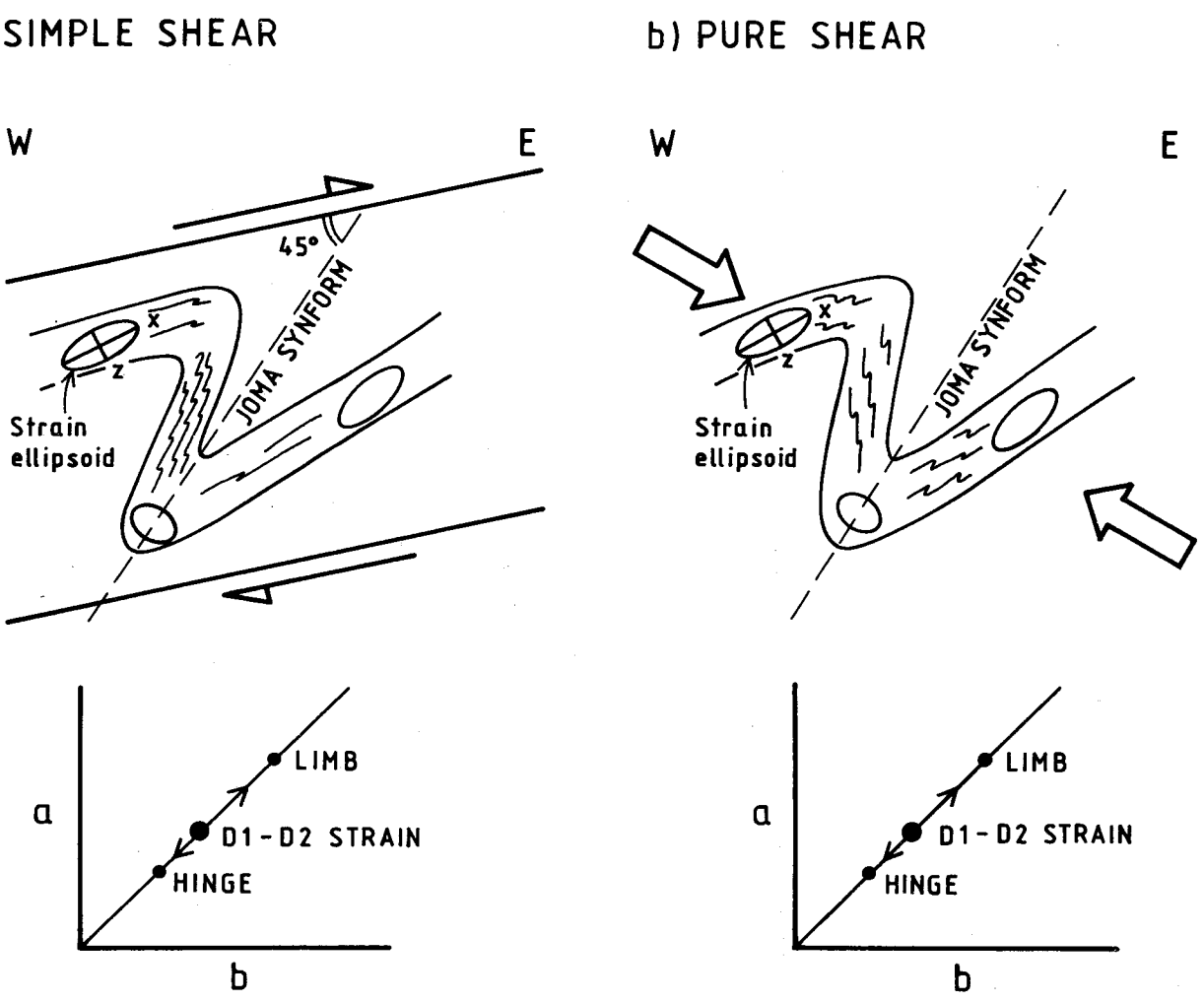

Fig.2.30 Diagram to show the effects on D1-D2 strains of (a) simple shear and (b) pure shear D3 deformation models. In the X-Z plane, D1-D2 strain on the hinge of the fold is decreased by D3, whereas those on the limbs are increased. The Y strain axis remains a direction of no strain and thus both models result in k=1 deformation paths.

FIG. 2.31

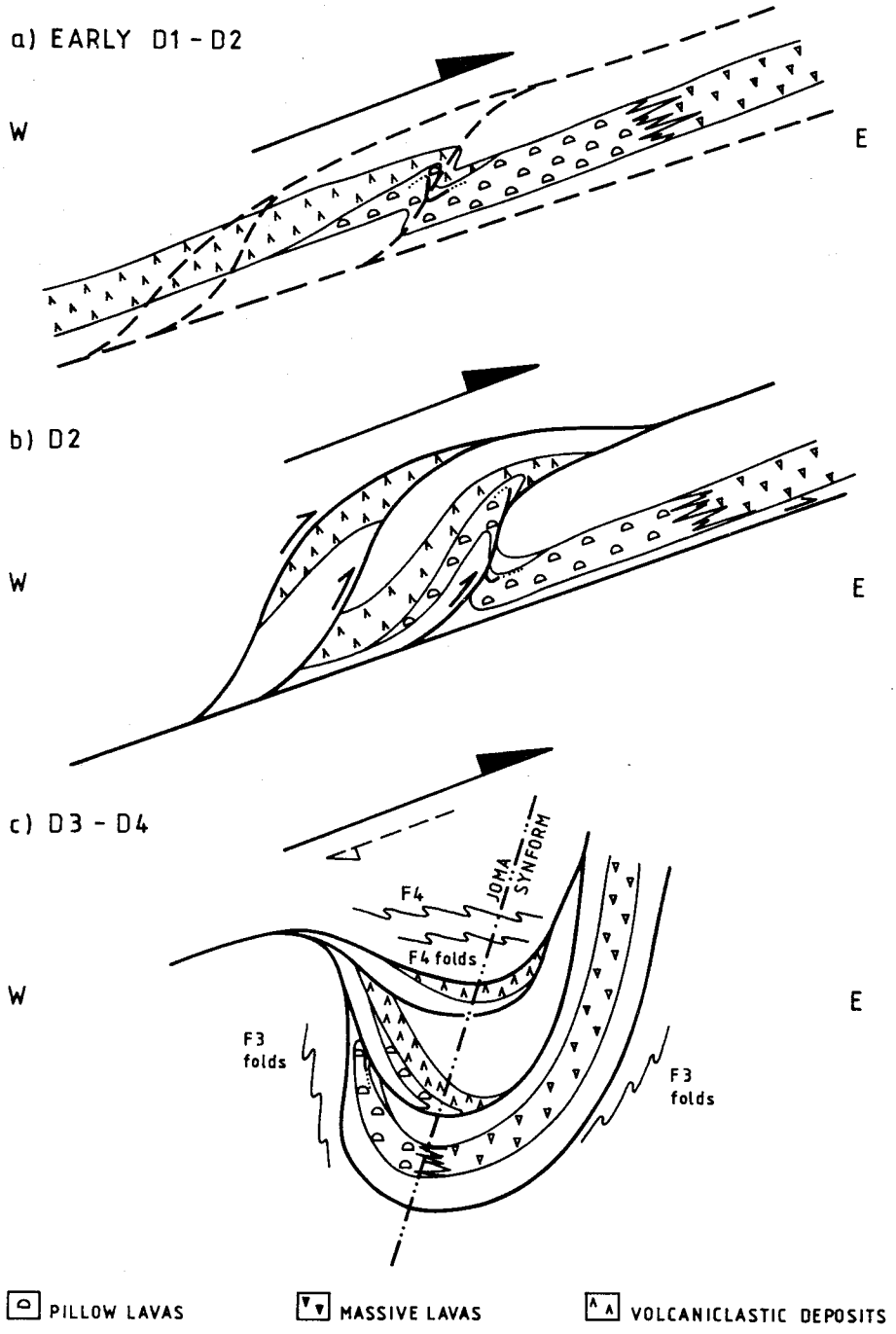

Fig.2.31 Model for the deformation history of the Leipikvattnet nappe. (a) In early D1-D2 times, greenstone units were part of a single horizon. An f2 fold marks the future location of the thrust at the lower contact of the middle greenstone. (b) Shearing and thrusting during D1-D2 times leads to a repeated stratigraphic sequence. Ramp and flat structures cause variation in the attitude of S2. (c) D2 thrusts lock and continuing shear produces the Joma synform which folds the D2 thrust planes. S3 is oriented at 45° to the shear plane. Flat lying F4 folds are caused by inhomogeneous D3 deformation.

be produced if D3 deformation were strong on both limbs of the Joma synform thus rotating the L2 lineations and F2 fold hinges towards the pure shear strain maximum which plunges moderately north. Since D3 deformation is not intense on the east limb of the Joma synform and the L2 distributions of zones A, B and C are indistinguishable, a dominantly simple shear mechanism is more probable.

D1, D2 and D3 deformation phases are therefore closely related and are the result of a constant orientation of shear plane, direction and sense. During D1-D2 deformation, strain was taken up largely by movement on thrust planes resulting in the emplacement of the Leipikvattnet nappe and the repeated stratigraphic sequence within it. D3 deformation folds these major thrusts, effectively stopping movement along them, and further shearing was taken up in the formation of the Joma synform. The amount of shortening achieved by the development of the nappe pile is likely to be at least an order of magnitude greater than that which produced the Joma Synform, and thus D3 represents the last stage in the shearing event.

F3 major folds in the Leipikvattnet nappe become increasingly more open westwards from the Joma synform. This indicates increasing D3 deformation to the east, suggesting that movement along the major thrusts stopped first in the east and continued longer in the west, resulting in increasing stress in the Joma area and causing the development of the Joma synform. This increasing stress would result in a late stage pure shear component to the D3 deformation with minimum (Z) axis oriented subparallel to the shear direction. This explains the steepening of S3 cleavage on the eastern limb of the Joma synform.

D4 minor structures occur as conjugate folds in which one component shows the same vergence but steeper attitude than the Joma synform. Higher up in the nappe pile, in the overlying Gjersvik nappe, the other component of the D4 conjugate set becomes dominant. The similar hinge orientations of F3 and F4 folds and the spatial relationship between D3 and D4 minor structures (section 3.2), suggests that their development overlapped in time, with D4 continuing later. It is therefore likely that D4,

like D3, is related to the last stages in the major shearing event. The steepening of the westward dipping D4 component correlates with the steeper S3 cleavage on the Joma synform east limb and thus signifies a pure shear component to the deformation during late D3 and early D4 times. This suggests that the flatlying component of F4 folds, which becomes dominant in the overlying Gersvik nappe, is also closely connected with D3 deformation. The Joma synform is laterally impersistant and thus forms a les-shaped 'bulge' in the tectonic pile. It is suggested that the flat-lying folds formed in response to subvertical compression at the margins of this lens.

SECTION 3 : THE JOMA MASSIVE SULPHIDE DEPOSIT

3.1 STRUCTURAL SETTING OF THE JOMA MASSIVE SULPHIDE DEPOSIT

The Joma massive sulphide deposit outcrops within the middle greenstone unit and lies in the hinge zone of the Joma synform. The deposit lies within the pillow lavas, close to the northern contact with volcaniclastic greenstones and comprises two arcuate outcrops, see Fig.3.1. In the major arc, sulphides outcrop discontinuously over a distance of some 1200m, while the lesser arc, which is situated approximately 50m to the northeast, outcrops over a distance of 200m. The massive sulphides are unexposed except along the river section and in the open pit, but have been mapped out by trenching and geophysical means, as a series of lenses shown in Fig.3.1. A map of the exposed north-eastern arc (Fig.2.24, section 2.3.3) shows that the sulphide layer is folded into a series of gently northwest plunging isoclinal F2 folds and the lenses of the unexposed sulphide outcrop therefore probably represent F2 fold hinges, separated by sheared or thrust out fold limbs.

The massive sulphides are composed of pyrite, chalcopyrite, pyrrhotite and sphalerite with varying amounts of matrix quartz, carbonate and amphibole. Textural and compositional layering on scales of millimetres to metres is common. The ore body shows a general compositional change from sphalerite-rich pyrite ore in the east to chalcopyrite-rich ores in the west. Associated with the chalcopyrite-rich ores are numerous silicate layers of greenstone, chlorite schist, albitite and carbonate which are intercalated with the sulphides. The most chalcopyrite-rich ore is a breccia composed of silicate and pyrite fragments in a chalcopyrite-pyrrhotite matrix.

Structural studies on the ore and associated silicate horizons have been concentrated on the most recently worked areas of the mine where the surfaces are still fresh. Detailed mapping and structural measurement has been carried out on levels 350,

Fig.3.1 Map showing the outcrop of the Joma massive sulphide deposit, the country rock lithologies and the lateral extent of underground mining.

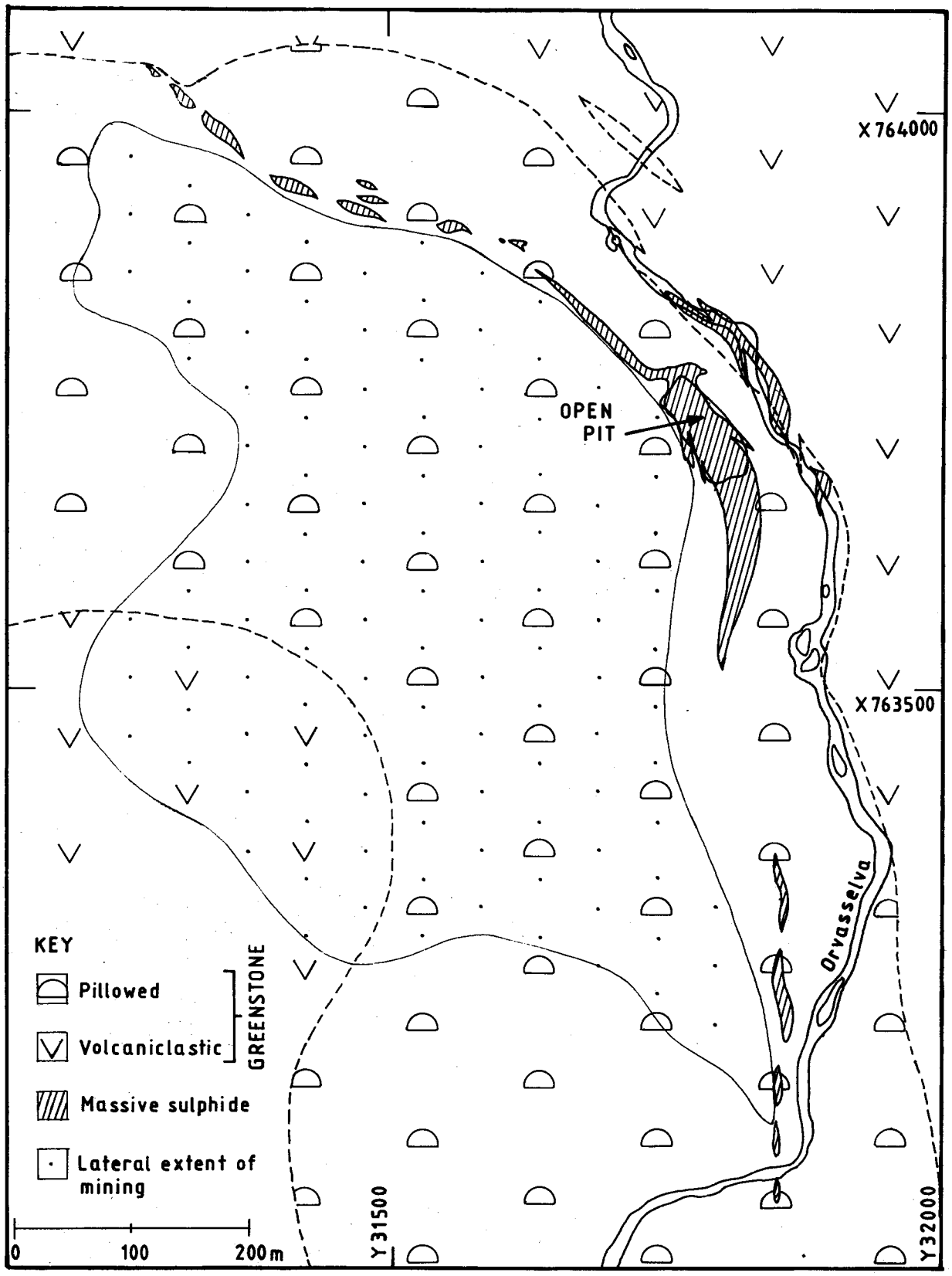

362, 375, 382, 387, 402, 416, 429 and 495, the locations of which are shown on Fig.3.2.

The deformation phases found in the Joma area can also be recognised underground. The main deformation phase, D2, has formed large scale isoclinal folds and is associated with intense shearing and thrusting. Due to this thrusting and shearing, most of the sulphide-silicate contacts now observed are tectonic in nature. F3 folding has been superimposed on the D2 structures and F3 folds are most intensely developed in the western part of the ore body where they cause the general attitude of the ore horizon to become steeply easterly dipping.

3.2 D2 DEFORMATION

The main penetrative cleavage and mineral lineation found throughout the greenstone country rocks and silicate lithologies intercalated with the sulphides belongs to the main D2 deformation phase. This penetrative schistosity is expressed in the sulphides as a compositional streaking of sphalerite in pyrite or elongation of chalcopyrite-pyrrhotite aggregates, and sometimes as a preferred orientation of silicates, e.g. amphibole, in the sulphide matrix. Fig.3.3(a) shows that a plot of the poles to S2 schistosity forms a point distribution with an maximum indicating gently northwest dipping orientation, indicating that the ore body lies in the hinge zone of the Joma synform. All measurements of D2 structures throughout the mine were taken from areas least disturbed by D3 and thus refer to the orientation of D2 structures on the F3 long limbs which dip gently west. D2 deformation in the sulphides and their country rocks is expressed as large scale folding and associated thrusting. Folding is dominant in the western part of the ore body where chalcopyrite-pyrrhotite ores are intercalated with silicate and carbonate horizons, and thrusting is dominant in the eastern part which is composed of massive pyrite-sphalerite ores.

3.2.1 F2 Folding.

Large scale isoclinal F2 folds with amplitudes of 100-300m

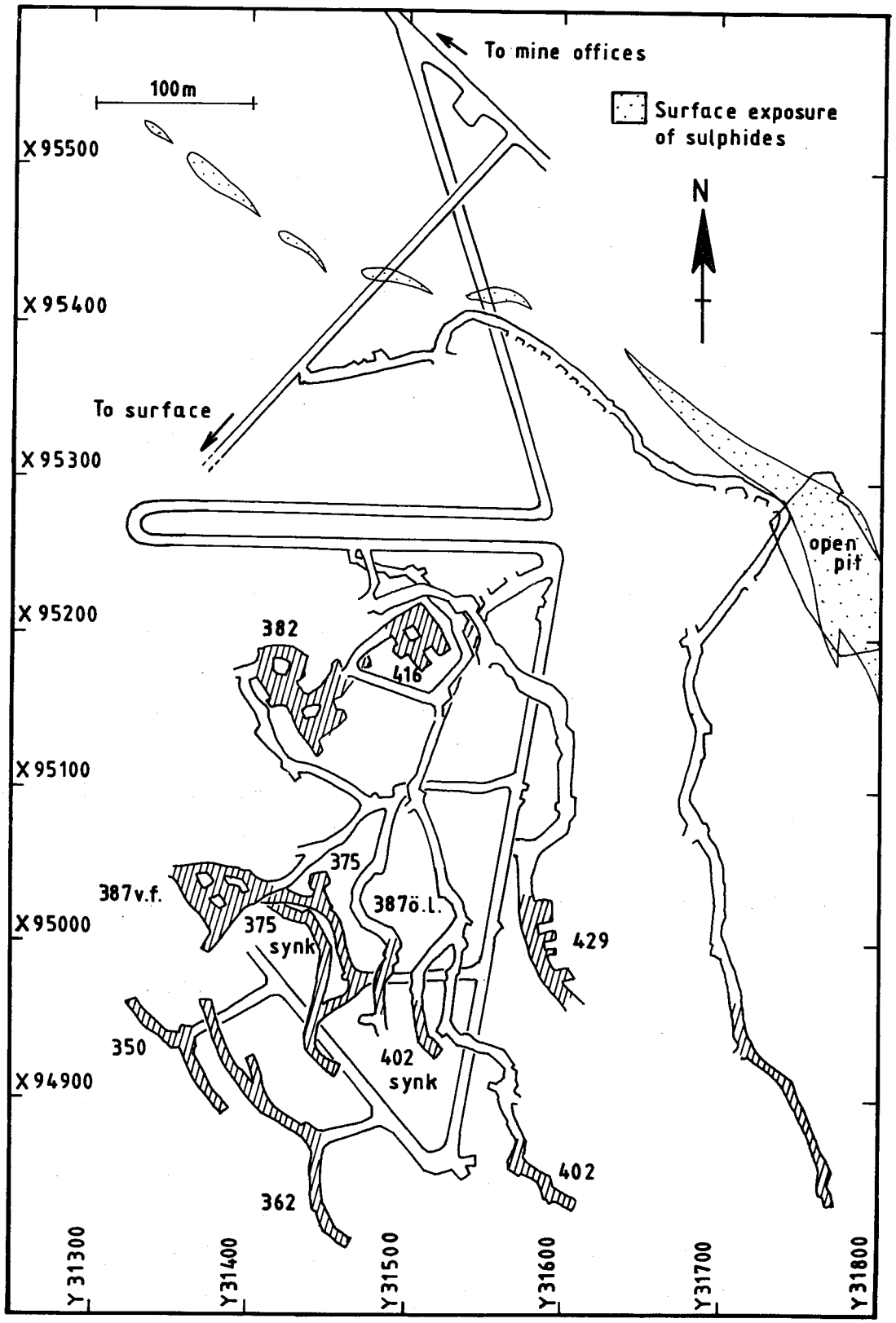

Fig.3.2 Map showing the areas of the mine studied, with connecting driveways. The exposure of the massive sulphides and the open pit are also indicated.

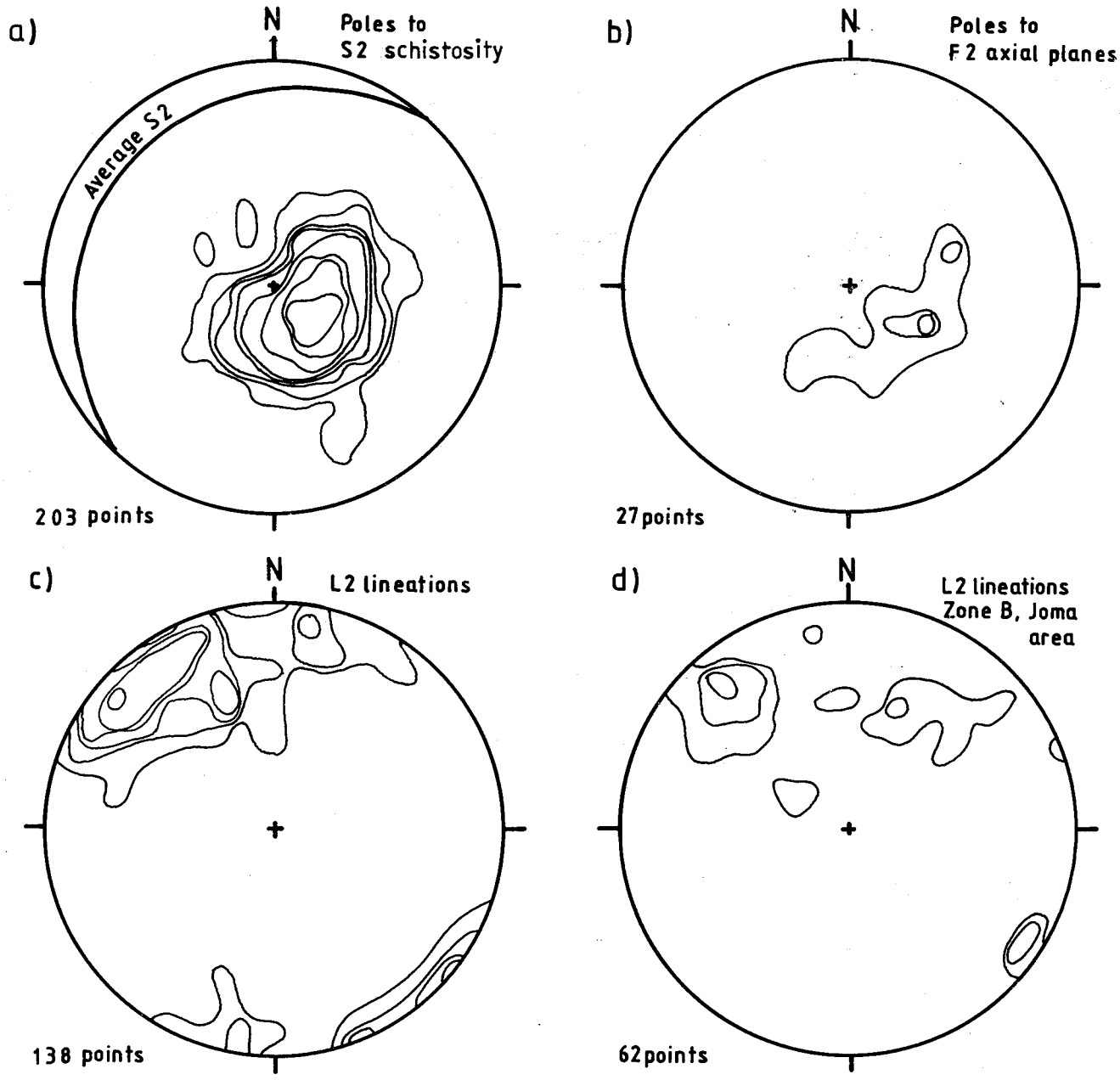

Fig.3.3 D2 structures plotted on Lambert equal-area projection stereonets. S2 schistosity, (a), and F2 axial planes, (b), show similar distributions. L2 lineations for the mine, (c), show a similarly oriented maximum to those for the area containing the outcrop of the massive sulphides, zone B, (d).

a) Level 382

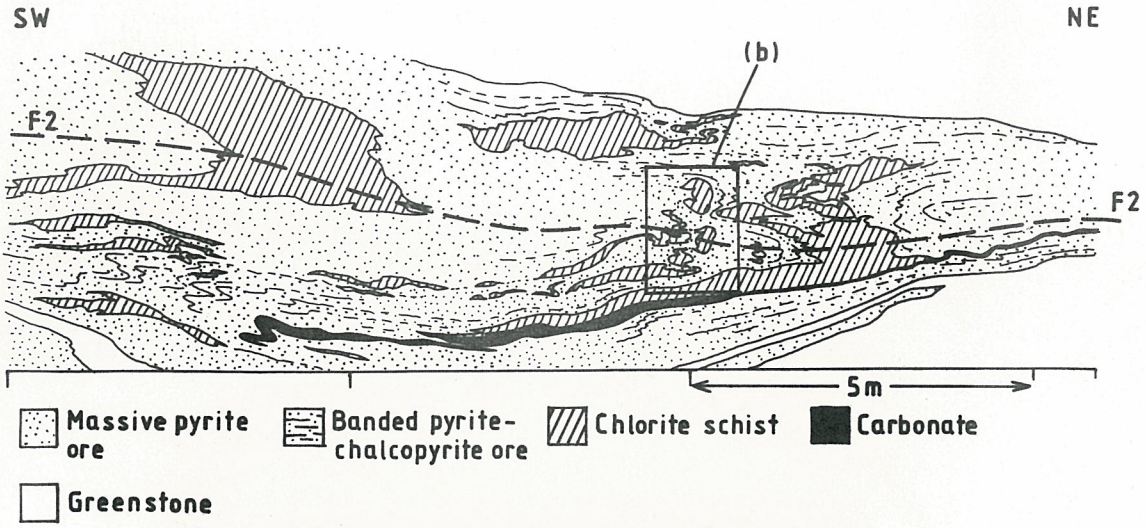

b)

Fig.3.4 (a) F2 hinge zone in chalcopyrite-pyrrhotite rich ores with intercalated silicate and carbonate horizons showing disruption of chlorite schist layer in the fold core, level 382. Minor F2 limbs have been sheared out leaving fold cores as isolated rafts in a sulphide matrix. (b) photograph of disrupted chlorite schist layer in area outlined in (a).

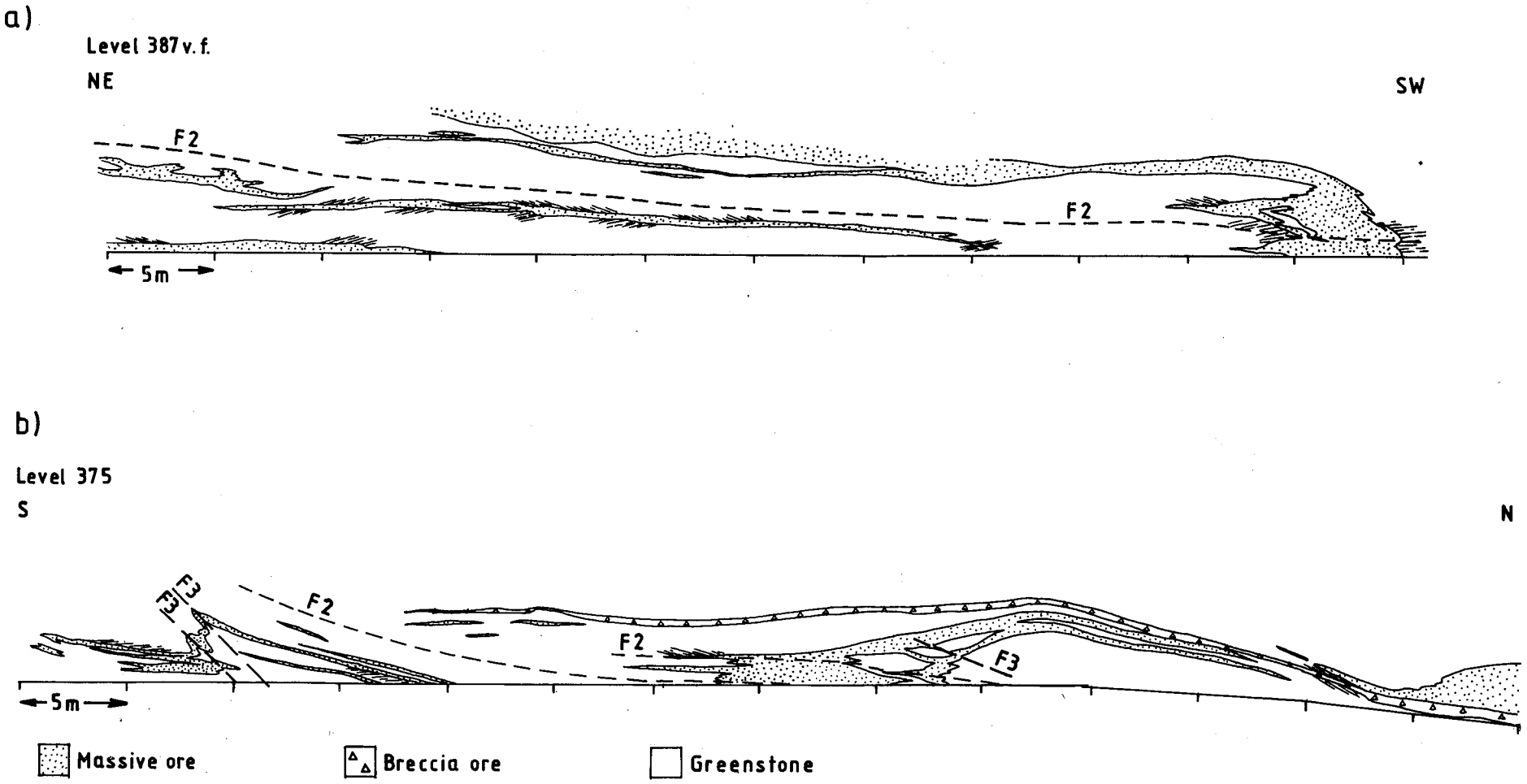

Fig.3.5 F2 hinge zones in chalcopyrite-pyrite ore showing development of numerous thin tectonic slivers of massive sulphides which cross-cut the schistosity in the greenstones, from levels 387 v.f. and 375.

a)

b)

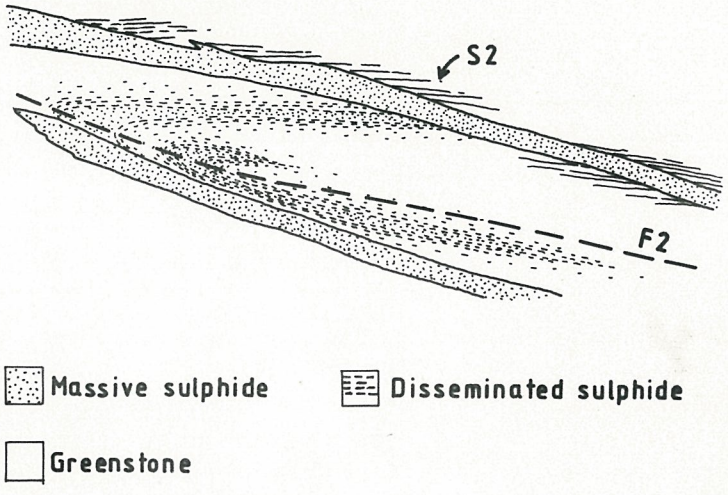

Fig.3.6 (a) Photograph of tectonic slice of massive sulhide showing folded textural layering in the core and contacts oblique to S2 schistosity in the greenstone. (b) Sketch showing folded gradational sulphide-greenstone contacts, representing possible original sedimentary layering. These are cut by tectonically emplaced massive sulphide layers with sharp contacts which cross-cut S2 schistosity.

occur in intercalated chalcopyrite-pyrrhotite ores, silicate and carbonate horizons of the western section of the ore body, e.g. on levels 382 and 387 v.f. Minor F2 folds, parasitic to the major folds, are common in thin silicate and carbonate layers. Stereoplots of poles to their axial planes and L2 lineations (F2 fold axes and mineral lineations) are shown in Fig.3.3(b) and (c). F2 axial planes have a distribution indistinguishable from S2 schsitosity in Fig.3.3(a), showing that S2 is axial planar to F2 folds. L2 lineations, composed of F2 fold axes and L2 lineations, show an arcuate distribution plunging gently to sub-horizontally west-northwest to north-northeast. The maximum of the distribution trends northwest, in agreement with the maximum for L2 lineations for the Joma area, see Fig.3.3(d).

F2 folds show thickened hinges and thinned limbs along which thrusting is a common feature. In the fold hinges, the silicate horizons have suffered strong ptygmatic folding, and in some cases chlorite schist layers have been sheared out along fold limbs to leave fold cores as isolated rafts in a sulphide matrix, see Fig.3.4(a) and (b). Where intercalated silicate horizons are less abundant, numerous thin slivers of sulphide are developed subparallel to the axial plane, see Fig.3.5(a) and (b). These occasionally show folded relict compositional and textural layering in their cores, indicating that they represent F2 folds with thrusts developed along their limbs, see Fig.3.6(a). Quartz-calcite veins occur along or subparallel to the contacts in the adjacent greenstones and are most common at sulphide layer terminations.

Along F2 fold limbs, layering and lithological contacts in the sulphides are commonly cut by sharply defined sulphide-greenstone contacts. At most contacts, the S2 schistosity in the greenstone is oblique. These features indicate that the greenstone-sulphide contact are tectonic. Gradational contacts, where massive sulphides grade through sulphide dissemination into greenstone, and are cut by thrust slices of massive sulphides with sharp contacts, represent probable original contacts, see Fig.3.6(b). These types of contact are, however, rare and the majority of sulphide-greenstone contacts are tectonic.

3.2.2 The Formation of Breccia Ore.

'Breccia ore' commonly occurs in F2 fold limbs, in the form of en echelon lenses and interconnected layers, see Fig.3.7(a). The breccia is composed of silicate, carbonate and sulphide fragments in a chalcopyite-pyrrhotite rich matrix. The fragments include banded pyrite-magnetite and fine grained pyrite ores, chlorite schist, greenstone, quartz, carbonate and pyrite grains. The brecciation process begins with the development of thrust lenses of banded pyrite ore and associated chlorite schist, which are separated by thin layers of actinolite and chlorite schist showing a strongly developed L2 mineral lineation, see Fig.3.8. Two or more generations of thrusts are common and individual lenses range from 6m, (Fig.3.7(b)), to a few cms long. The thrust planes are later penetrated by chalcopyrite and pyrrhotite which separates the lenses. Further deformation folds and rolls the lenses and further fragmentation is caused by the development of fractures which are filled by the chalcopyrite-pyrrhotite matrix or carbonate.

Where the matrix forms a high proportion of the rock, chalcopyrite-pyrrhotite show schlieren type textures and the fragments become highly contorted, see Fig.3.9. Quartz and pyrite fragments become well rounded. Fragments within the pyrrhotite matrix tend to be smaller and show better rounding, indicating a concentration of shearing in this sulphide mineral. Contacts between breccia ore and other sulphide ore types range from sharp, where the breccia ore shows an increase in strain towards the contact, to gradational, in which breccia ore grades through ore composed of tectonic lenses to undisturbed ore. The presence of a pre-existing foliation within the fragments, now disorientated and folded, indicates a tectonic origin for the breccia. Textures such as rolled and contorted fragments, rounded pyrite and quartz fragments and increasingly finely streaked matrix towards the contacts, suggests that they have acted as zones of 'decollement' along which shearing has been concentrated, thus allowing differential movement of adjacant blocks. Breccia ore lenses and layers occur at contacts between chalcopyrite-pyrrhotite rich and massive pyrite ores, between chalcopyrite-pyrrhotite ore and silicate lithologies and as

a) Leve 75 synk

SE NW

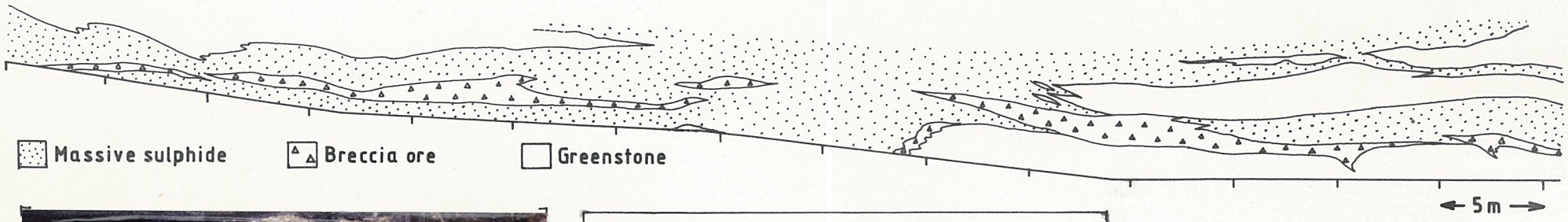

b)

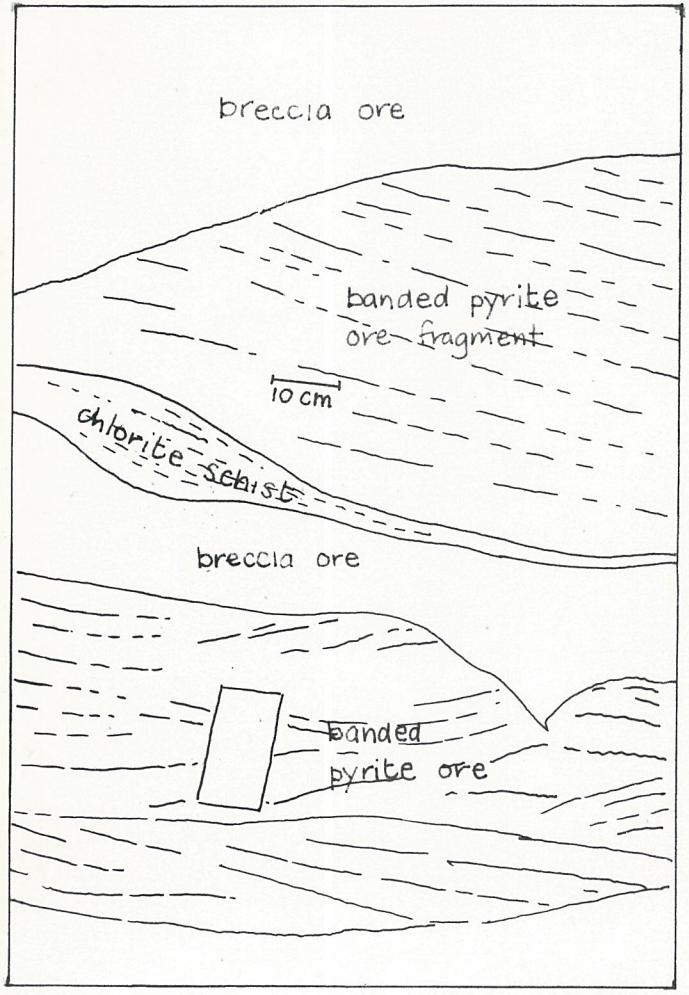

Fig.3.7 (a) En echelon lenses of breccia ore on the upper limb of an major F2 fold, from level 375. (b) photograph and corresponding sketch of a large pyrite ore fragment in breccia ore from level 387 ø.1.

Fig 3.8

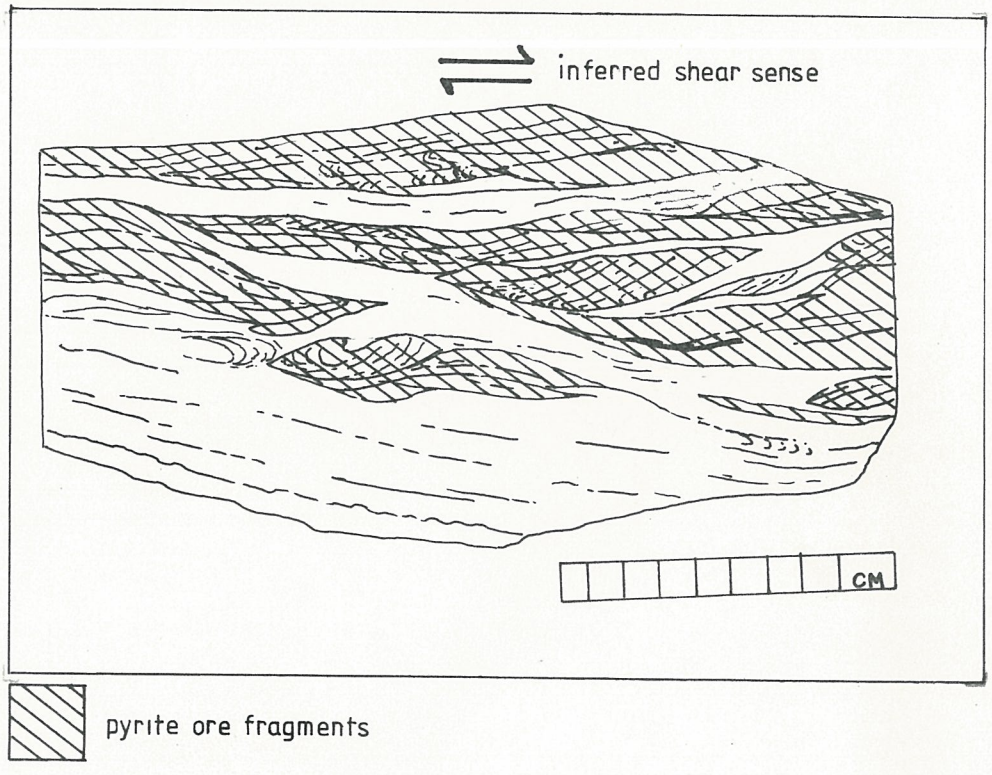

Fig.3.8 Photograph and corresponding sketch of slab showing tectonic lenses of pyrite ore in chalcopyrite-pyrrhotite matrix, from breccia ore, level 375.

Fig.3.9

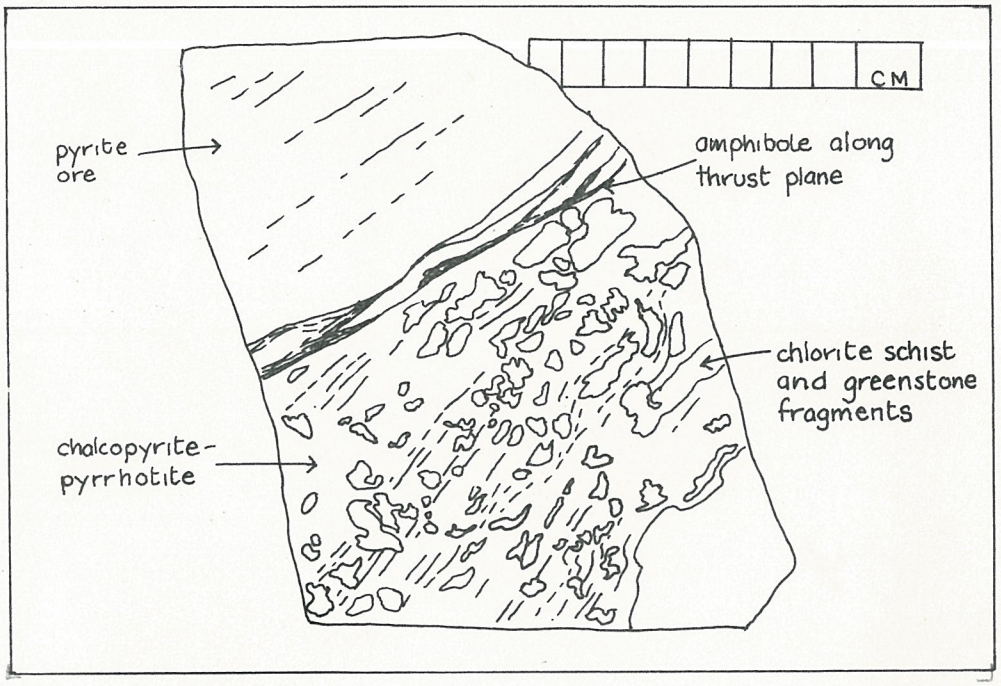

Fig.3.9 Photograph and corresponding sketch of breccia ore showing greenstone, chlorite schist, carbonate and quartz fragments in a chalcopyrite-pyrrhotite matrix, from level 375.

layers in greenstone adjacent to chalcopyrite-pyrrhotite ores. The fragmentation of silicate lithologies and pyrite ore types allows the migration of chalcopyrite and pyrrhotite within these zones and the presence of breccia ore layers in greenstone indicates that they have travelled distances of several tens of metres parallel to layering.

3.2.3 D2 Thrusting.

Eastwards from the western part of the ore body, the silicate and carbonate horizons become less abundant and chalcopyrite-pyrrhotite ores give way to dominantly pyrite ores, with locally abundant sphalerite. This transition is accompanied by a change in the style of the D2 deformation from folding to thrusting. Thus, in the eastern part of the ore body, large scale folds are rarely seen and the ore is composed of a series of thrust-bounded lenses. This results in local dramatic thickening and thinning of the ore horizon, e.g. on level 362, the massive sulphide unit thins from over 10m to 0.5m in thickness over a horizontal distance of some 50m. Smaller scale lenses of massive sulphide separated by greenstone are common at the terminations of larger lenses (Fig.3.10(a)), and thin layers of sulphide thrust into the greenstones commonly occur at massive sulphide lens contacts, see Fig.3.10(b). Within the massive sulphide lenses, thin (1mm to 0.5m) layers of chlorite schist, actinolite schist and carbonate, laterally continuous over several tens of metres, commonly separate different ore types, e.g. amphibole bearing from non-amphibole bearing pyrite ore (level 495) and chalcopyrite from pyrite ore (levels 362 and 387). These layers often split and rejoin, enclosing lenses of massive ore. Many layers show pinch and swell morphology, and in the thicker sections the S2 schistosity is commonly oblique to the contacts with massive ore. The obliquity of S2 shistosity and the separation of different ore types indicates that these layers mark the location of thrusts within the massive sulphide ores. These layers can be followed to the major sulphide-greenstone contacts where they are either cut abruptly by the contact or thicken and become layers of greenstone country rock.

As in the western part of the ore body, all sulphide-green-

a)

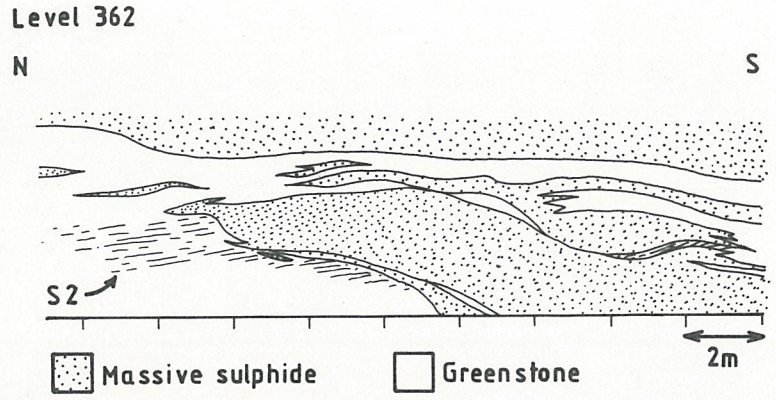

b)

Fig.3.10 (a) tectonic lenses of massive pyrite ore in greenstone showing sharp contacts which cross-cut S2 schistosity in the greenstones, from level 362. (b) photograph of thin thrust wedge of massive pyrite-sphalerite ore extending from main sulphide-greenstone contact, from level 429.

stone contacts are sharp and commonly display discordance with internal layering in the sulphides and S2 schistosity in the greenstones, showing that they are tectonic in nature. From the orientations of S2 schistosity and tectonic greenstone-sulphide contacts, intersections lineations were calculated and these are plotted in Fig.3.11(a). The intersection lineations show sub-horizontal plunges with highly variable trends, the highest concentration of which is parallel to L2 lineations, see Fig.3.11(c). Fig.3.11(b) shows a plot of poles to greenstone-sulphide contacts which form a point distribution with a maximum indicating a gently west dipping orientation. The intersection of the average S2 plane (from Fig.3.3(a)) with this average greenstone-sulphide contact, plots near the maximum of the intersection lineations of Fig.3.11(a).

3.2.4 D2 Sense of Shear.

As discussed in section 2.3.3, D2 deformation is associated with the main shearing event that led to the development of the nappe sequence, and is therefore dominantly simple shear. This is compatible with the widespread development of thrusting in the massive sulphides. Since thrusting takes place along the greenstone-sulphide contacts, (gently west dipping in the mine area) these contacts are equivalent to the shear plane while the shear direction is approximated by the L2 mineral lineation (gently northwest plunging).

In theory, folds develop with their axes perpendicular to the shear direction and their vergence can be used to tell the shear sense, see Fig.3.12(a). With increasing simple shear deformation, the fold axes rotate towards the shear direction, (Fig.3.12(a)). This effect is enhanced by the large competency differences which exist between the silicates and their sulphide matrix, so that F2 fold hinges rotate very rapidly into the shearing direction. All F2 fold axes measured are subparallel to the L2 mineral lineation (shear direction) and cannot therefore be used to determine the shearing sense.

The intersection between S2 schistosity and sulphide contacts, however, show a wide range of orientations from

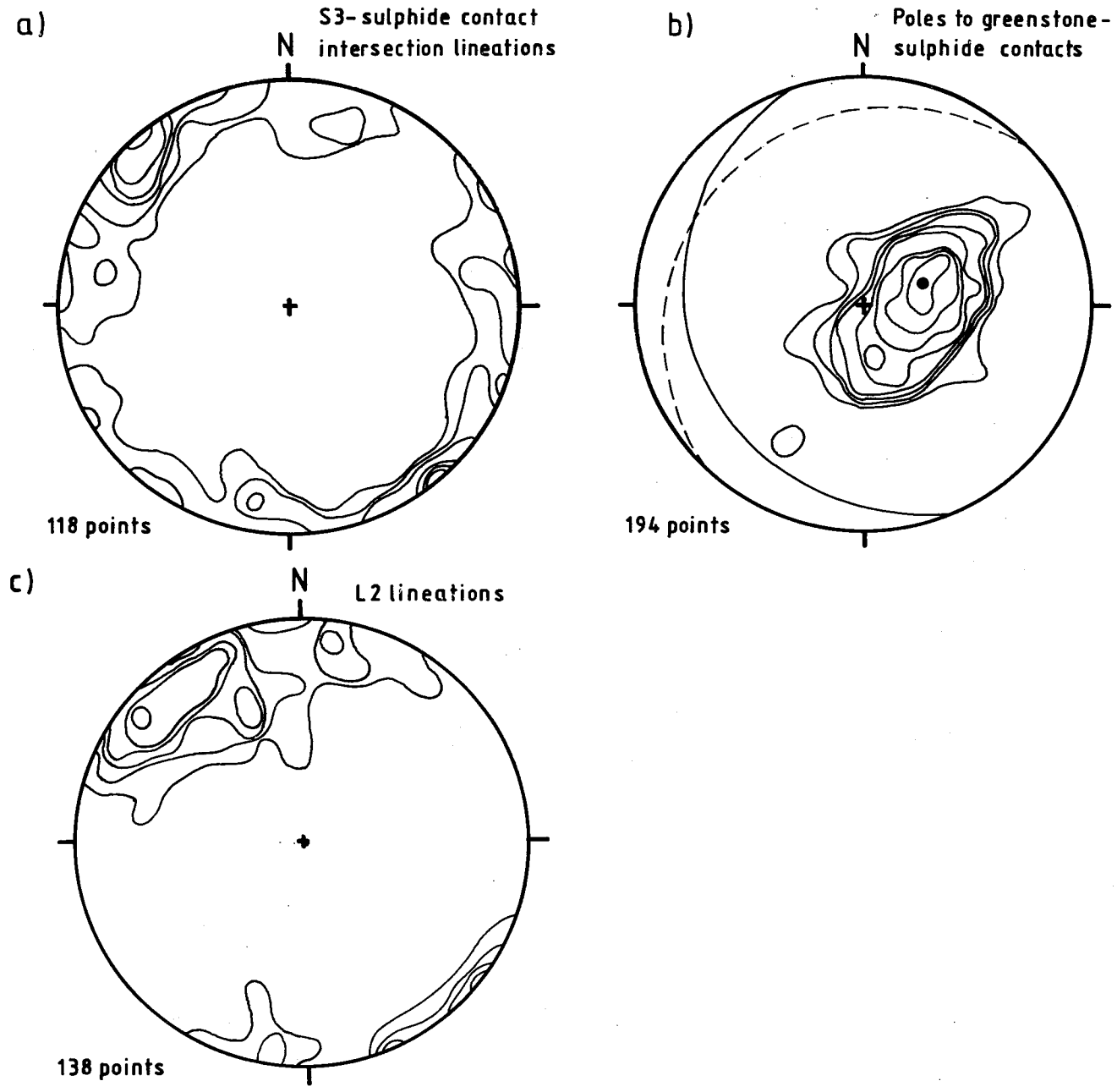

Fig.3.11 (a) stereoplot of intersection lineations formed by S2 schistosity in greenstone and greenstone-sulphide contacts. The maximum for the distribution is subparallel to the maximum for L2 lineations shown in (c). (b) poles to sulphide-greenstone contacts show a point distribution with a maximum indicating a gentle westerly dip. The intersection between this average contact and the average S2 schistosity lies subparallel to the maximum for the intersection lineations in (a).

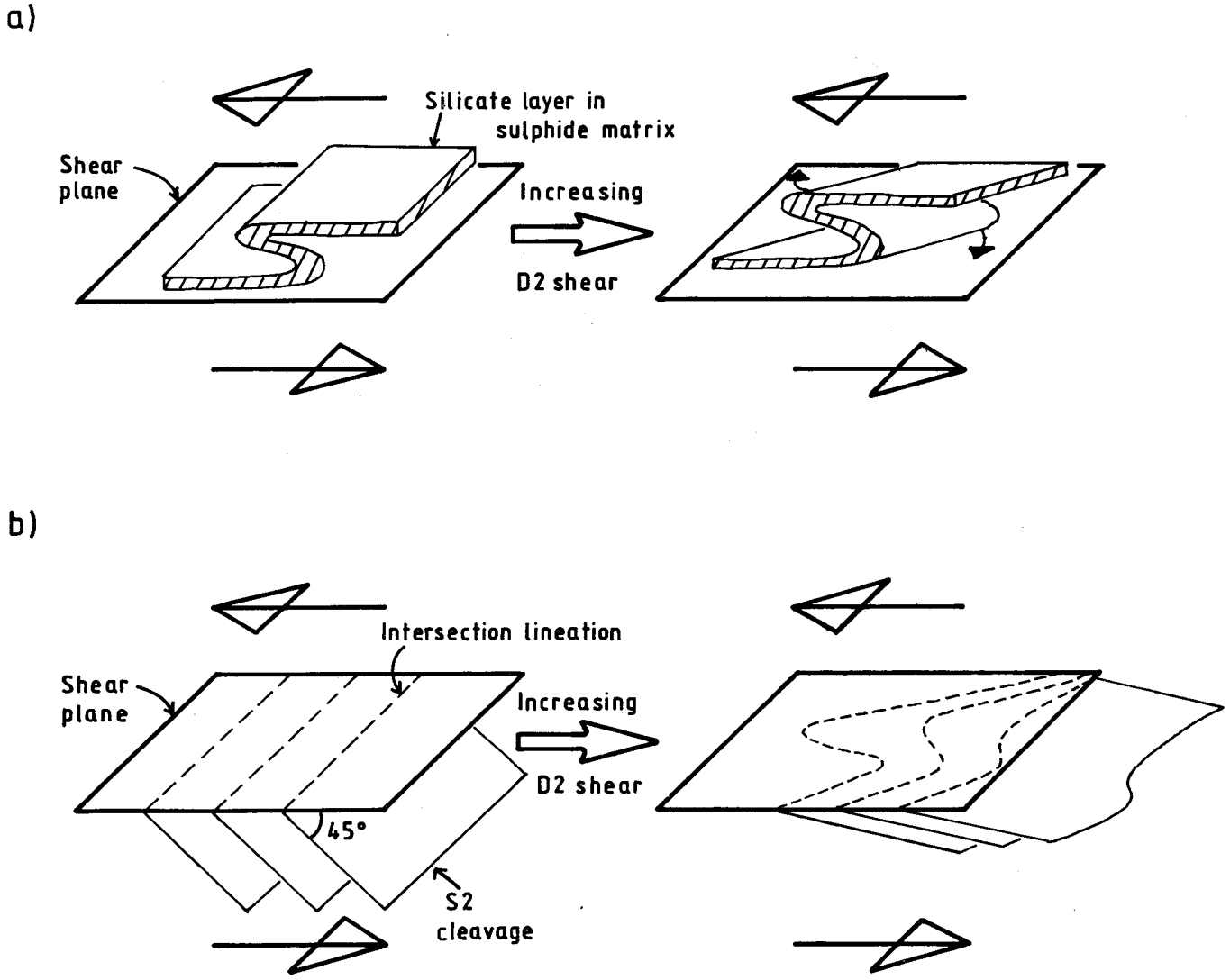

Fig.3.12 (a) sketch showing the behaviour of shear folds during simple shear deformation. When the folded layer has a competancy greatly exceeding that of the matrix, the fold hinges rotate rapidly into the shear direction. (b) sketch showing the relationship of S2 schistosity to the shear plane. Intersection lineations are initialy perpendicular to the shear direction but become highly variable with increasing shear.

perpendicular to parallel to the shear direction. In theory, the intersection between the cleavage and the shear plane is perpendicular to the shear direction throughout the deformation, see Fig.3.12(b). In practice, however, it's trend becomes highly variable as the schistosity approaches the shear plane and shows a tendency to rotate towards the shear direction (L2 lineation), see Fig.3.12(b), creating the pattern shown by the intersection lineations in Fig.3.11(a). Where the intersection lineation is oblique to the shearing direction, the relationship between the schistosity and contact orientations gives the shear sense.

The shear sense is most clearly seen in sections oriented subparallel to the L2 mineral lineation (shear direction) which trends northwest, e.g. on the north-south trending wall, level 362, Fig.3.10(a). Sections oblique to L2, show variable sense of shear due to the range of intersection lineation trends, e.g. the northeast trending wall, level 387 v.f., Fig.3.5(a). The relationship between schistosity and sulphide contacts in these sections indicates that, in the majority of cases, that the overlying rocks moved in a southeasterly direction. This shear sense is also indicated by the orientation of thrust lenses in the breccia ore (Fig.3.8), and from the thrust slivers of sulphide in greenstone at the margins of the massive sulphide lenses in the eastern section of the ore body. In some cases, the reverse sense of shear is indicated for internal thrusts marked by thin chlorite schist and greenstone layers. This suggests differential rates of movement between massive sulphide lenses, i.e. that some lenses have moved faster than others, such that reversed shear occurred on some internal slides.

3.3 D1 DEFORMATION

A penetrative schistosity pre-dating the dominant S2 schistosity has been described from the quartzitic phyllites, in section 2.3.4, indicating the presence of a D1 phase of deformation. In the ore horizon, if D2 were the first phase of deformation, original sulphide-greenstone contacts should be seen in the major F2 fold hinges, since thrusting is concentrated on the F2 fold limbs. However, the contacts in the F2 fold hinges

show similar characteristics to tectonic contacts on fold limbs and lenses of greenstone intercalated with the sulphides are folded in F2 hinges. Also, thin chlorite, greenstone and carbonate horizons thought to mark thrust planes and contacts between ore types observed to be cut by the sulphide-greenstone contact, are also folded in F2 hinge zones. These factors indicate that a phase of thrusting occurred before the development of the large scale F2 folds and this early deformation correlates with the D1 phase identified in the quartzitic phyllites. A few possible refolded fold patterns occur in F2 hinge zones, e.g. on level 382 (Fig.3.5(a)), but these patterns are difficult to interpret, due to the discontinuous and lens-like nature of the silicate lithologies within the sulphides. No early S1 schistosity or L1 mineral lineation has been identified and thus it is likely, as is the case in the quartzitic phyllites, that D1 is not a distinctly separate phase but an early expression of the D2 deformation which has become refolded later in the same event.

3.4 D3 DEFORMATION

D3 deformation is expressed in the ore body as tight to open F3 folds which are superimposed on D2 structures. They are associated with an S3 crenulation cleavage which is developed in the greenstones and silicates intercalated with the suphides. F3 folding is most intense in the western part of the ore body, causing a steepening of the dip. D3 deformation is inhomogeneous, and F3 folds occur in stacks which form lens-like pods of intense D3 deformation. Within a stack, individual folds are discontinuous both along and across the strike of their axial planes.

3.4.1 Variation in F3 Fold Attitude.

F3 Fold axial planes are moderately to steeply northwest dipping in the greenstone country rocks, and show similar orientations to those for the Joma area. F3 folds which fold the greenstone-sulphide contacts commonly become more shallowly dipping in the sulphides and approach F2 axial plane

orientations. Fold axes trends become highly variable and, in some cases F3 folds, identified by the folded S2 schistosity, show F2 axial plane and axis orientations. Fig.3.13(a) shows F3 fold axial planes and crenulation cleavages, and Fig.3.13(b) shows F3 folds axes and L3 intersection lineations. The distribution of poles to F3 axial planes in Fig.3.13(a) shows a maximum corresponding to a moderately dipping axial plane with a trend towards more shallow dips. The F3 fold axes and L3 lineations show a maximum at subhorizontal, northeast-southwest trends, and a further trend towards more westerly plunges. The maximum for both distributions corresponds to the general directions found for zone B of the Joma area, shown in Fig.3.13(c) and (d), and thus the additional trends towards more shallow axial planes and more westerly fold axis plunges are due to the effects of deformation in the sulphides. A plot of axial plane dip against axis plunge in Fig.3.14, shows that as the fold axial plane becomes more shallowly dipping, the axis plunge directions become more variable and includes more westerly trends.

3.4.2 Reactivation of D2 Structures During D3.

Adjacent thin chlorite and actinolite schist layers and greenstone-sulphide contacts, marking D2 thrust planes, often show markedly differing intensities of F3 folding, see Fig.3.15(a). Similar features are shown by greenstone lenses with F3 folds which do not penetrate the lower thrust contact (Fig.3.15(b)), and by folds in the greenstone-sulphide contact which do not penetrate the layering in the immediatly overlying sulphides (Fig.3.15(c)). All of these features indicate that the shortening caused by D3 folding has also reactivated the D2 thrust planes, allowing the adjacent rocks to remain undisturbed. The breccia ore, the location of intense D2 shearing, also occasionally shows reactivation in F3 hinge zones, where the chalcopyrite-pyrrhotite matrix has penetrated along F3 axial planes and partially broken up the chlorite schist layer adjacent to the breccia ore, see Fig.3.16.

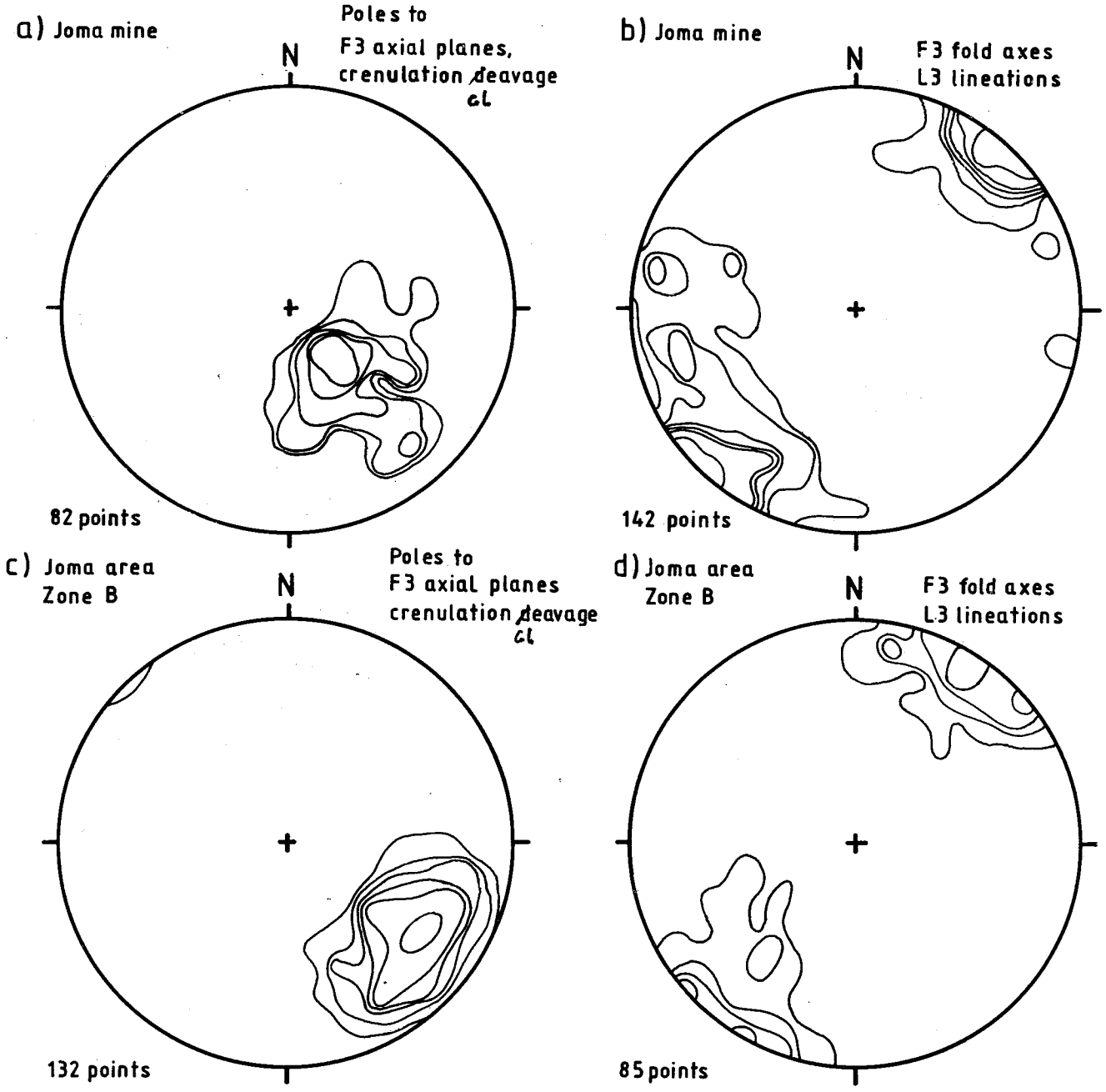

Fig.3.13 Stereoplots showing D3 structures of the mine compared with those of the area containing the ore body outcrop. Comparison of (a) and (c) shows the flattening of S3 cleavage and F3 axial planes in the sulphides, and comparison of (b) and (d) shows the rotation of L3 lineations towards the shear direction (L2 lineation maximum).

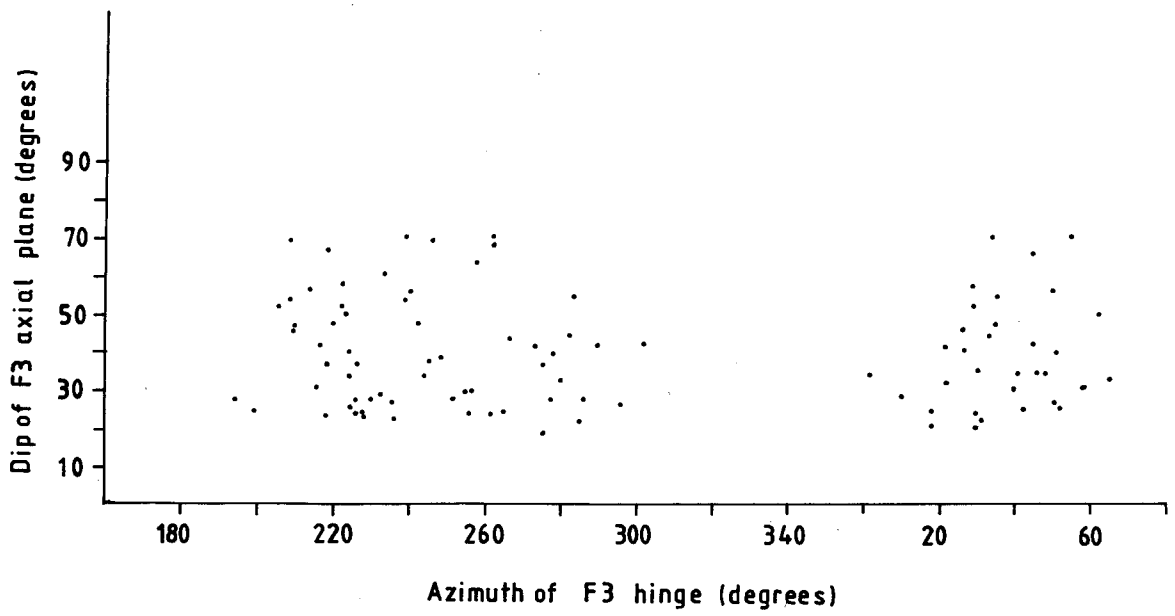

Fig.3.14 Graph showing the relationship between F3 axial plane dip and F3 fold hinge trend. The plot shows that as the dip of F3 axial planes decreases, hinge trends cover a wider range towards more westerly trends.

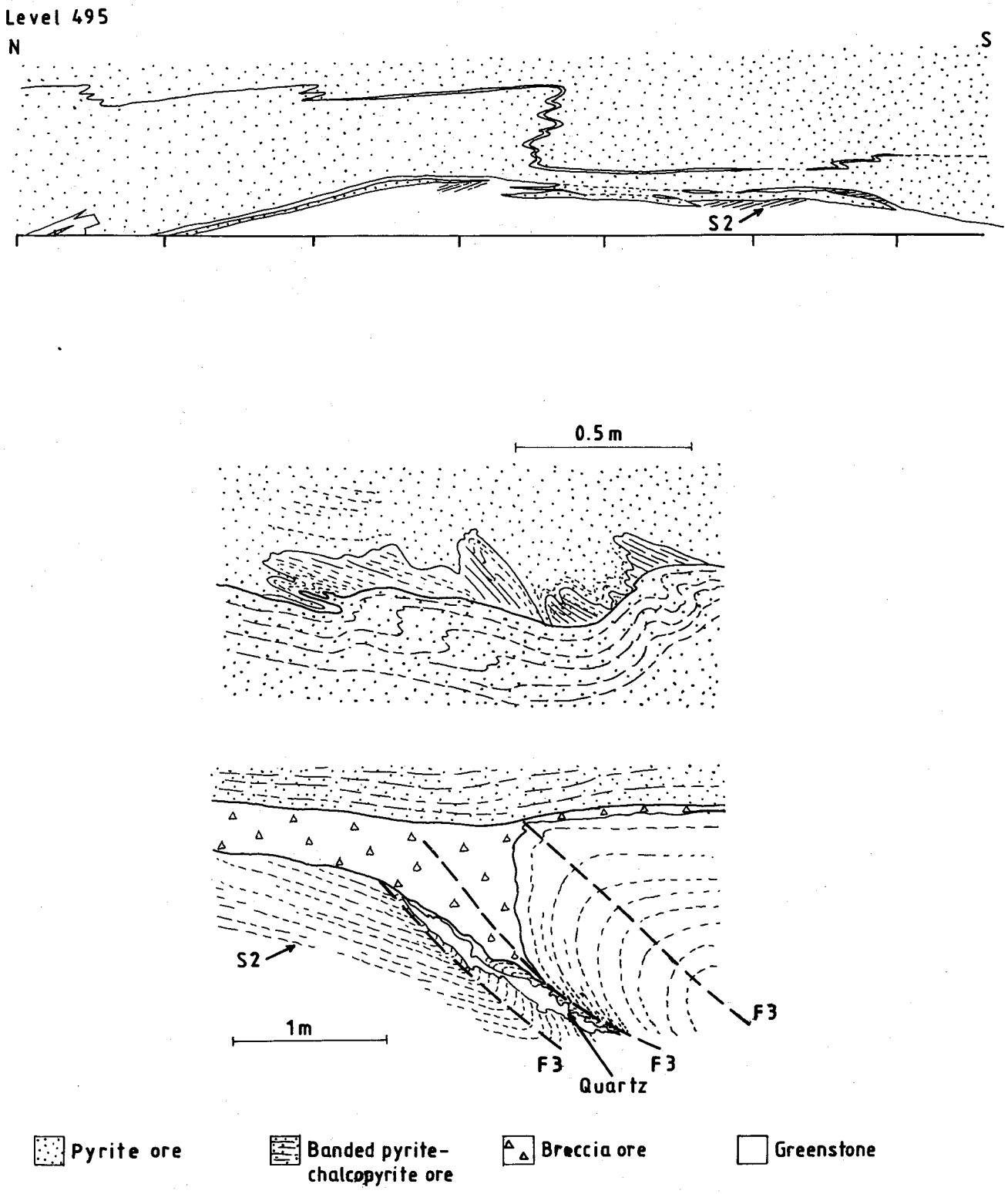

Fig.3.15 Reactivation of D2 slides during D3. (a) F3 folds in a thin chlorite schist layer do not penetrate the main sulphide-greenstone contact, level 495. (b) minor F3 folds in a greenstone lens, lying on a D2 thrust plane, do not fold the lower contact. (c) F3 fold in sulphide-greenstone contact does not fold the layering in the overlying sulphides. In all cases the discrepancy in D3 shortening has been accomodated by slip on D2 thrust planes.

a)

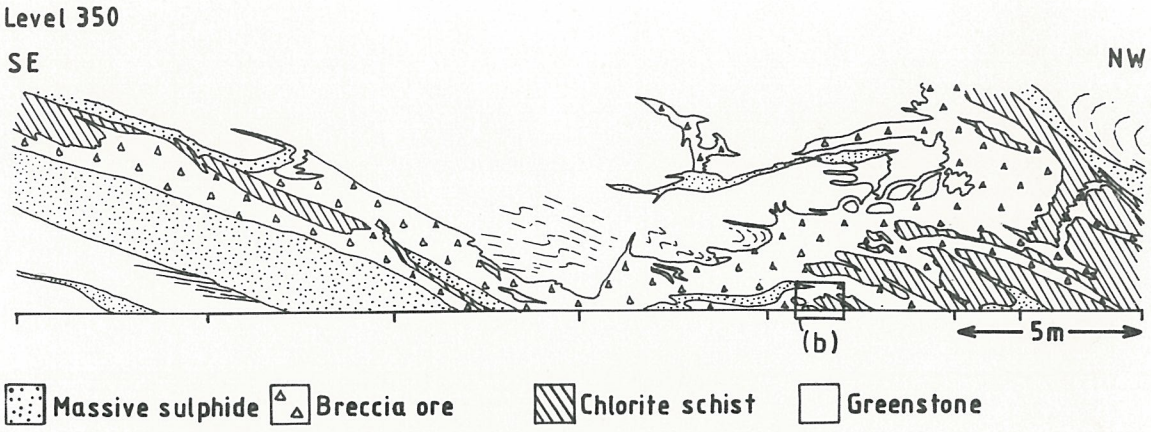

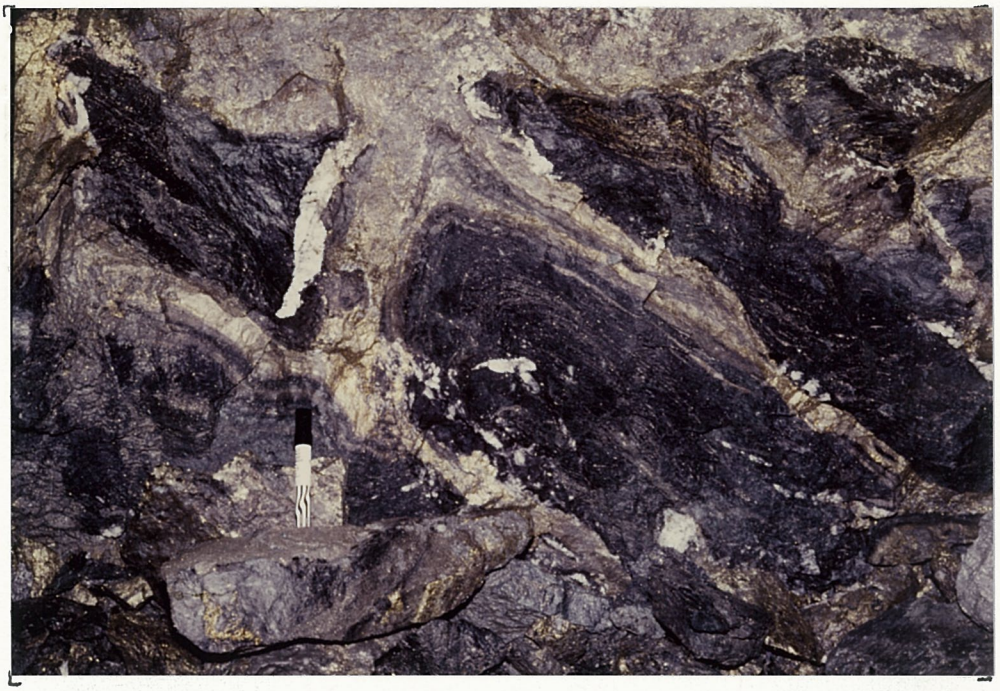

Fig.3.16 (a) reactivation of breccia ore in hinge zone of major F3 fold. The chalcopyrite-pyrrhotite matrix has penetrated along the F3 axial planes and fractures, resulting in the breakup of the chlorite schist layer. (b) photograph of the section outlined in (a).

3.4.3 D3 Veins and Fractures.

Abundant veins cut the S2 schistosity and therefore belong to the D3 phase of deformation. Fracturing is most intense within the greenstones adjacent to the massive sulphides, but also occurs in silicate layers intercalated with the sulphides, and to a lesser extent within massive pyrite ore. Veins range from a few cm to 2m long and from a few mm to 15 cm broad. Their morphology ranges from vein-like to lens-shaped and they occur as single fractures or in en echelon sets, see Fig.3.17. Fractures are filled dominantly by quartz and calcite, with variable amounts of chlorite, actinolite, chalcopyrite and pyrrhotite. Calcite occasionaly shows curved fibrous growth at a high angle to the fracture walls. Fracture edges are most commonly straight, but can also show complexly stepped margins.

Poles to fracture planes are plotted in Fig.3.18 which shows two maxima, one more diffuse corresponding to dipping steeply to moderately dipping fracture planes and a second corresponding to steeply southeast dipping fractures. The dominant set of fractures lies subparallel to S3 and is most commonly located along F3 axial planes. This set contains the largest veins which often show offset across adjacent edges in agreement with the sense of shear required to produce F3 folds. The subdominant set, dipping steeply southeast, are smaller and show no or minor amounts of offset with the opposing sense of shear to that shown by the dominant set. The two sets variably offset each other or converge to a common area where the offset sequence is indiscernible and they are therefore coeval. In the greenstones, where fractures are most abundant, the two sets form trellice like network of veins, see Fig.3.17(b).

3.4.4 Peircement Structures.

In silicate layers within the sulphides and at greenstone-sulphide contacts, F3 folds have developed into 'piercement structures'. In these structures, the F3 folds have developed tight synforms with associated fracturing of the silicate lithology along the axial plane. Such piercement structures are most abundant in the western part of the ore body where F3

Fig. 3.17

(a)

(b)

Fig.3.17 (a) photograph of lens-shaped, calcite-chlorite filled D3 fractures in greenstone. (b) photograph of abundant F3 veins forming a trellice like network in greenstones.

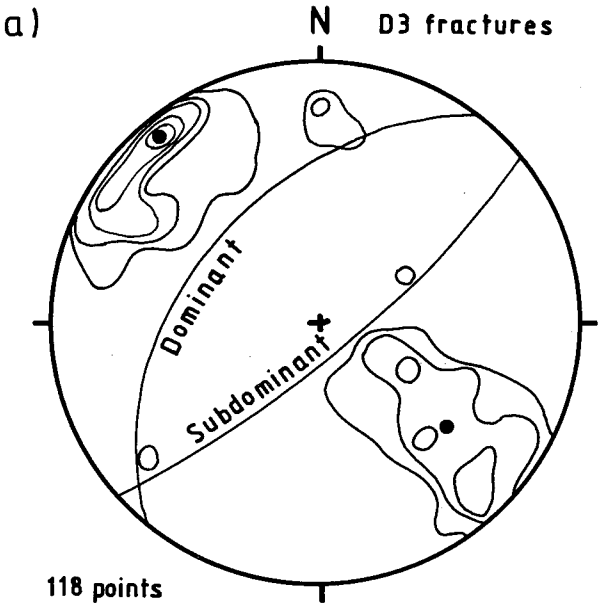

Fig.3.18 Stereoplot showing the distribution of D3 fractures and veins. The distribution shows two maxima, representing the dominant set subparallel to F3 axial planes dipping moderately northwest, and the subdominant set of subvertical, northeast trending fractures.

folding is most intense. They are found dominantly within chlorite schist layers in the chalcopyrite-pyrrhotite ores, and in greenstones adjacent to the sulphide contact. They occur rarely within albitite layers intercalated with the sulphides. The majority of piercement structures develop in synformal F3 folds but also occasionaly occur in antiformal folds. Their development is confined to F3 folds.

From a study of F3 folds in various stages of piercement structure development, the evolution of the structures can be traced. An F3 fold with a rounded antiform and tight synform is developed, see Fig.3.19. The layering in the adjacent sulphides together with included layers of other silicate lithologies and carbonates, follows the fold outline. A fracture develops along the overturned F3 limb and sulphides, preserving their original layering, penetrate along the fracture. At a later stage of fracture development, movement occurs along the fracure, opening up a parallelogram-shaped space which is then filled dominantly by calcite and quartz with lesser chlorite, stilpnomelane, amphibole, chalcopyrite, pyrrhotite and sphalerite. Initial fracture deposits, often calcite, show fibrous growth of crystals perpendicular to the fracture walls, and it is probable at this stage that crystal growth keeps pace with the rate of fracture opening. This is succeeded by a non-fibrous, coarse-grained mass of other minerals which probably grew in an open fluid filled space. The fracture so developed penetrates the whole layer if layer thickness is less than about 0.5m. In thicker layers, fractures do not penetrate the whole layer but isolated lenses and discontinuous veins are developed along the continuation of the fold axial plane. As the deformation proceeds these fracture fillings can become folded or boudinaged themselves and the original parallelogram shape deformed into an 'double axe-head' shape (Fig.3.20), and finally into separated lenses of vein material. A diagrammatic representation of this evolution is shown in Fig.3.22.

3.5 RELATIONSHIP BETWEEN D2 AND D3 DEFORMATION PHASES.

From the analysis of the Joma area, D3 deformation has

Fig. 3.19

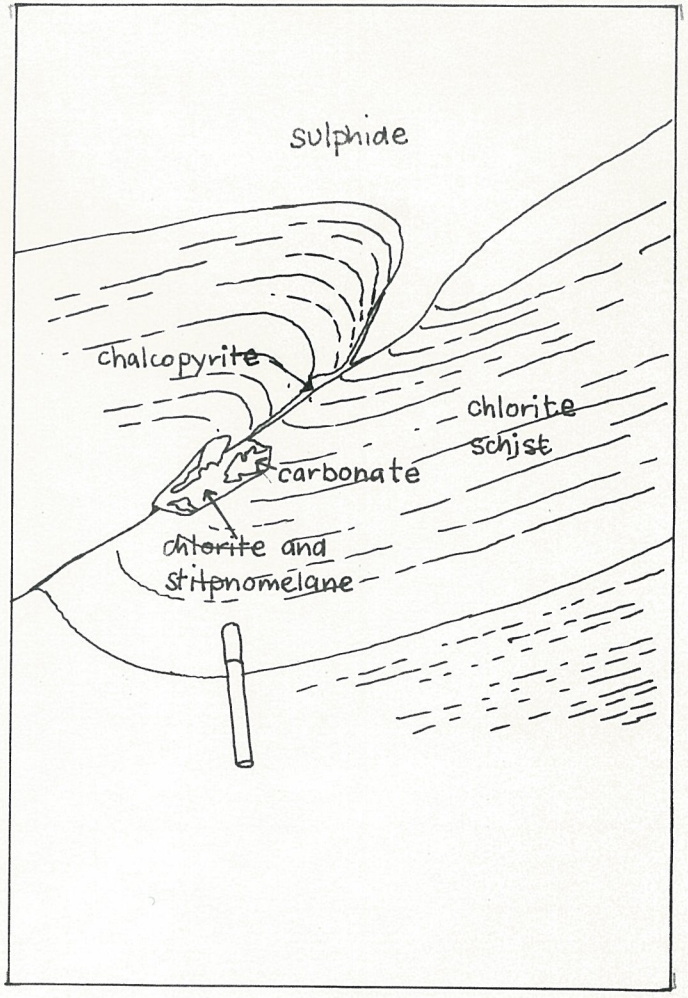

Fig.3.19 Photograph and corresponding sketch of a piercement structure formed in a chlorite schist layer in massive sulphides showing a tight synform in the upper contact. Sulphide has been mechanically emplaced along part of the axial planar fracture and the remainder is filled with calcite, quartz and chlorite.

Fig. 3.20

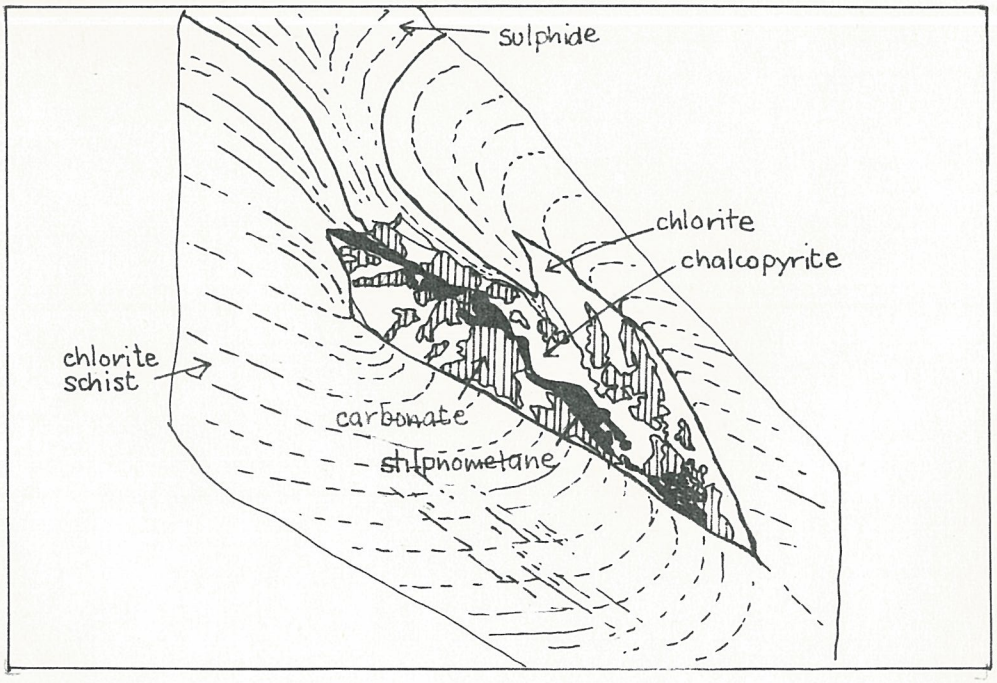

Fig.3.20 Photograph and corresponding sketch of piercement structure detail showing parallelogram-shaped open fracture now filled with calcite, quartz, chlorite, stilpnomelane and chalcopyrite.

resulted from shear on a similar shear plane orientation, direction and sense to D2. The reactivation of shear on D2 planes, and the vergence of D3 folds also indicate a similar shear plane orientation, direction and sense during D2 and D3 phases in the massive sulphide deposit. The large competency contrast that exists between sulphide and silicate lithologies, has led to a greater intensity of D3 deformation in the sulphides than in the adjacent greenstone country rocks. Thus D3 structures in the sulphides show features attributable to higher strains than those in the greenstones. The flattening of the F3 axial planes towards S2 and the increase in the range of the fold axes orientations towards northwesterly plunges indicates modification due to shear on the D2 shear plane orientation in the L2 direction. F3 axial planes in the adjacent greenstones show axial planes which dip moderately northwest, at approximately 45° to the average greenstone-sulphide contact, the angle at which cleavage first develops in a shear zone, see Fig.3.21(a). F3 folds in the sulphides have suffered more intense shearing which has rotated the axial planes towards the D2 thrust planes and axes towards L2, as indicated on Fig.3.21(b).

Fracturing and vein development, a marked feature of D3 deformation, shows a close relationship to the D2 shearing event, see Fig.3.21(a). The dominant set of fractures which is subparallel to S3, lies at approximately 45° to the D2 shear plane while the subdominant set lies at 90°, representing a conjugate shear set to the D2 shear plane. Using the L2 maximum as the shear direction, the two sets of fractures intersect close to the D2 strain Y direction and are therefore compatible with D2 deformation.

The orientation of the dominant set of fractures indicates that, under homogeneous simple shear strain, they should progressively close. Thus the extensive development of this set of fractures in the greenstones immediately adjacent to the massive sulphides and in the silicate layers within the sulphides implies tensile stress during D3 deformation in a direction approximately parallel to D2 shearing. Ptygmatic folding of silicate layers in F2 hinge zones and the flattening of F3 folds in the sulphides indicates that the sulphides have a much lower

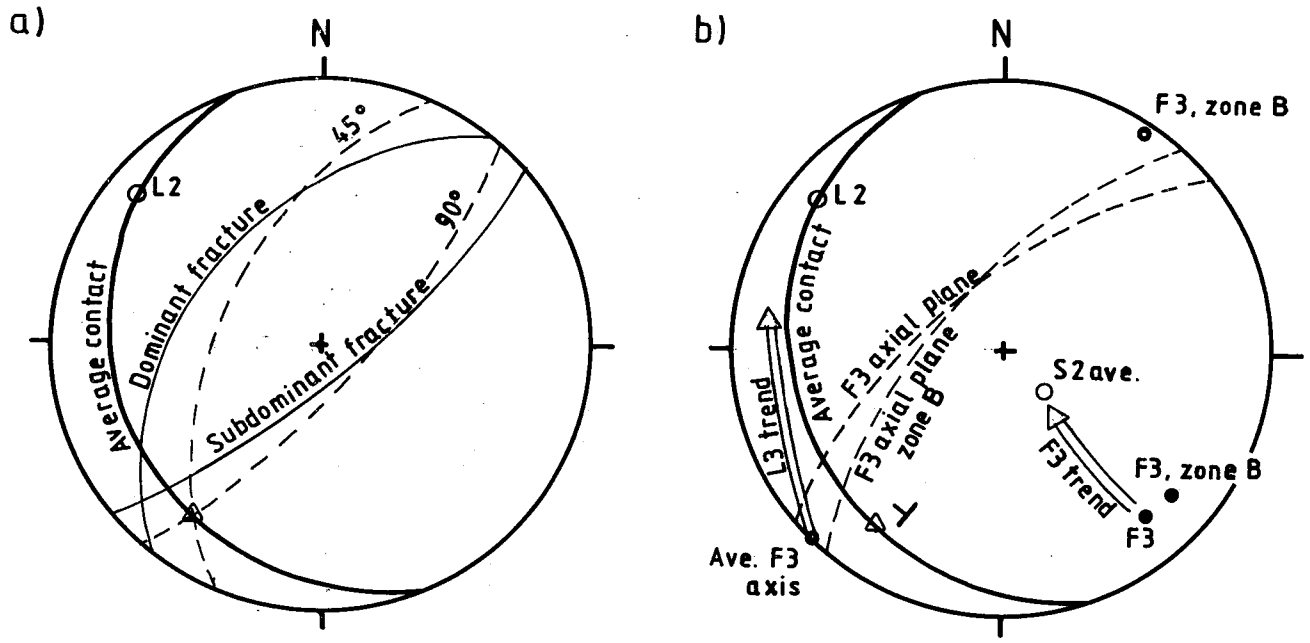

Fig.3.21 Stereonet showing the relationship bewteen (a) F3 fractures, sulphide-greenstone contacts (D2 shear plane) and L2 lineations (shear direction) and, (b) F3 fold axial planes and axes, sulphide-greenstone contacts (shear plane) and L2 lineations (shear direction).

competency than the greenstone country rocks and intercalated silicate layers. This competency difference leads to a concentration of deformation and thus greater extension in the sulphides than in the silicate lithologies. The silicates respond with boudinage initiated by fracturing in thinner layers enclosed in sulphide and by the development of extension fractures parallel to S3 crenulation cleavage in thickerlayers and the greenstone country rocks.

During D2 deformation, the differing amounts of deformation in sulphides and silicates were accomodated by movement along thrust planes. This led to the development of tectonic lenses and layers of sulphide which have been thrust into the country rocks. Fracturing and vein development occured largely along these thrust planes or parallel to S2 schistosity in the country rocks. During D3, the formation of the Joma synform and associated folds effectively locked the D2 thrust planes for all but minor movement. The greater amount of shearing occuring in the sulphides than in the greenstone country rocks could not then be accomodated by movement along thrust planes and the resulting tension developed in the greenstones initiated extensive fracturing. This accounts for the greater intensity of fracturing during D3 than D2 deformation.

Piercement structures show evidence of both shortening by folding and extension by fracturing. Any layer oriented oblique to the shear plane at an angle greater than 90o to the shear direction will suffer shortening under simple shear and folding if a competency contrast exists, see Fig.3.22(a). If the layer has a competency close to that of the matrix, folding will continue and the layer will be rotated through large angles until it is finally extended again by the same simple shear deformation. However, where competency contrasts are large, rotation towards the shear plane, contrary to that expected from simple shear alone, can occur and this provides a possible mechanism for the formation of the piercement structures, see Fig.3.22(b).

A layer orientated slightly obliquely to the shear plane begins to fold, simultaneously rotating against the shear

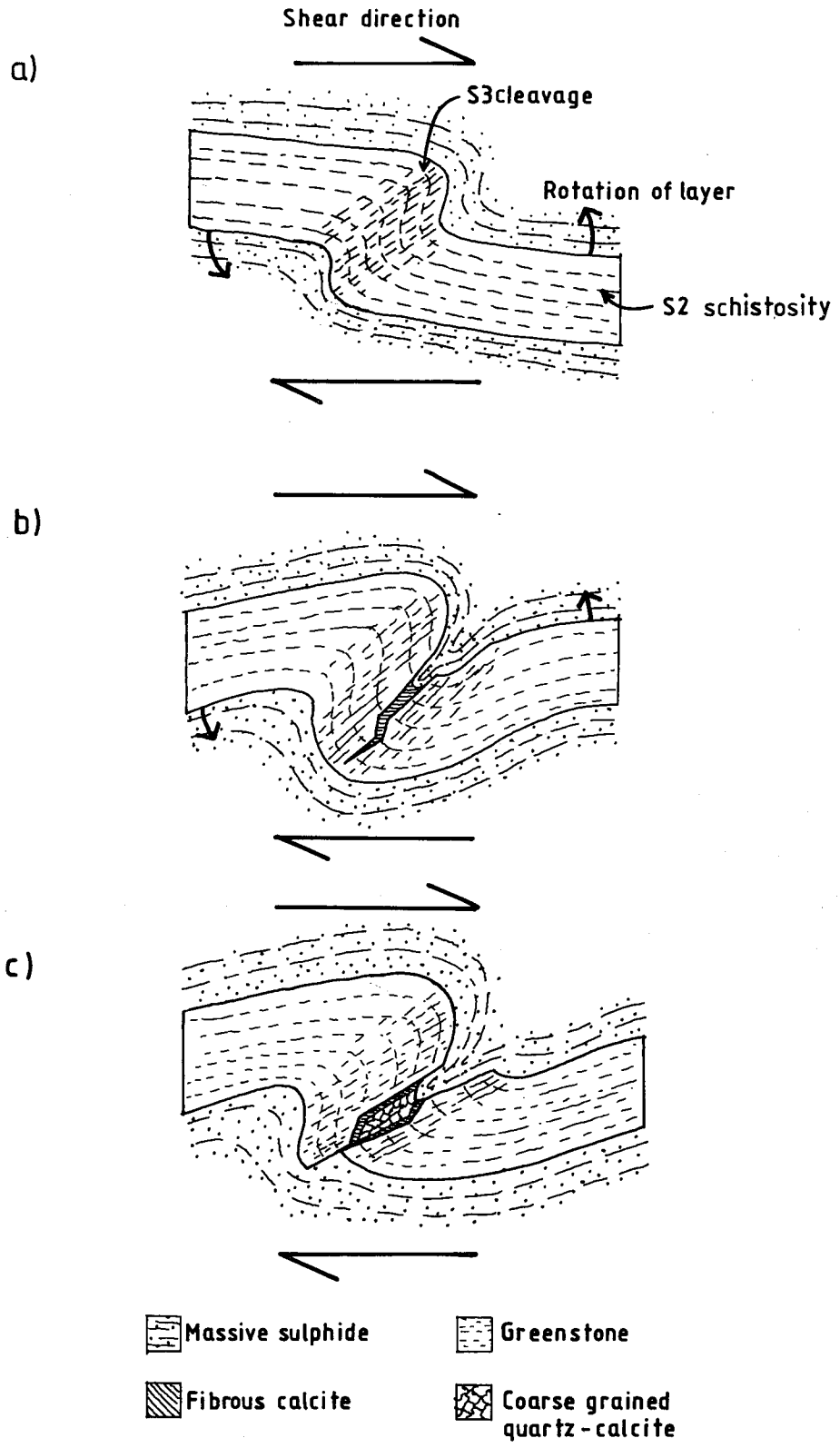

Fig.3.22 A model of piercement structure developement. (a) a silicate layer in sulphide developes an F3 fold with a sharp synform. (b) after rotation of the layer towards the shear plane, a tension fracture developes along the axial plane which is filled with fibrous calcite. (c) movement along the fracture results in an open void which fills with calcite and quartz.

direction towards the shear plane. The layer thus rotates into a position where extension rather than shortening occurs and fracturing and boudinage result. Other layers, initially parallel to the shear plane or in an orientation favourable to extension, show boudinage alone with no initial F3 folding. Thus very small differences in layer orientation with respect to the greenstone-sulphide contacts can result in folding followed by boudinage, i.e. piercement structure development, or boudinage alone. Once folding and rotation has occurred, fracturing is encouraged by the development of S3 crenulation cleavage in the F3 fold axial planes, which provides a plane of weakness in a suitable orientation. As the majority of piercement structures are synformal, it is probably that the difference in density between the sulphides and silicate lithologies has played a part. Thus, the overlying, heavier sulphides encourage the development of sharp cuspate synforms, which are an the early stage of piercement structure developement.

3.6 ORE BODY GEOMETRY.

The major D2 and D3 structures described in the previous sections can be traced throughout the ore body using selected profiles contructed for the upper part by Olsen (1978) and for the lower sections by Reinsbakken (1986). F2 and F3 hinge lines were traced through the profiles using the ore body footwall, and contours constructed on the footwall itself. Horizontal projections of F2 and F3 hinges and contours on the ore body footwall are shown in Fig.3.23, 3.24 and 3.25.

Fig.3.23 shows the major F3 hinge traces in the ore body footwall with their steep, overturned limbs shaded. They show the characteristic northeast-southwest F3 trend and are clustered in the western part of the ore body where D3 is most intense. The folds plunge overall gently southwest, in agreement with minor F3 folds and L3 lineations in the ore body and with those of the Joma area, (section 2.3.2). The lens-shaped patterns shown by the steep limbs shows that, similar to minor F3 folds, they are laterally impersistent.

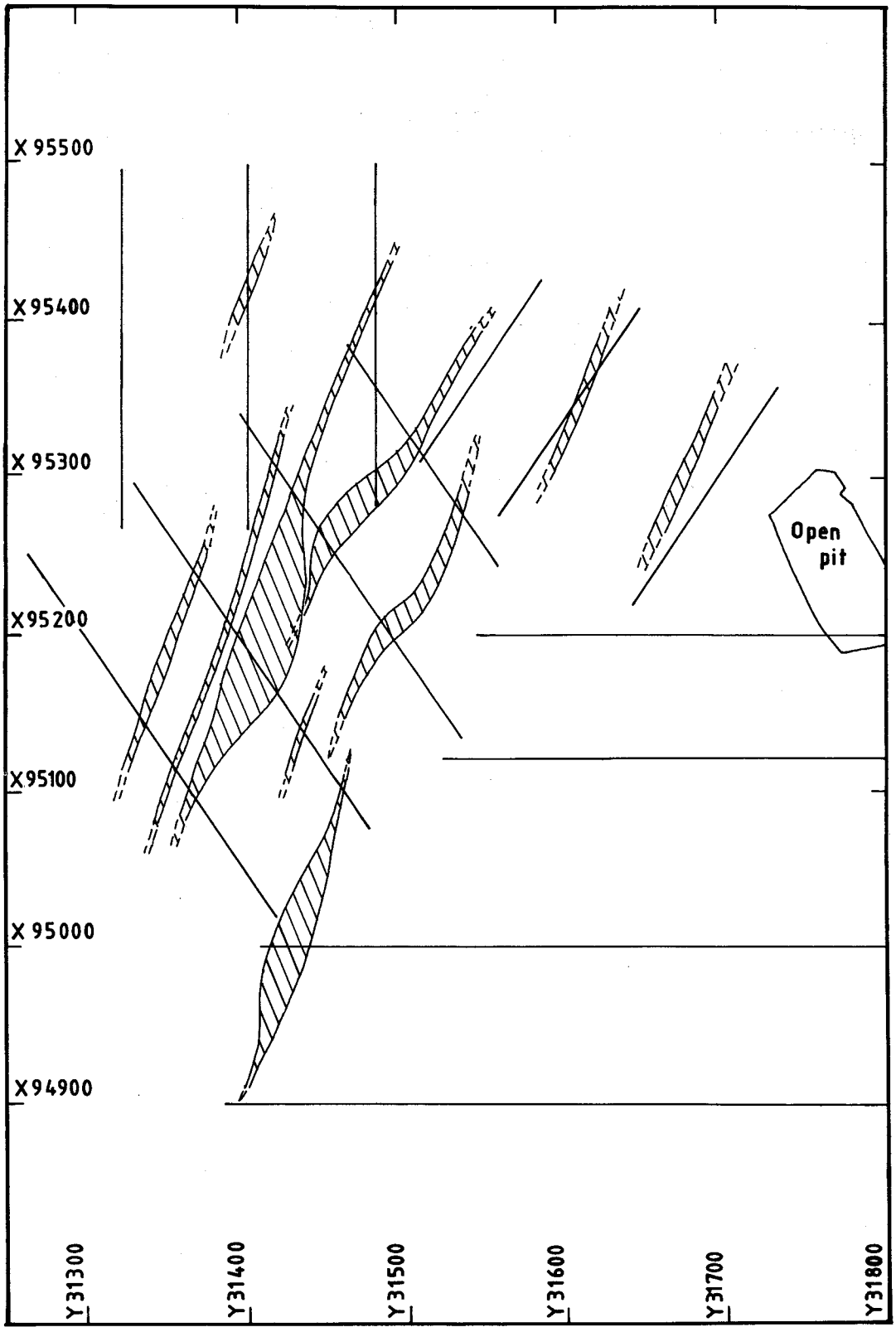

Fig.3.23 Map of major F3 fold hinge traces in the ore body footwall throughout the Joma mine. Steep F3 limbs are shaded. F3 folds are concentrated in the western section of the ore body.

Fig.3.24 shows the major F2 fold hinge traces in the footwall of the ore body where they are least disturbed by D3. Short overturned F2 limbs are shaded. F2 hinges show the characteristic northwesterly trend of L2 lineations with some deviation to the west in the northern part of the ore body due to folding by the D3 Joma synform. The folds are gently northwest plunging in the eastern part and gently southeasterly plunging in the western and northern parts of the ore body. Hinges in the eastern part of the ore body, where D2 thrusting is dominant, represent the tips of thrust wedges. These can be traced westwards into the major F2 folds showing that the major F2 folds develop into thrust wedges as the ore type changes from chalcopyrite-pyrrhotite rich ores with intercalated silicate and carbonate horizons, to massive pyrite-sphalerite ores.

Fig.3.25 shows the contours constructed for the orebody footwall. The ore horizon dips gently east in the eastern part and is folded by the Joma synform to dip gently southwest in the northern part. In the western section, F3 folding is intense, causing the ore horizon to dip generally steeply to moderately east to southeast. The influence of the zone of F3 folding is minor in the north and becomes increasingly intense to the south, showing that the whole F3 zone is discontinuous. F2 folding causes tight folds in the contours. In the northeastern part of Fig.3.25, the enclosed contours are caused by the presence of a large thrust wedge of massive sulphides that is exposed at the surface as the 'elvegangen'.

In order to show the relationship between ore types, deformation styles and phases and the morphology of the ore body, a diagrammatic east-west section through the ore body has been constructed combining all the major features, Fig.3.26(a). This section shows the major ore lithologies and lies oblique to F2 and F3 fold trends. The eastern section of the ore body, composed dominantly of pyritic ores, forming a series of en echelon D2 thrust lenses. Thin silicate and carbonate horizons mark the location of thrust planes inside the sulphides. Westwards, the ore grades into chalcopyrite-pyrrhotite rich ores with intercalated silicate and carbonate layers and the style of D2 deformation changes to folding with thrusting developed on the

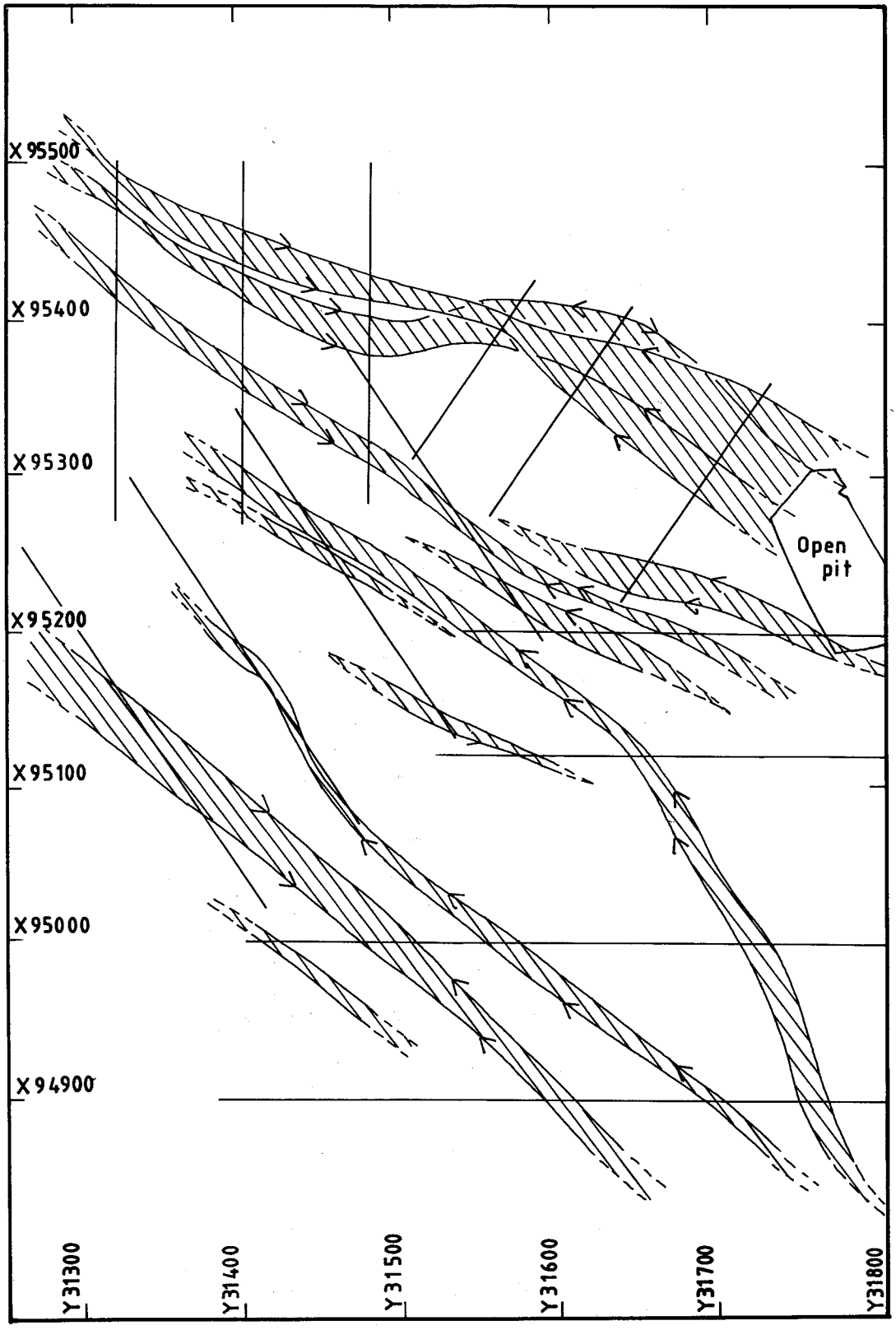

Fig.3.24 Map of major F2 fold hinge and thrust wedge tip traces in the ore body footwall throughout the Joma mine. Overturned short limbs of folds are shaded. Tips of thrust wedges in the eastern part of the ore body pass into fold hinges in the western part.

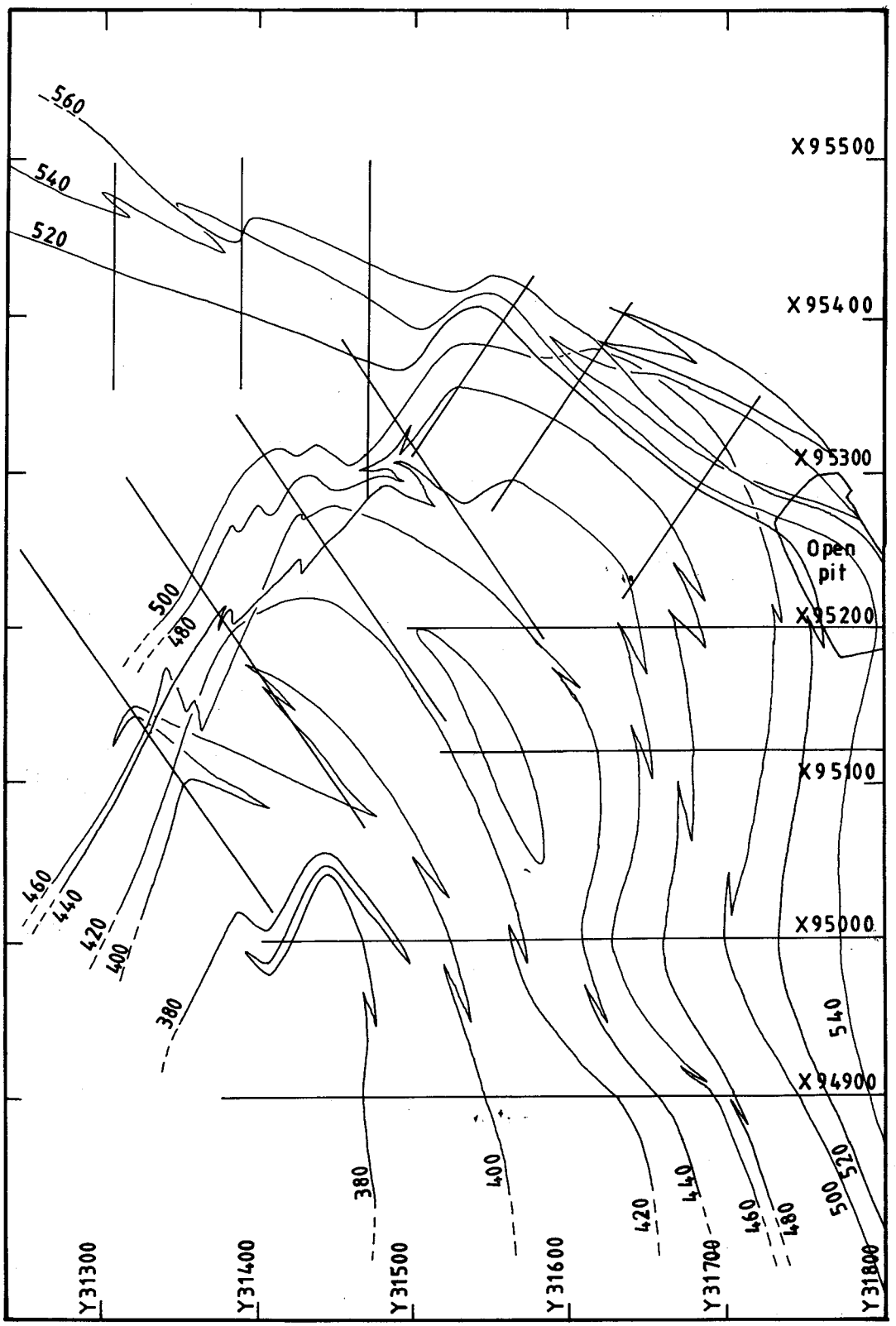

Fig.3.25 Contours in the ore body footwall throughout the Joma mine. The footwall contact dips gently southwest in the eastern section of the ore body and is folded in the western section to become steeply east dipping.

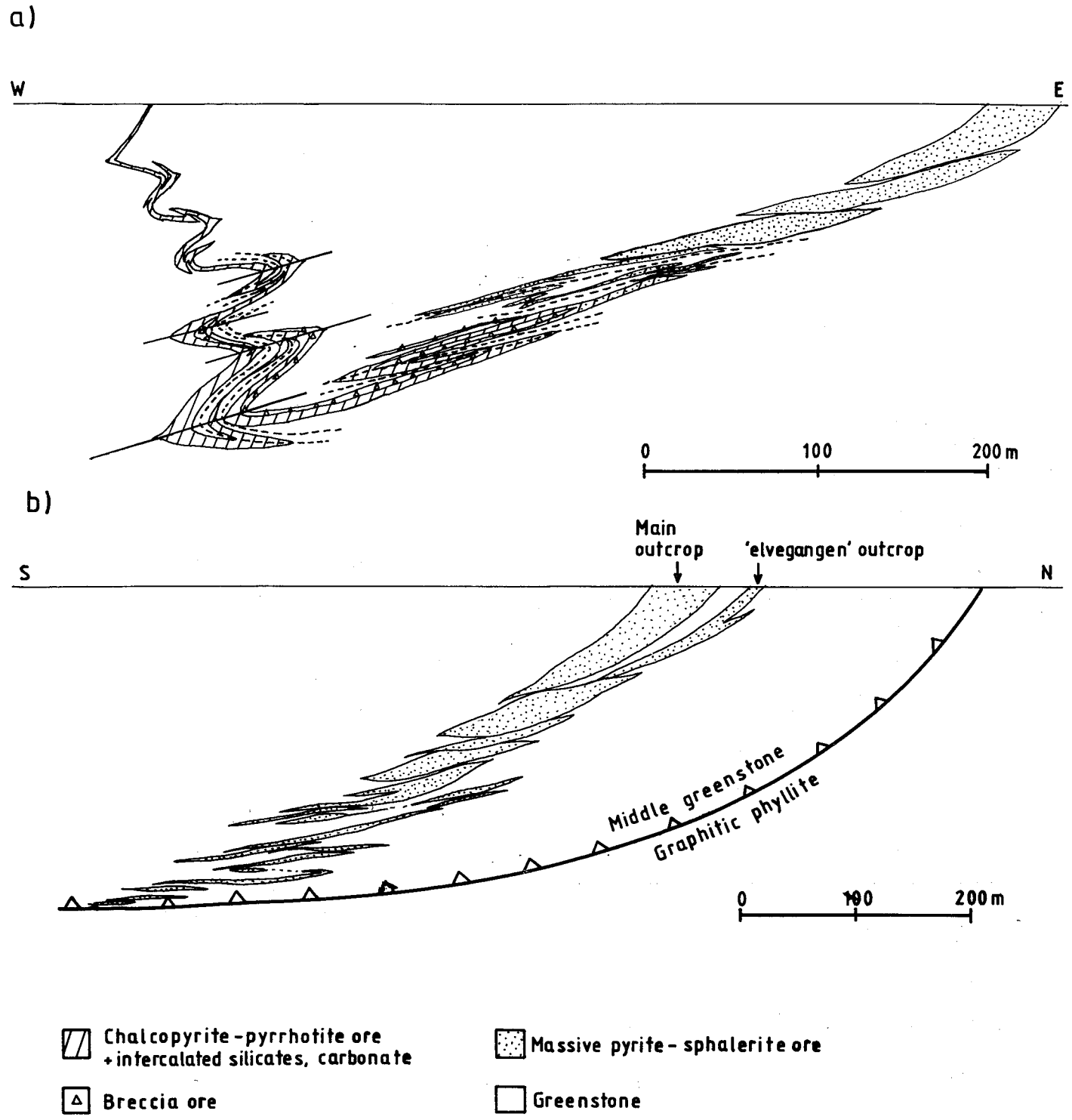

Fig.3.26 (a) diagrammatic east-west section through the Joma ore deposit showing changes in D2 deformation style from thrusting in the east to folding in the west. F3 folds refold F2 folds in the west. (b) diagrammatic north-south section through the Joma ore body showing the increase in intensity of D2 deformation towards the middle greenstone lower thrust contact. The ore body is cut at depth by the thrust.

fold limbs. The short F2 fold limbs are commonly thrust out, while breccia ore layers mark zones of intense shearing on the long limbs. F3 folds are largely confined to the western section of the ore body where they refold F2 folds and D2 thrust planes, and cause an overall steepening of the ore body dip.

D2 deformation, folding and thrusting, increases in intensity with depth. Drill hole (Reinsbakken, Part II) and geophysical data (Løgn and Bølviken 1974) indicate that the ore horizon approaches the lower contact of the middle greenstone with depth. The contact has been shown, in section 2.3.3, to be the locality of a major thrust zone along which the middle greenstone has been tectonically emplaced in the sequence. This thrust zone accounts for the increase in D2 intensity with depth and has cut the ore horizon at depth. Fig.3.26(b) shows these features in a diagrammatic north-south section through the ore body.

SECTION 4 : SUMMARY AND CONCLUSIONS

4.1 SUMMARY OF THE STRUCTURE OF THE JOMA AREA AND SULPHIDE DEPOSIT.

Four phases of deformation have been identified in the Joma area. The main deformation phase, to which the generally flat-lying penetrative schistosity and northwest trending, mineral lineation belongs, is D2. This phase is associated with the main nappe emplacement event and the formation of minor thrusts that form the lower contacts of the inner, middle and probably also the outer, greenstone units. F2 folds are occasionally seen to fold an S1 schistosity and F1 folds to which F2 folds are coaxial. Thus, D1 deformation is interpreted as an early stage of D2 deformation. Fold vergences and the outcrop pattern of pillow lavas indicate the presence of a major F2 fold in the middle greenstone with the Joma sulphide deposit located in the overturned limb. The fold and the ore horizon are both cut at depth by the thrust at the base of the middle greenstone.

The D2 structures are refolded by a northeast trending, major F3 fold, the Joma synform. F3 fold axial planes and associated crenulation cleavage dip moderately to steeply northwest and fold hinges plunge gently northeast or southwest. Zones of L3 lineation plunge, trending obliquely across the greenstone units, imply a pre-D3 variation in the S2 schistosity surface interpretedas a 'ramp and flat' structure associated with the thrust at the base of the middle greenstone. From the folded L2 lineation patterns, finite strains and the distribution and orientation of D3 deformation, D3 and D2 deformations are sub-coaxial and dominantly simple shear. D3 deformation is therefore interpreted as a late stage in the nappe emplacement event.

D4, the latest phase of deformation, is confined to minor structures adjacent to the upper thrust boundary with the overlying Gjersvik nappe. D4 structure show an antithetic relation-

ship to D3 structures such that as D3 deformation decreases in intensity, D4 structures become dominant. These structures are thought to form as a result of compression caused by the formation of the Joma synform.

All deformation phases indentified in the Joma area are present in the Joma massive sulphide deposit. D2 structures, with which the penetrative schistosity in the greenstones and textural layering in the sulphides is associated, show a variation in style corresponding to a composition change across the ore body. In the east, where the sulphides are chalcopyrite and pyrrhotite rich and contain intercalated silicate layers, isoclinal F2 folds with amplitudes of 100 to 300m are developed. The folds show thickened hinges in which the silicate layers have suffered intense folding and disruption, and thinned limbs along which thrusting has led to the emplacement of thin slivers of sulphide into the greenstone country rocks. In the eastern section of the ore body the sulphides are massive and pyrite-sphalerite dominated. Here intense thrusting has led to the development of numerous tectonic lenses within which slides are marked by thin, laterally persistent, silicate and carbonate layers. The tips of thrust lenses pass westwards into the hinges of F2 folds. Due to abundant thrusting, the majority of sulphide-greenstone contacts are now tectonic and a phase of thrusting, pre-dating D2, correlated with D1, is indicated by the folding of such tectonic contacts in F2 fold hinges. D2 deformation increases markedly with depth as the ore horizon approaches the lower thrust contact of the middle greenstone. The obliquity of S2 schistosity to the sulphide-greenstone contacts implies a southeasterly directed sense of movement on the majority of the thrust contacts.

D2 structures are refolded during D3 and F3 folding is most intense in the western section of the ore body. As in the country rocks, F3 folds are discontinuous and occur in lens-shaped zones of intense folding. Within the sulphides, reactivation of the D2 thrust planes during D3 has caused a flattening of the F3 axial planes and rotation of F3 fold hinges toward the D2 thrust planes and the L2 lineation direction, respectively. Abundant D3 fractures and veins in the adjacent

greenstones form two sets, the first subparallel to the F3 axial planes and the second, subparallel to conjugate shears to the D2 thrust planes. They indicate tensional stresses in the greenstones during D3 deformation, thought to be caused by the competency contrast between greenstone and sulphide.

4.2 THE EFFECTS OF DEFORMATION ON ORE THICKNESS

The results of two phases of deformation on the Joma ore body has been to greatly modify the original tabular form of the ore horizon and intense early (D1-D2) deformation has resulted in drammatic changes in thickness over short distances. Tectonic thickening has occurred in the hinge zones of F2 folds and, to a lesser extent, F3 folds, in the western section of the ore body. Vertical thickening occurs in the steep limbs of F3 folds due to change in attitude of the ore horizon. Thinning of the ore horizon occurs in the limbs, especially short limbs, of F2 folds in the western section, and at the edges of thrust lenses, in the eastern section of the ore body.

The structural styles of the two fold phases can be used as a guide to changes in ore thickness and to locate zones of thick ore. In the eastern section of the ore body, massive pyrite-sphalerite sulphides have developed thrust lenses whose edges trend northwest parallel to the L2 lineation. They tend to be arranged en echelon so that, traversing the ore body in a southerly direction, successive lenses occur at increasingly greater depths to the southwest i.e., in a direction perpendicular to the trend of thrust lenses, see Fig.4.1(b). In the western section of the ore body, chalcopyrite-pyrrhotite ores with intercalated silicate horizons, have led to the development of large scale F2 folds. Their thickened hings form rod-shaped zones trending parallel to the L2 lineation and plunging gently northwest or southeast, see Fig.4.1(a). Zones of exaggerated ore thickness in steepened F3 limbs trend perpendicular to F2 hinges, plunging gently northeast. Where these two hinge trends intersect, pod-like areas of greatest ore thickness occur, see Fig.4.1(a). Since F3 folding is confined to the western section, these pods occur only in this part of the ore body.

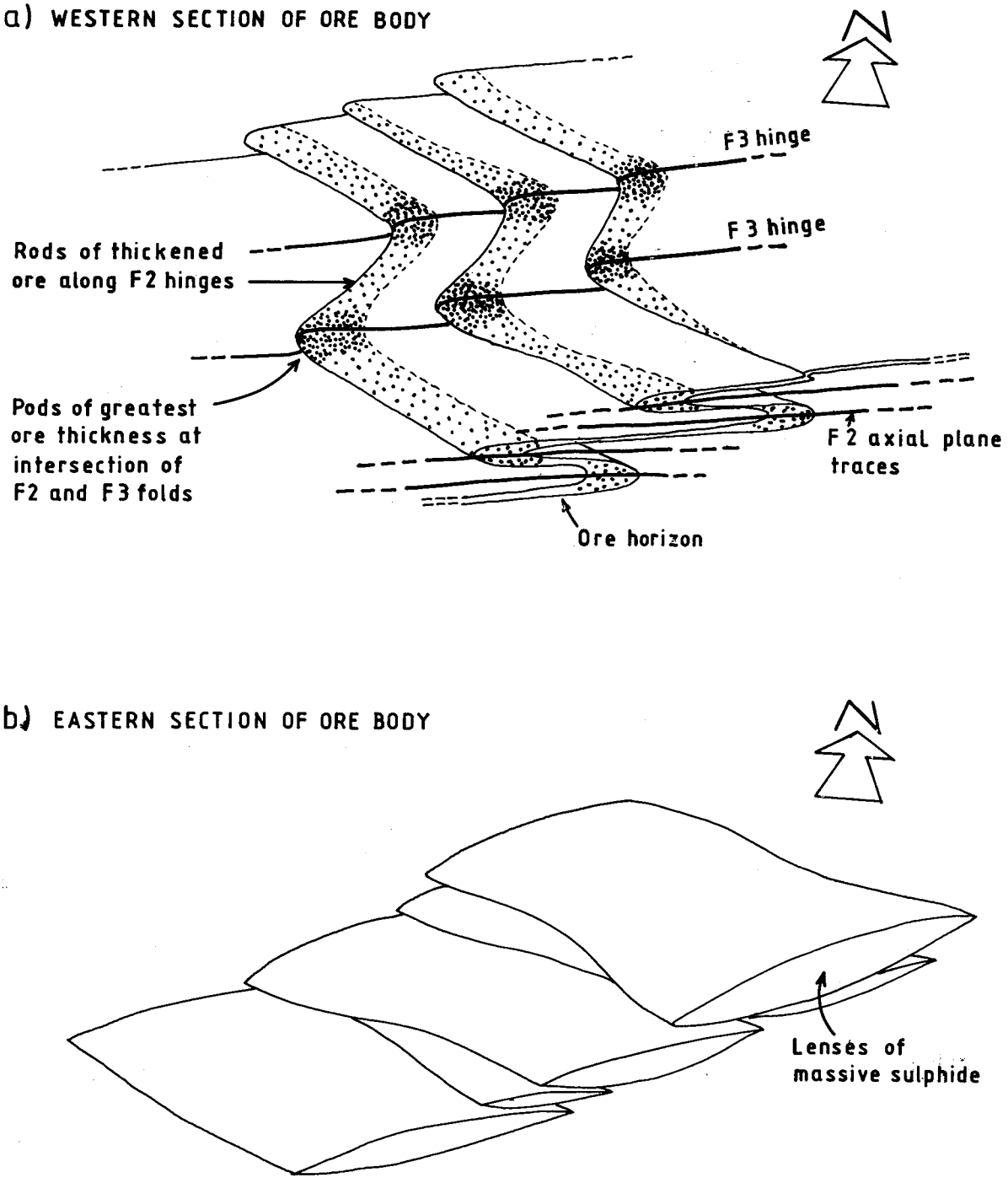

Fig.4.1 Three dimensional sketches of the Joma ore horizon showing the effect of D2 and D3 deformation on ore thickness. a) F2 folds in the western section of the ore body result in rod-like zones of thickened ore. Thickest development of ore occurs at the intersection of F2 and F3 hinges. b) in the eastern section of the ore body, the ore is divided into a series of en echelon thrust lenses.

4.3 THE CONTINUATION OF THE GREENSTONE UNITS IN THE LEIPIKVATTNET NAPPE AND FURTHER ORE OCCURENCES

The structural analysis of the Joma area has shown that the repetition of the three greenstone units is tectonic and that the Joma massive sulphide deposit is cut by a thrust located at the base of the middle greenstone. The L2 mineral lineations approximate the shear direction and the relationship between S2 shistosity in the greenstones and the tectonic sulphide-greenstone contacts indicates that the middle greenstone has been translated in a southeasterly direction. The remainder of the Joma deposit should therefore be situated within the Leipikvattnet nappe to the west of the presently known ore body. To investigate the continuation of the three greenstone horizons beyond the presently mapped area, their outcrop has been traced on the 1:50,000 maps of the Huddingsvatnet area (Kollung 1979) and Røyrvik area (Kollung and Lutro 1985).

To the south of the Joma area, the Leipikvattnet nappe forms a steeply dipping belt trending north-northeast, see Fig.4.2. The inner greenstone outcrops in a thin strip adjacent to the main thrust with the overlying Gjersvik nappe. Thin graphitic phyllite layers within the greenstone probably represent the location of minor thrusts connecting with the lower contact of the inner greenstone lens in the Joma area, as indicated on Fig.4.2. The outcrops of the middle and outer greenstone units thin southwards and can be traced for approximately 10 and 7 kms respectively. Both units show folding on their structurally upper contacts and all three greenstone units show smooth unfolded lower contacts. Since these are known to be the location of thrusts in the cases of the inner and middle greenstone units, it is thus likely that the lower contact of the outer greenstone is also tectonic. As the lower thrust contacts are unfolded, the folding of the upper contacts is coeval with thrusting and therefore D2 in age.

In the extreme south of the area in Fig.4.2, the rocks between the three greenstone units are composed of thin intercalated layers of graphitic phyllite, quartzitic phyllite and

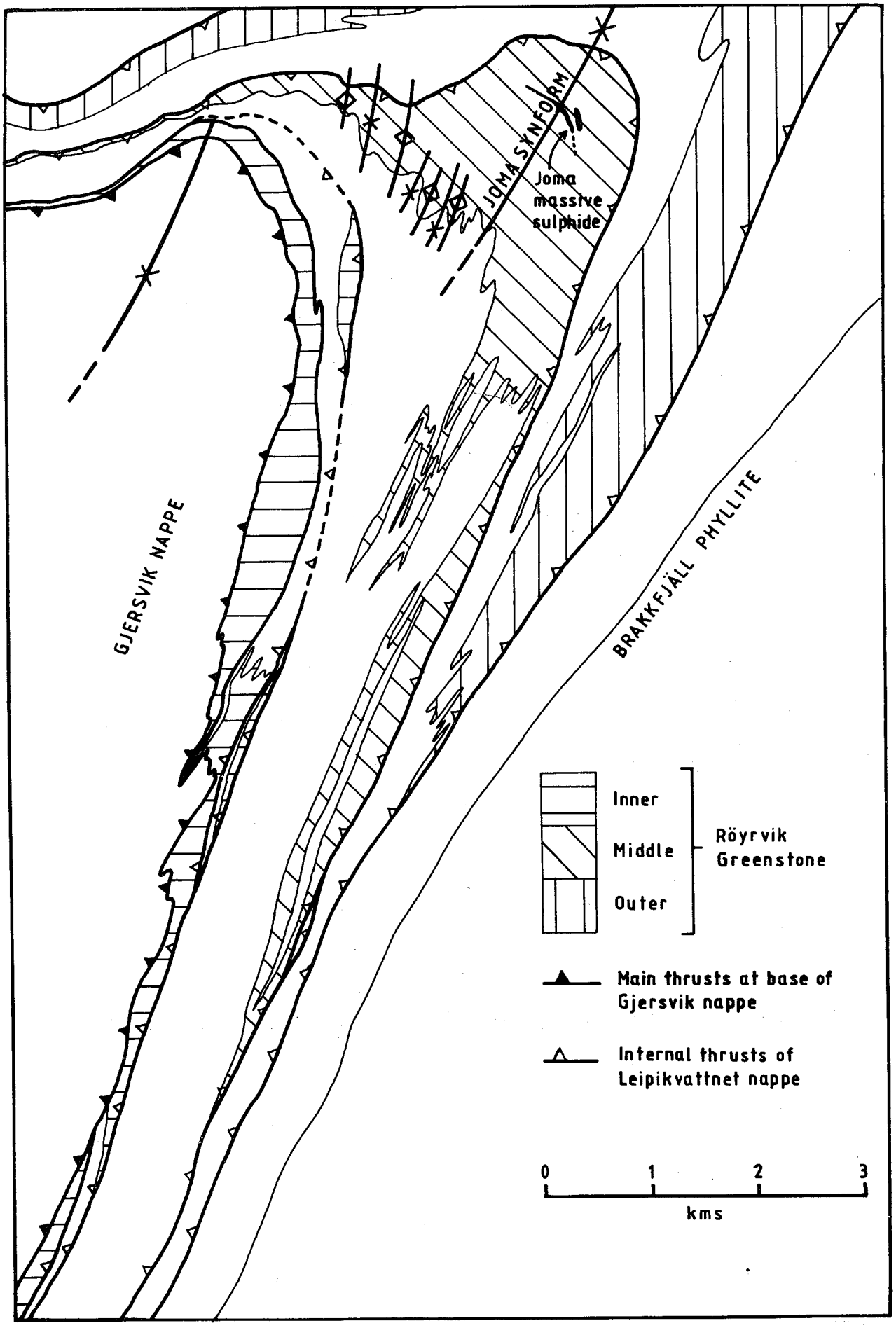

Fig.4.2 The geology of the Leipikvattnet nappe to the south of the Joma sulphide deposit, from the 1:50,000 map of Kollung (1979).

greenstone. This interlayering is probably due to attenuated isoclinal F2 folding and small scale thrusting. The layering trend can be used to trace the southern continuation of the thrusts at the bases of the middle and outer greenstone units, showing that they gradually converge with the main thrust at the base of the Gjersvik nappe, see Fig.4.2.

To the west, the Leipikvattnet nappe trends generally east-west and is folded by an open F3 antiform trending northeast and plunging gently southwest. Fig.4.3, showing the region to the west of the Joma area, is based on the 1:50,000 map (Kollung and Lutro 1985) and incorporates the results of detailed 1:5,000 mapping in the Gåsvannet area (Horbach 1985). As in the area to the south of Joma, the inner greenstone forms an almost continuous, thin strip of outcrop, adjacent to the main thrust contact with the Gjersvik nappe. The outcrop of the outer greenstone can be followed, progressively thinning westwards. The middle greenstone, in contrast, passes westwards into a series of thin, en echelon lenses trending obliquely to the inner greenstone and major thrust. It is probable that these lenses are tectonic in character and they are interpreted as a series of imbricate minor thrusts underlying the inner greenstone. West of Gåsvannet, the middle greenstone is again represented by a single thin greenstone layer.

Several occurrences of sulphide impregnation associated with carbonate horizons and one occurence of massive sulphide, at Borvasselv, have been mapped by Horbach (1985) in the imbricated greenstone layers to the east of Gåsvannet, see Fig.4.3. The sulphides are associated with lithologies similar to those found in the Joma massive sulphide deposit (carbonate and chlorite schist). They also lie to the west of the main deposit, the predicted direction for the location of the missing portion of the sulphide body, and are separated from the main deposit by a series of thrusts. They therefore represent the best candidate for the section of the Joma massive sulphide deposit which was separated from the main body by thrusting at the base of the middle greenstone. A sketch of the structure of the middle greenstone is shown in Fig.4.4.

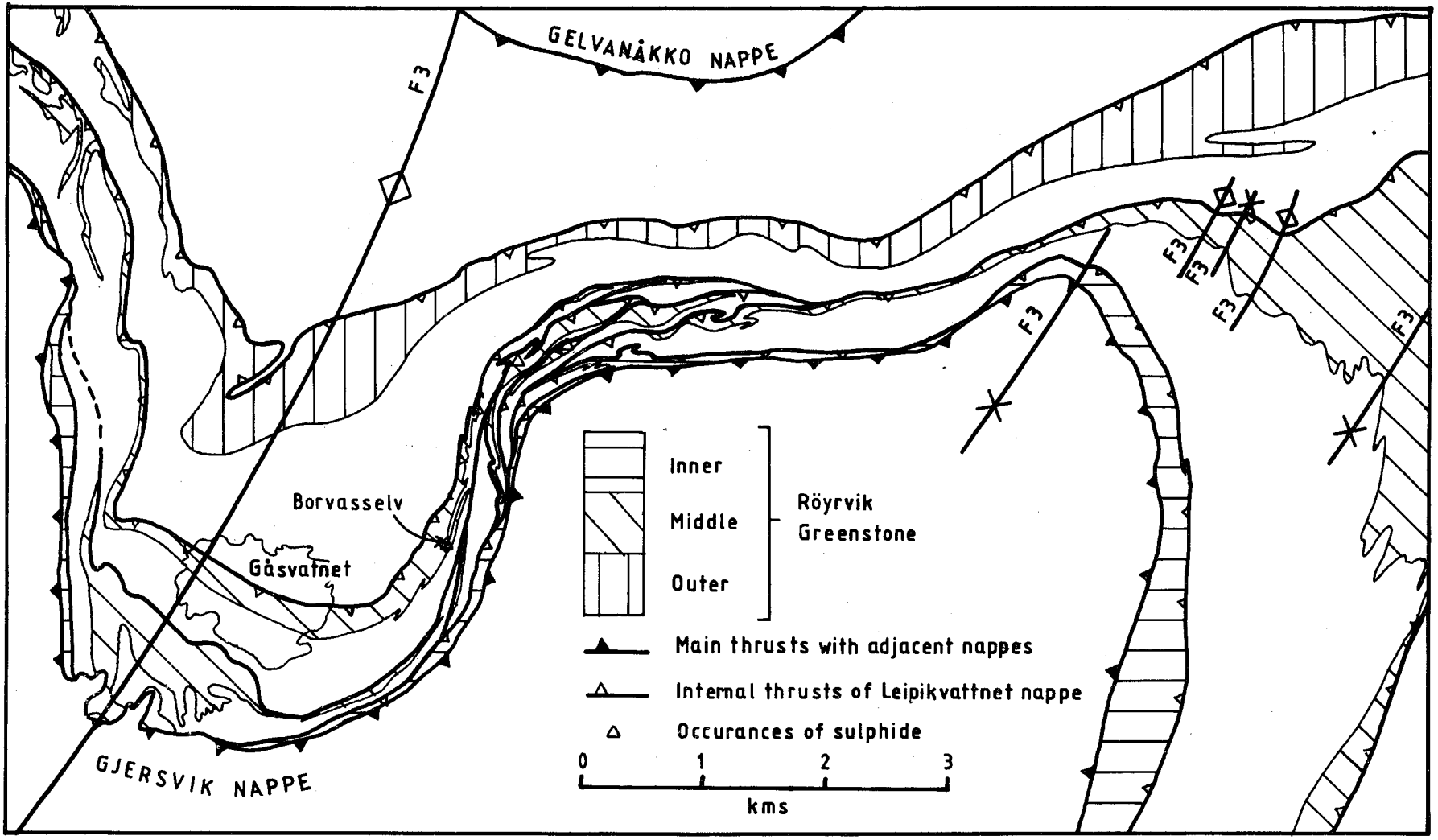

Fig.4.3 The geology of the Leipikvattnet nappe to the west of the Joma sulphide deposit compiled from the 1:50,000 map of Kollung and Lutro (1986) and 1:5,000 map of Horbach (1985).

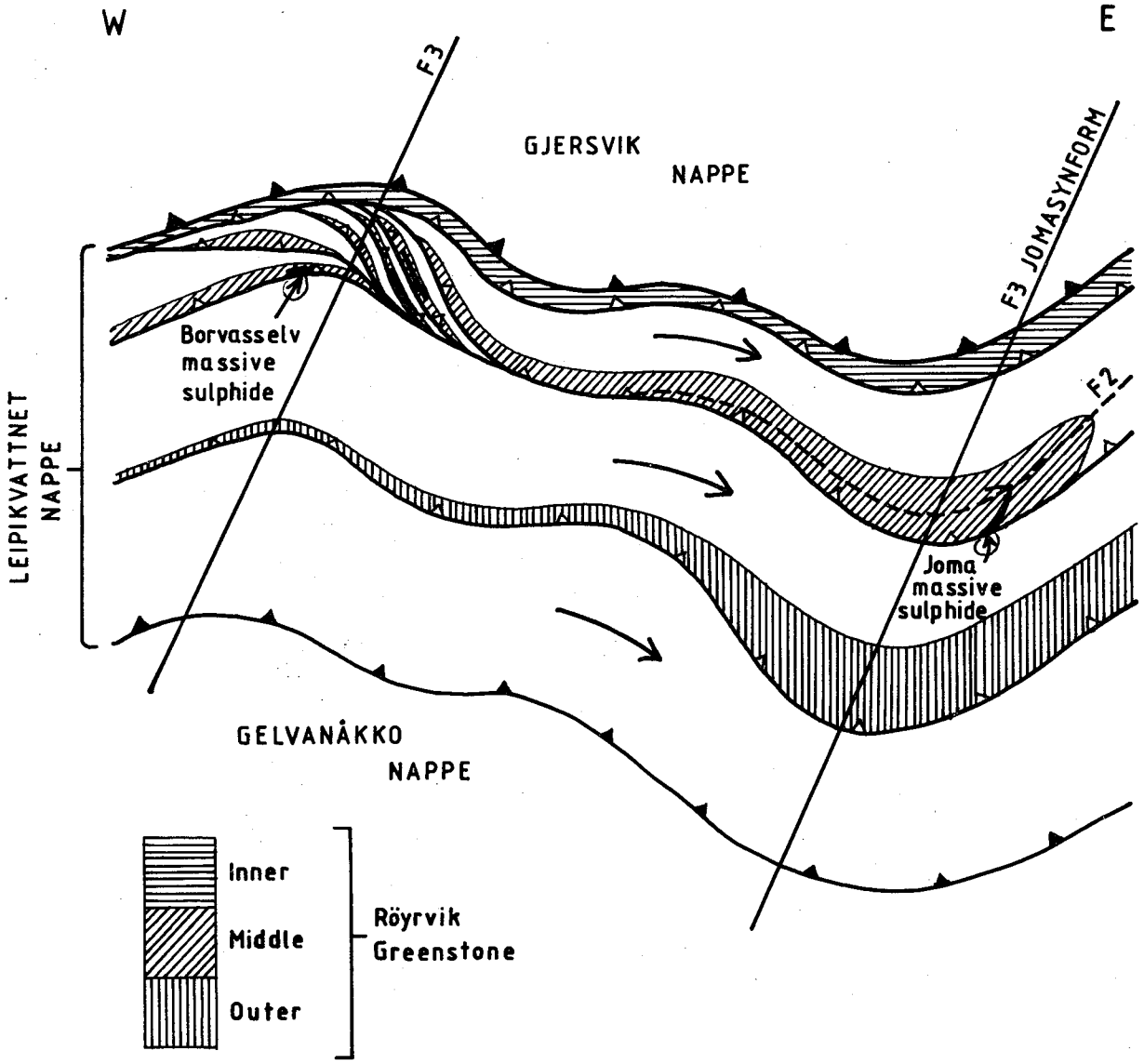

Fig.4.4 Sketch east-west section showing the structure of the Leipikvattnet nappe and the relationship between the Joma ore deposit and sulphide occurences at Borvasselv.

4.4 CORRELATION OF THE JOMA AREA WITH THE REST OF THE NORTH CENTRAL SCANDINAVIAN CALEDONIDES

The Leipikvattnet nappe forms one of the higher tectonic units of the Köli nappe comlex outcropping in the north central Scandinavia. A map of this region, Fig.4.5, shows that the Leipikvattnet nappe forms a discontinuous outcrop stretchingfrom the north side of the Grong-Olden culmination to north of the Bjørgefjell massive. Much of the geological mapping and structural studies in the region were completed during the 1960's and 1970's by the Swedish and Norwegian Geological Surveys (Zachrisson 1964, 1969, Nilsson 1964, Kollung 1971, Trouw 1973, Stephens 1977,1982, Sjöstrand 1978, Roberts 1979, Lutro 1979, Sandwall 1981). Other studies include those centered on ore deposits such as Skorovas (Halls et.al. 1977), Stekenjokk (Zachrisson 1971, Juve 1977) and Joma (present study) and those by Aukes et.al. (1979) in the Lierne district, southern Jämtland and Häggbom (1978) and Ramberg (1981) in the Storfjället nappe. Comprehensive reviews of the tectonostratigraphy are given by Stephens et.al. (1985) and Stephens and Gee (1985). A compilation of the major tectonic boundaries of this area, based on Stephens and Reinsbakken (1981) with additional information from Häggbom (1978), Ramberg (1981) and unpublished data (Reinsbakken), is shown in Fig.4.5.

Between three and five phases of deformation have been recognised in various areas of the Seve-Köli nappe complex. Intermediate in the deformation history are a series of north to northwest trending open folds which that can be traced for over 100 km along strike (Zachrisson 1969). The Joma synform forms a part of one of these folds and can therefore be used to correlate the structures of the Joma area with those of other areas.

Pre-D3 deformation is everywhere correlated with the nappe emplacement event. Up to three phases of deformation are recognised and in several places the earliest phase is almost completely overprinted by the penetrative schistosity, now represented only by relict folds and schistosity (Trouw 1973, Stephens 1977, Sjöstrand 1978, Lutro 1979). The dominant

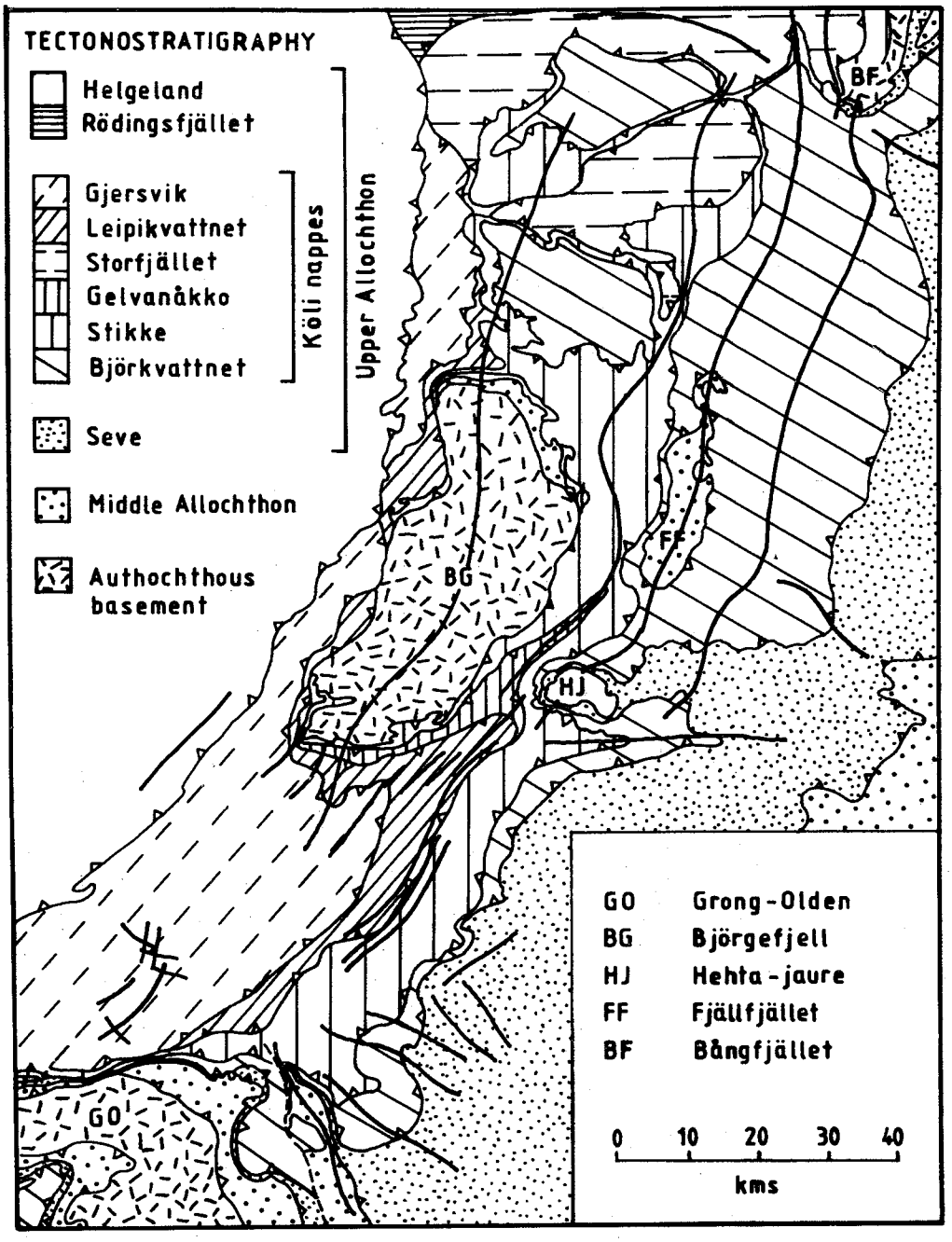

Fig.4.5 Compilation of the major tectonic boundaries of the north central Scandinavian Caledonides after Stephens and Reinsbakken (1981) with additional information from Haggbom (1978), Ramberg (1981) and unpublished data (Reinsbakken). The traces of the major F3 folds are indicated as thick solid lines.

schistosity is in some areas partially overprinted by a crenulation cleavage associated with folding and minor thrusting. Locally this crenulation cleavage becomes penetrative and in its turn overprints the previous schistosity (Trouw 1973, Sandwall 1981). Mineral lineations and folds hinges associated with penetrative schistosity trends north to northwest, while folds associated with the crenulation cleavage trend at high angles to the mineral lineation.

These phases represent different stages in a recurring deformation cycle associated with nappe emplacement. A penetrative schistosity and mineral lineation parallel to the transport direction is developed by dominantly simple shear deformation. This schistosity is later deformed by a crenulation cleavage and folds with hinges oriented subperpendicular to the transport direction. With progressive deformation the crenulation cleavage becomes penetrative and the fold hinges are rotated into the shearing direction. The previous schistosity becomes completely overprinted and ocurs only in rarely preserved relicts. The different stages in this deformation cycle shown by different areas, indicates that the deformation event associated with nappe emplacement was inhomogeneous and it is therefore not possible to correlate schistosities in widely separated areas.

Pre-D3 deformation in the Joma area also shows evidence of this deformation cycle. D1 represents the penetrative schistosity of an early cycle which has been completely overprinted by D2, and is now only rarely preserved. S2 schistosity represented the final stages of the following cycle and, since it has not suffered any further pre-D3 deformation, the next cycle was not initiated before the nappe emplacement event was completed.

D3 deformation deforms the major thrust planes and therefore postdates the major nappe emplacement event. F3 folding occurs in two coeval sets. The dominant set trends north to northeast with moderately northwest dipping to subvertical axial planes, while the subdominant set trends west to northwest with subvertically dipping axial planes. Only the dominant set, to which the Joma synform belongs, is developed in the Joma region.

Individual F3 folds are commonly discontinuous and the major fold traces are composed of sets of en echelon fold traces, as shown by the trace of the Joma synform as it approaches the overlying Gjersvik nappe, see Fig.4.5.

D3 deformation in the Joma area, where F3 fold axial planes dip moderately northwest, have been shown to be dominantly simple shear with a similar shear plane, direction and sense to D2 deformation. F3 folding is therefore interpreted as a late stage compression associated with the nappe emplacement event. During D2, this compression was taken up as movement on shear planes and dominantly simple shear deformation of the nappes. During D3, when the major thrusts were locked, the last stages of this compression resulted in an increasing component of pure shear and the development of subvertical F3 axial planes. At Joma, the steepening of axial planes in the eastern limb of the Joma synform suggests and increasing pure shear component to the east.

D4 deformation consists of flat lying kinks, folds and crenulation cleavage with hinges trending variably northeast. In the Joma area, D3 and D4 deformation occur in adjacent areas with little overlap. A similar relationship occurs in the Gelvanåkko nappe (Stephens 1982) and in the lower Köli of the Lierne district (Aukes et.al. 1979). D3 and D4 deformation also show corresponding degrees of intensity in adjacent areas i.e., zones of intense D4 deformation occur adjacent to zones of intense D3 deformation. This suggests that these phases of deformation are closely related and it is thought that the flat-lying F4 folds developed in response to subvertical stresses initiated at the margin of 'bulges' in the tectonic pile caused by the formation of discontinuous F3 folding.

In summary, all deformation phases can be related to the major nappe emplacement event. The translation of the nappes themselves, in a south to southeaterly direction, is associated with several cycles of simple shear dominated pre-D3 deformation. After major movement on the thrust planes ceased, the last stages of compression lead to the development of large scale open F3 folding. Flat lying D4 structures then developed in reponse to stresses set up by inhomogeneous D3 deformation.

REFERENCES:

Anger, C., Eisbein, P. (1963): Erzmikroskopische Beobachtungen an der Schwefelkies-Kupferkies-Lagerstatte Joma, Grong-Revier (Norwegen). Berg. Wiss., 15, 93-97.

Augustithis, S.S. (1982): Atlas of sphaeroidal textures and structures and their genetic significance. Theophrastus Publ., Athens.

Aukes, P.G., Reymer, A.P.S., de Reuter, G.W.M., Stel, H., & Swart, H.T. (1979): The Geology of the Lierne district, north-east of the Grong culmination, central Norway. Nor. geol. unders. Nr. 354, Bull. 52, 115-130.

Bjørlykke, H. (1959): Rapport over geologisk arbeid i Grongfeltet i tiden 17-29 juli 1959. Internal report, Norsk Bergverk.

Boyer, S.E. & Elliot, D. (1982): Thrust Systems. A.A.P.G. Bull., 66, 1196-1230.

Cheeney, R.F. (1983): Statistical Methods in Geology. Publ. Allen and Unwin., 169 pp.

Eidsmo, O. Foslie, G., Malvik, T., Vokes, F.M. (1984): The mineralogy and recovery of silver in some Norwegian base-metal sulphide ores. In: Proc. Second International Congress in Applied Mineralogy in the Mineral Industry, Los Angeles, California, 1984. Ed. Park, Hausen and Hagni, 891-910.

Foslie, S. (1925): Unpublished 1:50,000 geological map of Huddingsvatnet area.

Foslie, S. (1926): Norges svovelkisforekomster. Nor. geol. unders., Nr. 127, 122 pp.

Foslie, S. (1949): Jomafeltet i Grong og dets malm forråd. Tidsskr. f. Kjemi. Bergv. Met., 9, 177-182.

Gendzwill, D.J. & Stauffer, M.R. (1981): Analysis of triaxial ellipsoids, their shapes, plane sections and plane projections. Math. Geol., 13, 135-152.

Häggbom, O. (1978): Polyphase deformation of a discontinuous nappe in the central Scandinavian Caledonides. Geol. Fören. Stockh. Förh., 100, 349-354.

Halls, C., Reinsbakken, A., Ferriday, I., Haugen, A. & Rankin, A. (1977): Geological setting of the Skorovas orebody within the allochthonous stratigraphy of the Gjersvik Nappe, central Norway. In: Volcanic Processes in Ore Genesis. Spec. Pap. No.7, Inst. Min. Met., Geol. Soc. London, 128-151.

Horbach, R (1985): Unpublished 1:5,000 geological map of the Gåsvatnet area, Nord-Trøndelag.

Horbach, R., Leissmann, W. (1985): Lagerstattenkunde schichtgebundener Sulfidvererzungen Paragenese, Geochemie und Genese der Vererzungen im Joma-Gebeit (Norwegen). Unpubl. progress report, Univ. Clausthal, Germany, 120 pp.

Juve, G. (1964): Geologisk kart - Joma kisforekomster Ornivået, målestokk 1:500. Grong Gruber A/S.

Juve, G. (1964): Skisse over Hovedmalmens skjæring med grunnstollen, horisontal planet, målestokk 1:200. Grong Gruber A/S.

Juve, G. (1977): Metal distribution at Stekenjokk: primary and metamorphic patterns. Geol. Fören. Stockh. Förh., 99, 149-158.

Kollung, S. (1979): Stratigraphy and major structures of the Grong district, Nord-Trøndelag. Nor. geol. unders., Nr. 354, Bull, 52, 1-52.

Kollung, S. (1979): Unpublished 1:50,000 geological map of Huddingsvatnet area.

Lutro, O. (1979): The geology of the Gjersvik area, Nord-Trøndelag, central Norway. Nor. geol. unders., Nr. 354, Bull. 52, 53-100.

Løgn, O. & Bølviken, B. (1974): Self potentials at the Joma pyrite deposit, Norway. In: Geo-exploration. Elsevier Scient. Publ. Co., Amsterdam, 11-28.

Munster, K. (1915): Rapport over Joma Kisforekomst. Pub. Kongsberg, 185 pp.

Nilsson, G. (1964): Berggrunden inom Blåsjöområdet i Nordvästra Jämtlandsfjällen. (English summary) Sver. geol. undersökn., Serie C, Nr. 595, 70 pp.

Oftedahl, C. (1958): Oversikt over Grongfeltets skjerp og malmforekomster. Nor. geol. unders., Nr. 202, 76 pp.

Olsen, J. (1980): Genesis of the Joma stratiform sulphide deposit, central Norwegian Caledonides. Proc. Fifth. Quadr. IAGOD Symp. E. Schweizerbart'sche Verlagsbachandlung, Stuttgart, Germany, 745-757.

Olsen, J. (1984): Joma - geologisk beskrivelse, sammenstilling av resultater fra kartlegging 1975-1977. Internal report, Grong Gruber A/S, 54 pp.

Ramberg, I.B. (1981): The Brakkfjellet tectonic lens: evidence of pinch-and-swell in the Caledonides of Nordland, north central Norway. Norsk Geol. Tidskr., 61, 87-91.

Roberts, D. (1979): Structural sequence in the Limingen-Tunsjøen area of the Grong District. Nor. geol. unders., Nr. 354, Bull. 52, 101-114.

Romaya, J.P. (1982): A field investigation of the geology and structure of the Joma mine area, Norway. Unpublished B.Sc. thesis, Royal School of Mines, Imperial College, London, 61 pp.

Romaya, J.P. (1982): A mineralogical and textural study of the Joma ore body, central Norwegian Caledonides. Unpubl. B.Sc. thesis, Royal School of Mines, Imperial College, London, 35 pp.

Sandwall, J. (1981): Caledonian Geology of the Jofjället area Västerbotten County, Sweden. Sver. Geol. Unders., Serie C, Nr. 778, 105 pp.

Shimamoto, T. & Ikeda, Y. (1976): A simple method for strain estimation from deformed ellipsoidal objects. I: Basic theory. Tectonophysics 36, 315-337.

Sjöstrand, T. (1978): Caledonian Geology of the Kvärnbergsvattnet area, northern Jämtland, central Sweden, stratigraphy, metamorphism and deformation. Sver. Geol. Unders., Serie C, Nr. 735, 107 pp.

Stephens, M.B. (1975): Pebble strain analysis in the Vojtja conglomerate of central Västerbotten, Sweden. Geol. Fören. Stockh. Förh., 97, 74-82.

Stephens, M.B. (1977): Stratigraphy and relationship between folding, metamorphism and thrusting in the Tärna-Björkvattnet area, northern Swedish Caledonides. Sver. Geol. Unders., Serie C, Nr. 726, 146 pp.

Stephens, M.B. (1982): Field relationships, petrochemistry and petrogenesis of the Stekenjokk volcanites, central Swedish Caledonides. Sver. Geol. Unders., Serie C, Nr. 786, 111 pp.

Stephens, M.B. & Gee, D.G. (1985): A tectonic model for the evolution of the eugeoclinal terranes in the central Scandinavian Caledonides. In: The Caledonide Orogen - Scandinavia and Related Areas. Gee and Sturt (Eds.), 935-978.

Stephens, M.B. , Gustavson, M., Ramberg, I.B., Zachrisson, E. (1985): The Caledonides of central north Scandinavia - a tectono-stratigraphic overview. In: The Caledonide Orogeny - Scandinavia and Related Areas. Gee and Sturt (Eds.), 135-162.

Stephens, M.B. & Reinsbakken, A. (1981): UCS Excursion No. B14, Successions related to island arcs in the Köli nappes, Central Scandinavian Caledonides. In: Excursions in the Scandinavian Caledonides. Uppsala Caledonide Symposium 1981.

Trouw, R.A.J. (1973): Structural geology of the Marsfjällen area, Caledonides of Västerbotten, Sweden. Sver. Geol. Unders., Serie C, Nr. 689, 115 pp.

Zachrisson, E. (1964): The Remdalen syncline, stratigraphy and tectonics. Sver. Geol. Unders., Serie C, Nr. 596, 53 pp.

Zachrisson, E. (1969): Caledonian geology of northern Jämtland - southern Västerbotten. Köli stratigraphy and main tectonic outlines. Sver. Geol. Unders., Serie C, Nr. 644, 33 pp.

Zachrisson, E. (1971): The structural setting of the Stekenjokk ore bodies, central Swedish Caledonides. Econ. Geol., 66, 641-652.

Zachrisson, E. (1973): The westerly extension of Seve rocks within the Seve-Köli nappe complex in the Scandinavian Caledonides. Geol. Fören. Stockh. Förh., 95, 243-251.

ACKNOWLEDGEMENTS

The project was carried out while the author held a two year, N.T.N.F. postdoctoral fellowship. Further financial support for field work came from Grong Gruber A/S. Thanks go to the Joma project steering committee; Prof.F.M. Vokes, Prof. R. Sinding-Larsen, Dr. P. Ihlen and A. Haugen, for their discussion and advice. I am indebted to Prof. F.M. Vokes for critically reading the whole manuscript and to Dr. A. Krill for his comments on Section 2. Thanks also go to A. Reinsbakken, co-worker, for his discussion throughout the life of the project.